December 2020

Modeling and Analysis of Scheduling Problems Containing Renewable Energy Decisions

Shasha Wang
Clemson University, sarahwsasa@gmail.com

Modeling and Analysis of Scheduling Problems Containing Renewable Energy Decisions

---

A Dissertation
Presented to
the Graduate School of
Clemson University

In Partial Fulfillment
of the Requirements for the Degree
Doctor of Philosophy
Industrial Engineering

---

by
Shasha Wang
December 2020

Accepted by:
Dr. Scott J. Mason, Committee Chair
Dr. Mary E. Kurz
Dr. Harsha Gangammanavar
Dr. Yongjia Song

Abstract

With globally increasing energy demands, world citizens are facing one of society's most critical issues: protecting the environment. To reduce the emission of greenhouse gases (GHG), which are by-products of conventional energy resources, people are reducing the consumption of oil, gas, and coal collectively. In the meanwhile, interest in renewable energy resources has grown in recent years. Renewable generators can be installed both on the power grid side and end-use customer side of power systems. Energy management in power systems with multiple microgrids containing renewable energy resources has been a focus of industry and researchers as of late. Further, on-site renewable energy provides great opportunities for manufacturing plants to reduce energy costs when faced with time-varying electricity prices. To efficiently utilize on-site renewable energy generation, production schedules and energy supply decisions need to be coordinated. As renewable energy resources like solar and wind energy typically fluctuate with weather variations, the inherent stochastic nature of renewable energy resources makes the decision making of utilizing renewable generation complex.

In this dissertation, we study a power system with one main grid (arbiter) and multiple microgrids (agents). The microgrids (MGs) are equipped to control their local generation and demand in the presence of uncertain renewable generation and heterogeneous energy management settings. We propose an extension to the classical

two-stage stochastic programming model to capture these interactions by modeling the arbiter's problem as the first-stage master problem and the agent decision problems as second-stage subproblems. To tackle this problem formulation, we propose a sequential sampling-based optimization algorithm that does not require a *priori* knowledge of probability distribution functions or selection of samples for renewable generation. The subproblems capture the details of different energy management settings employed at the agent MGs to control heating, ventilation and air conditioning systems; home appliances; industrial production; plug-in electrical vehicles; and storage devices. Computational experiments conducted on the US western interconnect (WECC-240) data set illustrate that the proposed algorithm is scalable and our solutions are statistically verifiable. Our results also show that the proposed framework can be used as a systematic tool to gauge (a) the impact of energy management settings in efficiently utilizing renewable generation and (b) the role of flexible demands in reducing system costs.

Next, we present a two-stage, multi-objective stochastic program for flow shops with sequence-dependent setups in order to meet production schedules while managing energy costs. The first stage provides optimal schedules to minimize the total completion time, while the second stage makes energy supply decisions to minimize energy costs under a time-of-use electricity pricing scheme. Power demand for production is met by on-site renewable generation, supply from the main grid, and an energy storage system. An ϵ-constraint algorithm integrated with an L-shaped method is proposed to analyze the problem. Sets of Pareto optimal solutions are provided for decision-makers and our results show that the energy cost of setup operations is relatively high such that it cannot be ignored. Further, using solar or wind energy can save significant energy costs with solar energy being the more viable option of the two for reducing costs.

Finally, we extend the flow shop scheduling problem to a job shop environment under hour-ahead real-time electricity pricing schemes. The objectives of interest are to minimize total weighted completion time and energy costs simultaneously. Besides renewable generation, hour-ahead real-time electricity pricing is another source of uncertainty in this study as electricity prices are released to customers only hours in advance of consumption. A mathematical model is presented and an ϵ-constraint algorithm is used to tackle the bi-objective problem. Further, to improve computational efficiency and generate solutions in a practically acceptable amount of time, a hybrid multi-objective evolutionary algorithm based on the Non-dominated Sorting Genetic Algorithm II (NSGA-II) is developed. Five methods are developed to calculate chromosome fitness values. Computational tests show that both mathematical modeling and our proposed algorithm are comparable, while our algorithm produces solutions much quicker. Using a single method (rather than five) to generate schedules can further reduce computational time without significantly degrading solution quality.

Dedication

This dissertation is dedicated to my dearest son, Ethan Yifei Wang, who showed me the happiness of being a mom; To my loving husband, Dr. Tianwei Wang, who has always supported me; To my parents, Lijuan Zhou and Jianzhong Wang, whom have given all of their love to me.

Acknowledgements

First and foremost, I would like to express my sincere gratitude to my advisor, Dr. Scott J. Mason, for his support, guidance, and motivation throughout my Ph.D. study. I really appreciate that he has provided me with the research freedom to explore on my own interests and the guidance to keep me on the right path. He also gave me the freedom to choose the location and time to do my research such that I can take good care of my family. He is the best advisor and mentor I have ever known.

I would also like to extend my gratitude to my committee members: Dr. Harsha Gangammanavar, Dr. Mary E. Kurz, and Dr. Yongjia Song. Dr. Harsha Gangammanavar was my research mentor when he was a post-doc at Clemson University. He taught me how to conduct research. I thank him for his patience, motivation, enthusiasm, and immense knowledge. Profound gratitude goes to Dr. Mary E. Kurz for her encouragement, insightful comments, and patient guidance throughout the process of my dissertation. I am thankful to Dr. Yongjia Song for his guidance and directions given to me for completing my dissertation. Special thanks go to Dr. Sandra D. Ekşioğlu for her suggestions and comments in completing this project during her time at Clemson.

I would like to thank my friends, Dr. Site Wang, Dr. Mowen Lu, Dr. Sreenath Chalil Madathil, Dr. Zahra Azadi, and Di Liu for providing their help and support in my research and life.

Last but not the least, many thanks to my dear husband, Dr. Tianwei Wang, who was always there for me and stood by me through both good times and bad. I also profoundly thank my parents for supporting me and encouraging me with their best wishes. Finally, thanks go to my little angel, Ethan Yifei Wang, for bringing me happiness and perspective during the writing of this dissertation.

Table of Contents

List of Tables

List of Figures

Chapter 1

Introduction

Protecting the environment is one of the most critical issues faced by citizens of the world today. As means to reduce the emission of harmful gases (e.g., sulfur dioxide (SO_2) and carbon dioxide (CO_2)), which are by-products of conventional energy resources, renewable and other environment-friendly energy resources have seen increased interest in recent years from academic researchers and industrial personnel. Figure 1.1 shows a forecast of energy consumption over time. Although oil, gas, and coal are still expected to dominate energy resources over the next 18 years, the total amount of energy supplied from them collectively decreases from 85% in 2015 to 75% by 2035 (see Figure 1.1a). Among all energy resources, renewable energy accounts for a small proportion but grows the fastest, with its share increasing from 3% in 2015 up to 10% during the same time period (see Figure 1.1b).

Furthermore, many countries and regions are planning to increase their utilization of renewable energy resources (Figure 1.2). As shown in Figure 1.2a, the European Union (EU) leads the way regarding the penetration of renewable energy generation, with its share of renewable generation doubling to 40% by 2035. China, the world's largest developing country, after starting with 0% renewable generation

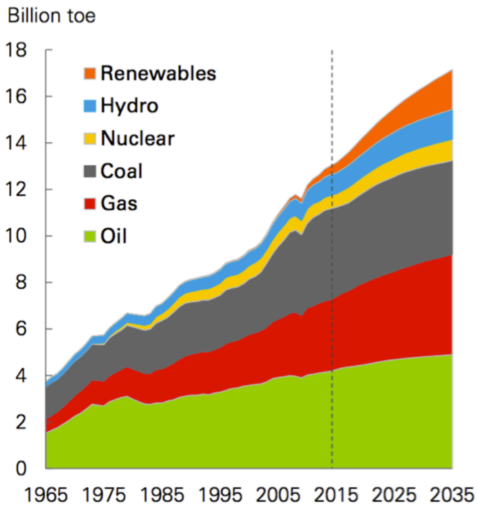

(a) Primary energy consumption

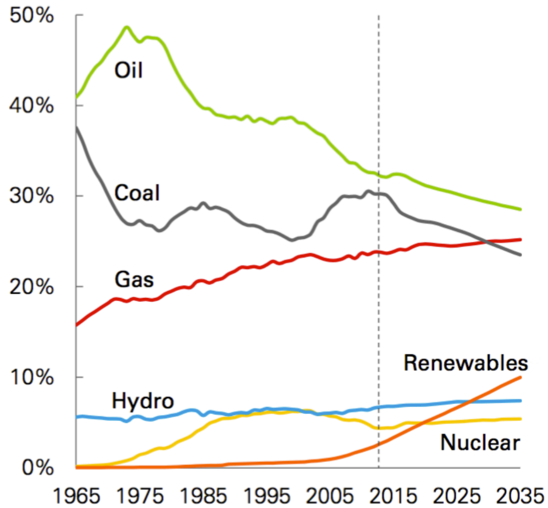

(b) Shares of primary energy

Figure 1.1: Forecast of primary energy consumption in the future
(Source: http://www.bp.com/content/dam/bp/pdf/energy-economics/energy-outlook-2017/bp-energy-outlook-2017.pdf)

in 1995, plans to increase generation to 20% by 2035. In fact, China will generate more renewable power than the EU and United States (US) combined over the next 18 years and will become the country that has the largest growth of renewable generation (Figure 1.2b). Some governments and organizations such as RE100 have committed to encouraging businesses to consider using 100% renewable power. Companies such as Microsoft and Apple have pledged that they will rely solely on renewable energy in the future, while many other companies and countries are currently considering switching to renewable energy resources.

However, an unfortunate reality of renewable energy resources like solar and wind energy is their inherent stochasticity. Any power system integrated with renewable energy resources may become unstable as renewable energy generation typically fluctuates with weather variations. Consider the daily solar energy generated at one location for a year (Figure 1.3) although the generation follows a certain distribution, it varies widely from 8:00 AM (100 on the x-axis) to 4:00 PM (200 on the x-axis).

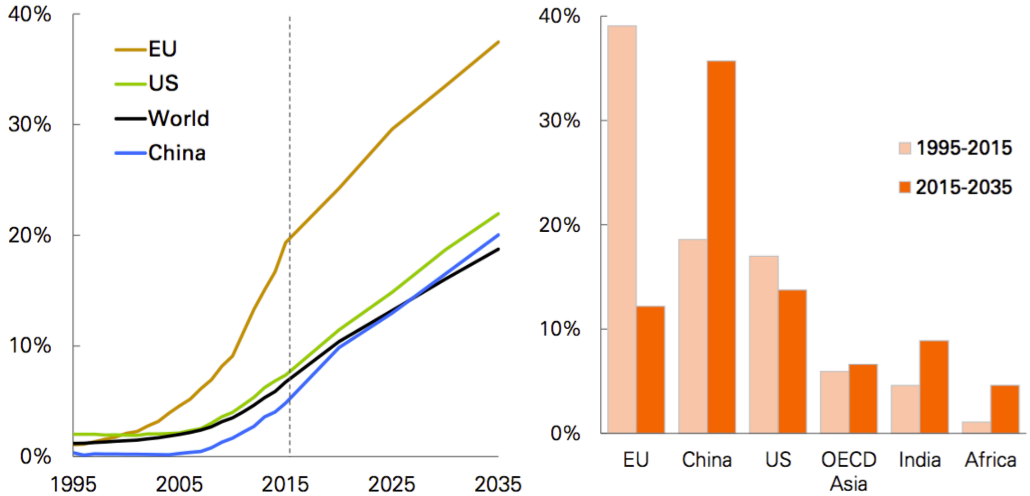

(a) Renewables share of power generation (b) Shares of renewable power growth

Figure 1.2: Forecast of renewable generation in the future
(Source: http://www.bp.com/content/dam/bp/pdf/energy-economics/energy-outlook-2017/bp-energy-outlook-2017.pdf)

Further, the generation level can range from 0 to 90 MW. Another critical point implied by Figure 1.3 is that without developing appropriate techniques to accommodate the uncertainty caused by unstable/non-constant generation levels, additional costs and potentially, energy shortages, will be incurred given any underestimation of the inherent stochasticity [1]. Clearly, improved decision support approaches for renewable energy generation and management are needed to help realize the benefits of renewable energy resources, both economically and reliably.

1.1 Topic Area 1: Energy Management in Power Systems

In power systems, high voltage power is transmitted via transmission lines from a central power plant to substations where the power is stepped down to a lower voltage. Then, the distribution network distributes this lower voltage power

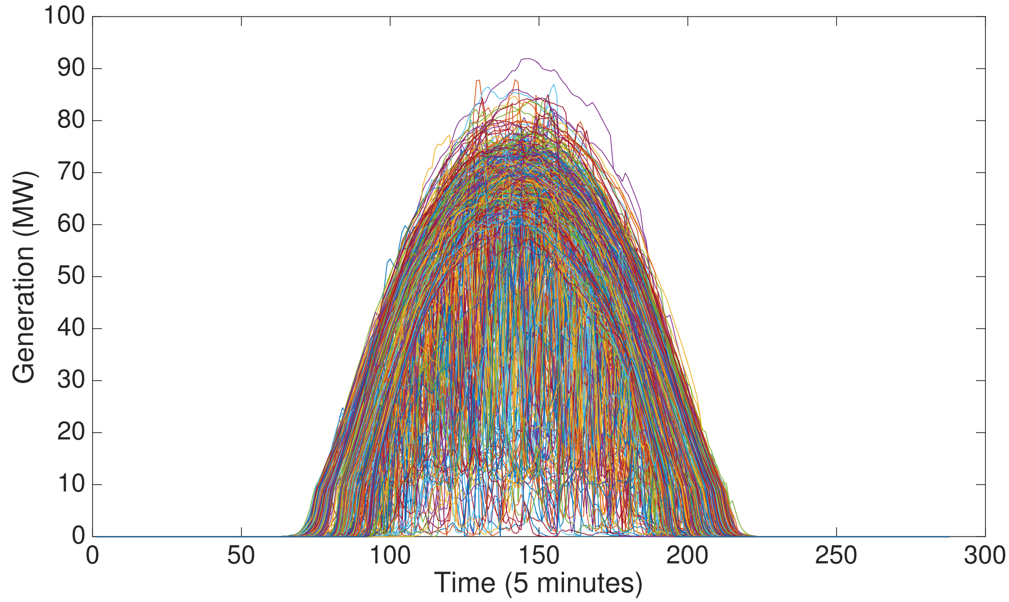

Figure 1.3: Solar generation level during a day at (-118.85, 35.35)

to customers. Generating energy in large central plants saves capital costs per kW of installed power. However, one drawback of the US's current power grid is that typically it relies on non-renewable resources that are environmentally unfriendly, such as gas or coal. Another disadvantage inherent in the US's large power grid is the reality of transmission inefficiencies that result from long-distance transmission. Further, when a part of the grid is affected due to maintenance actions or power outages, the entire grid is impacted. To overcome all these drawbacks, microgrids, which can improve efficiency, reliability, and security [2, 3], are emerging as alternate sources of power generation. As defined by the US Department of Energy Microgrid Exchange Group [4], "a microgrid is a group of interconnected loads and distributed energy resources within clearly defined electrical boundaries that acts as a single controllable entity with respect to the grid."

A microgrid can be operated as part of a power system or in an islanded mode in terms of connecting to or being disconnected from the main grid. When microgrids are connected to a power grid (Figure 1.4), microgrids can either purchase power from or sell power to the main grid. In addition, a microgrid can connect to neighboring microgrids such that it can purchase power from or sell power to its neighbors. To be able to sell power to the power grid or its neighbors, microgrids must have local (distributed) energy generation.

In addition to conventional energy resources such as gas, diesel, and fuel oil, the popularity of incorporating renewable energy resources into microgrids is evident, as researchers have been focused on increasing renewable energy penetration in microgrids [5, 6, 7, 8, 9]. For example, the average annual renewable energy penetration in Kodiak, Alaska, the second largest island in the US, has increased to 99.7% since the Kodiak Electric Association first set a goal of 95% renewable resources penetration in 2007.

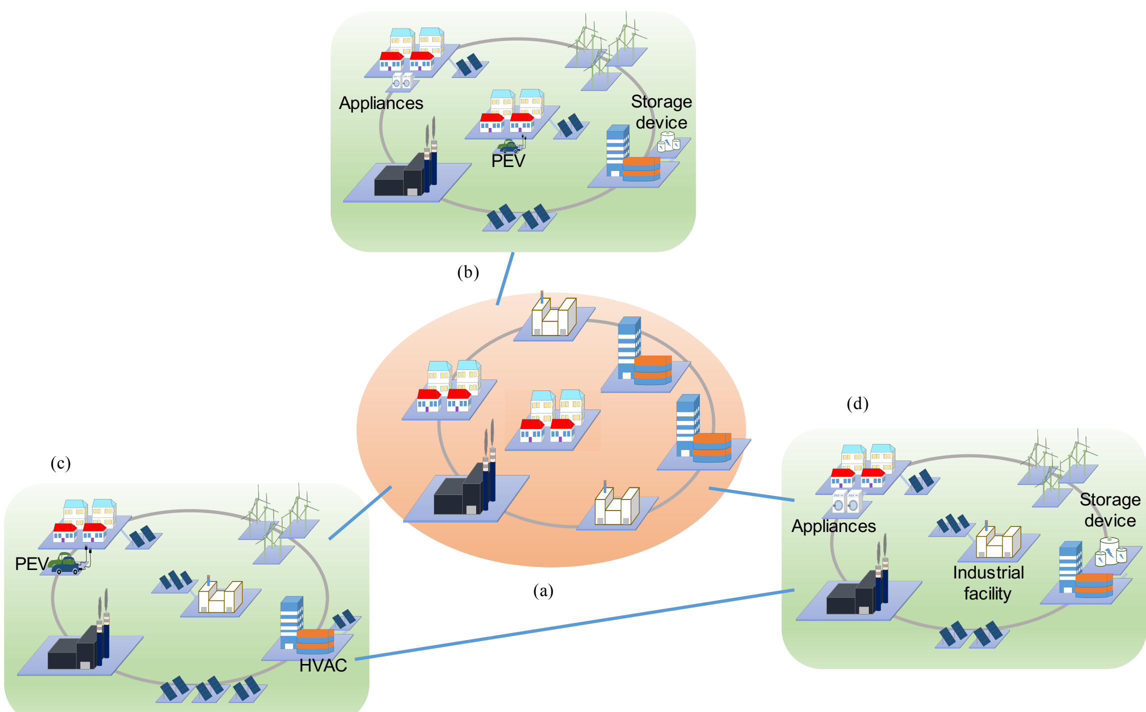

Figure 1.4: An example of power system

According to the US Energy Information Administration, 37% of the nation's renewable energy was generated by wind and solar in 2014. Unfortunately, the inherent stochasticity in both the wind and the solar radiation can cause power grids to become unstable as generation fluctuates with weather variations. As a result, if the energy in microgrids is not managed efficiently, renewable energy resources can increase microgrid operational costs. For example, if 1) microgrid renewable generation is insufficient to serve local users during time periods of high electricity prices and 2) energy storage systems were not charged sufficiently during periods of low electricity prices, then the microgrid must purchase energy from the power grid or run local conventional generators to satisfy power demand—both of these options are more expensive than using renewable generation.

With the development of the smart grid, which uses digital communication technology to detect and react to local changes in power usage, end-use customers' activities can be diverse as they can adjust their energy demands in response to changes in electricity prices. For example, a household may choose to do laundry at 3:00 pm rather than 7:00 pm if cheaper electricity prices prevail in the afternoon. Such customer-driven demand response can benefit the power system by increasing power system flexibility, helping to secure the power system by load curtailment and shifting, and reducing costs by reducing generating capacity requirements. These response activities, which are not only undertaken by households, but also by members of the industrial and commercial sectors, need to be investigated further in the energy management research.

Although a number of researchers have studied energy management in general, no prior research investigates demand response in microgrids containing renewable energy resources that are connected to the main power grid. Given the importance of and potential benefits resulting from this topic area, the first phase of my dissertation research will focus on developing a stochastic optimization framework for coordinating operations of the main power grid with multiple microgrids. Various energy management settings (e.g., demand response) will be considered in the power system along with the uncertainty of renewable energy generation. The goal of this research phase is to provide models and solution methodologies that can help decision makers to operate power systems efficiently and economically.

1.2 Topic Area 2: Production Scheduling with On-site Renewable Energy in Industrial Plants

As one type of end-use customer of power systems, manufacturing plants typically purchase their needed power from the electricity grid to run productions. As reducing production costs is one of the main goals of any manufacturing plant, effective scheduling, often plays a crucial role in most manufacturing and production systems in achieving such the economic goals. Scheduling is performed at a variety of temporal levels. Medium-term scheduling allocates jobs to factories in specific workweeks for completing expected customer orders, while short-term scheduling considers allocation decisions for specific resources such as machines and people over a short time horizon (e.g., a shift or a day) for actual customer orders. Scheduling methods and algorithms typically focus on optimizing cost- and/or time-related objectives/performance measures.

In different manufacturing plants, the production environment can vary according to the number of machines, machine types, speed, and/or layout configuration, to name only a few types of variants. The simplest machine environment is a single machine that processes individual jobs [10]. It can be thought of as a simplified version of all other, more complicated machine environments, such as flow shops and job shops [11, 12]. A flow shop consists of a set of m machines processing n jobs such that each job has to follow the same route (machine order/sequence) during its processing. Job shops are similar to flow shops in that jobs are processed by a number of different machines according to a pre-specified sequence. However, in a job shop, each job has its own unique, predetermined process route to follow.

While today's production schedules minimize costs, we assert that they do consider the electricity costs associated with production. With the development of the smart grid, manufacturing plants are faced with additional challenges of accommodating electricity price-based programs to improve their production economics. For example, the time-of-use electricity pricing schemes are designed to motivate customers to use more energy at off-peak time periods. Under this scheme, users are charged higher rates for consuming power at popular (peak) time periods when demand is at its highest and cheaper rates at other time periods. Similarly, real-time electricity pricing schemes are used by utilities to incentivize customers to shift their energy demands from peak periods to low-demand periods, as electricity prices vary hour-to-hour according to wholesale market prices.

A small number of research studies in the production literature focus on reducing the environmental impacts caused by the emission of hazardous gases, such as sulfur dioxide (SO2) and carbon dioxide (CO2), which are by-products of conventional energy sources. Sulfur dioxide is one of the gases that caused London's lethal smog in the winter of 1952 [13]. The mortality rate for the smog period from December 1952 to February 1953 was remarkably high. Reducing the emission of such harmful gases is another reason renewable and environment-friendly energy resources are receiving attention from academics and practitioners alike. Given the intermittent nature of renewable energy resources (e.g., the highest and lowest generation levels in Figure

1.3 are 90 MW and 0 MW, respectively), an excess (shortage) of power can occur when demand levels are below (exceed) the available generated power. To increase the utilization of renewable energy, batteries, which can store unutilized energy, commonly are used. Batteries can save conventional energy costs if they are charged when there is an abundance of energy and electricity prices are low, and discharged when power is needed and electricity prices are high.

Therefore. the second phase of my dissertation research will focus on integrating production scheduling decisions with on-site renewable energy resources for manufacturing processes in different machine environments. My research will capture the stochasticity of renewable energy resources and comprehend the operations/usage of energy storage systems while considering various electricity pricing schemes, such as time-of-use and real-time pricing. The goal of this phase of my dissertation research is to develop effective scheduling decision support algorithms for decision makers in manufacturing plants that are considering renewable energy alternatives.

1.3 Research Contributions

The high cost and limited sources of fossil fuels, the global desire for clean energy resources, and the need to reduce carbon footprint have made renewable energy resources attractive alternatives in both residential and industrial sectors. However, the intermittent nature of renewable energy resources introduces challenges to full power systems integration, given their uncertain generation schedules. These challenges are not only faced by power grids but also faced by end-use customers when on-site renewable generation is one of their available energy supplies. My dissertation research studied two different application areas of renewable energy resources: power systems and end-use customers. The specific research contributions in my dissertation are as follows:

First, we develop a stochastic programming model for multiple grid-connected microgrids with various energy management settings. Both conventional and renewable generations are sources of energy for the main grid and microgrids. Further, grid-connected microgrids can purchase power from the main grid. Our stochastic framework captures the stochasticity of renewable energy resources and the interactions between the main grid and microgrids in which each microgrid has its own heterogeneous optimization problems, operating time periods, and stochastic processes. To tackle this problem formulation, we developed a sequential sampling-based optimization algorithm that does not require a priori knowledge of probability distribution functions or selection of samples for renewable generation.

Second, we develop a time-indexed mixed-integer linear program for an energy decision problem in a flow shop. The energy sources available for the manufacturing process are 1) power purchased from the main power grid, 2) on-site renewable generation, and 3) discharged energy form energy storage systems. The mathematical model considers both machine status-related energy consumption and time-related energy consumption under a time-of-use pricing scheme. The objective of our model is to minimize both total weighted completion time and energy costs simultaneously. As energy supply decisions can be made after production scheduling decisions and the realization of renewable generation, this problem naturally breaks into a two-stage stochastic program. Therefore, a two-stage stochastic decomposition algorithm is developed to solve this important, practically-motivated problem. The ϵ-constraint approach is integrated into our algorithm to evaluate the two objective functions.

Finally, we extend the flow shop energy decision problem to a job shop environment under a real-time pricing scheme. The real-time pricing tariff brings another uncertainty in the model in addition to on-site renewable generation: electricity prices will impact the second-stage objective function in a two-stage stochastic program as they are objective function coefficients. As most job shop scheduling problems are known to be NP-hard, the computational time should prove unacceptably long for solving this problem at any practical scale using commercial solvers. Therefore, we develop a hybrid multi-objective evolutionary algorithm that integrates a mathematical approach with NSGA-II [89]. Five methods are developed to calculate fitness value for the flow shop scheduling problem and commercial solver is used to compute the optimal energy costs.

Chapter 2

Stochastic Optimization for Energy Management in Power Systems with Multiple Microgrids

S. Wang, H. Gangammanavar, S. D. Ekşioğlu, and S. J. Mason, "Stochastic optimization for energy management in power systems with multiple microgrids." IEEE Transactions on Smart Grid, vol. 10, no. 1, 1068-1079, 2019.

Nomenclature

Sets

$\mathcal{N}$	$:= \{0, 1, 2, \ldots, N\}$, the set of agents ($n = 0$ is the main grid)
$\mathcal{T}$	$:= \{0, 1, 2, \ldots, T\}$, set of discrete time decision epochs

In the following definitions, $t \in \mathcal{T}, n \in \mathcal{N}$ will hold, unless otherwise mentioned.

$\mathcal{B}_n$	buses
$\mathcal{L}_n$	transmission lines

$\mathcal{I}_n$	interconnection lines connected the main grid and microgrid n, $n \in \mathcal{N} \setminus \{0\}$
$\mathcal{G}_n$	conventional generators
$\mathcal{R}_n$	renewable generators
$\mathcal{D}_n$	demands
$\mathcal{D}_n^f$	fixed demands
$\mathcal{D}_n^v$	flexible demands
$\mathcal{V}_n^i$	industrial facilities
$\mathcal{V}_n^h$	buildings that have heating, ventilation, and air conditioning systems
$\mathcal{V}_n^b$	storage devices
$\mathcal{V}_n^p$	plug-in electrical vehicles
$\mathcal{V}_n^a$	home appliances

Subset $\mathcal{G}_{ni} \subseteq \mathcal{G}_n$ denotes conventional generators connected to bus $i \in \mathcal{B}_n$. Similarly, we have the subsets $\mathcal{R}_{ni}$ and $\mathcal{D}_{ni}$.

Parameters

D_{njt}	fixed demand (MW), $j \in \mathcal{V}_n^f$
D_j^i	total flexible demands (MW) required by industrial facility, $j \in \mathcal{V}_n^i$
D_j^a	total flexible demands (MW) required by home appliances, $j \in \mathcal{V}_n^a$
D_{jt}^h	minimum level of demand (MW) required by heating, ventilating, and air conditioning system $j \in \mathcal{V}_n^h$
Δ_{jt}^h	flexible portion of demand (MW) adapted by heating, ventilating, and air conditioning system, $j \in \mathcal{V}_n^h$

S_j	total demand required by PEV, $j \in \mathcal{V}_n^p$
c_{njt}^g	conventional generation cost per MW, $j \in \mathcal{G}_n$
c_{ijt}^b	selling price of power per MW, $(i,j) \in \mathcal{I}_n$
d_{ijt}^p	penalty for under-utilizing the power already purchased (per MW), $(i,j) \in \mathcal{I}_n$
d_{nit}^r	penalty for under-utilizing the renewable power (per MW), $i \in \mathcal{R}_n$
d_{nit}^ℓ	penalty for unmet demand (per MW), $i \in \mathcal{D}_n$
$\mathcal{A}_n^v$	feasible region for decisions a_{njt}
V_{nit}	voltage of bus $i \in \mathcal{B}_n$
X_{nij}	reactance of line $(i,j) \in \mathcal{L}_n$
v_n	weight of agent n
a_j^{min}, a_j^{max}	bounds of utilized power (MW), $j \in \mathcal{D}_n$
s_j^{min}, s_j^{max}	bounds of charging/discharging activities for storage devices and plug-in electrical vehicles (MW), $j \in \mathcal{V}_n^b \cup \mathcal{V}_n^p$
$p_{nij}^{min}, p_{nij}^{max}$	bounds of power flow (MW) distributed by line $(i,j) \in \mathcal{L}_n$
$[\underline{\tau}_j^i, \bar{\tau}_j^i] \subseteq \mathcal{T}$	operation time interval for industrial facility $j \in \mathcal{V}_n^i$
$[\underline{\tau}_j^p, \bar{\tau}_j^p] \subseteq \mathcal{T}$	operation time interval for plug-in electrical vehicle $j \in \mathcal{V}_n^p$
$[\underline{\tau}_j^a, \bar{\tau}_j^a] \subseteq \mathcal{T}$	operation time interval for home appliance $j \in \mathcal{V}_n^a$
$\tilde{\omega}_{njt}$	random variable, renewable generation (MW), $j \in \mathcal{R}_{ni}$

Decision Variables

b_{ijt}	transaction power (MW) between the main grid and microgrid n, $(i,j) \in \mathcal{I}_n$, $n \in \mathcal{N} \setminus \{0\}$
g_{njt}	conventional generation level (MW) at main grid, $j \in \mathcal{G}_n$
a_{njt}	power (MW) utilized to meet demand, $j \in \mathcal{D}_n$

s_{njt}	state of storage devices/plug-in electrical vehicles, $j \in \mathcal{V}_n^b \cup \mathcal{V}_n^p$
p_{nijt}	power flow (MW) distributed by line $(i, j) \in \mathcal{L}_n$
u_{jit}^p	unused purchased power (MW), $(j, i) \in \mathcal{I}_n$
u_{nit}^r	unused renewable generation (MW), $i \in \mathcal{R}_n$
u_{nit}^ℓ	unmet demand (MW), $i \in \mathcal{D}_n$
θ_{nit}	voltage angle of bus $i \in \mathcal{B}_n$

2.1 Introduction

Microgrids have recently emerged as an alternative for reducing greenhouse gas emissions and transmission losses [14, 15]. A microgrid (MG) is a small-scale power grid that is comprised of distributed energy resource systems, storage devices, local demands, and a distribution network [16, 17]. The capacity of such a distributed energy resource system varies from 1500 kW to 1000 MW, which is smaller than a centralized conventional power station [18]. Among all distributed energy resources used in MGs, renewable energy sources (RESs), such as wind and solar, have obtained more attention. Besides reducing greenhouse gas emissions, RESs are easy and economical to obtain, especially in islands and outermost regions [8]. Many researchers have investigated methods to increase the penetration of RESs in MGs such as using storage devices [19]. However, the inherent stochasticity of renewable resources, such as wind and solar, introduces operational challenges of MGs. An attractive feature of MGs is their ability to operate both as part of a larger power grid [20, 21] as well as in an islanded mode [8, 22]. MGs can transact power with the larger grid when they are connected, thereby acting as a source/sink for deficient/excess power in the system. In times of stress, such as during a storm or service interruption, an MG can break off from the larger grid and operate independently on its own. These capabilities can provide additional reliability options to power system operations. Energy managers [16] at microgrids make generation decisions according to information provided by local generation capacity, customer demand, and the amount of power transacted with the main grid.

For these reasons, there has been a growing number of publications that focus on the operations of MGs in the presence of renewable energy resources and/or storage devices. These works have attempted to capture the interactions between MGs and system operators. The setting in [20] was addressed using a simulation-based testing method where economic dispatch decisions at MGs are solved in a primary level and a secondary level optimization seeks to minimize overall operating costs. In [21], TSO-DSO-MGs interactions are captured via an optimization problem that is solved using diagonal quadratic approximation method and a variant of alternating directions method of multipliers. Networked MGs using a bi-level programming model were presented in [23]. A deterministic equivalent mathematical program with complementarity constraints of the bi-level program built using a scenario reduction technique is proposed as a solution approach. In these studies, authors attempt to optimize all MGs simultaneously, which can result in a large optimization problem. In order to achieve computational viability, they consider only a small number of MGs in the system and resort to a limited sample representation of uncertainty. However, it is expected that in the future, the main grid will interact with a large number of MGs. Alternatively, energy management in a multi-agent setting and in the context of electricity markets has been studied by [24, 25, 26]. These problems are solved using agent-oriented programming, Lagrangian-relaxation genetic algorithms, and a combination of stochastic programming and game theory, respectively. Once again, these works are limited to a small set of MGs to achieve computational viability. Moreover, developing solution approaches that converge in uncertain problem settings is still an area of active research. We adopt a stochastic programming approach to tackle some of these issues. Stochastic programming has previously been applied successfully to power system operation problems as they provide convenient tools to model complicated interactions, physical restrictions, and uncertainties [27]. In our work, we propose a novel approach to model this multi-agent setup and a sequential sampling algorithm to solve this problem, which provide provably convergent solutions.

MGs allow integrating smart grid control systems and innovative energy management technologies with traditional operations. In a smart grid, customers are allowed to adjust their energy consumption according to real-time electricity prices. The adjustable appliances either have flexible ranges of power demand or can shift their demand between periods. This behavior, which is called demand response, brings operational flexibility while imposing newer challenges on energy management systems. Most of adjustable demands considered in literature are storage devices and plug-in electrical vehicles [19, 28, 29]. In [20] and [29], the authors provide mathematical models for general adjustable demand. However, the type of adjustable demands varies including industrial, commercial, and residential. Ding *et al.* [30] study non-schedulable and schedulable tasks in industrial facilities. Goddard *et al.* [31] study heating, ventilation, and air conditioning demand response control in commercial buildings. Li *et al.* [32] present detailed models of appliances commonly used in households and investigates the optimal demand response schedule that maximizes customer's net benefit. Chen *et al.* [33] propose stochastic optimization and robust optimization approaches for real-time price-based demand response management for residential appliances. In this work, we propose a detailed mathematical model that captures heterogeneous management systems with adjustable demands and incorporates physical power network restrictions.

In light of the above contents, the main contributions of this paper are:

1. A stochastic programming model that extends the classical two-stage formulation to accommodate multiple subproblems. In the power systems context, this model is designed for a centralized arbiter, who is charged with generating and supplying power to a set of utilities and MGs with various weights (priorities), in the main grid. Each MG is allowed to respond to the decision of the centralized arbiter and a stochastic realization of renewable generation.

2. A comprehensive model that allows MGs to use different energy management systems. This leads to heterogeneous agent optimization problems, operating time periods, and stochastic processes. To the best of our knowledge, our work is the first to consider such a setup.

3. An extension of the two-stage stochastic decomposition (2-SD) to solve models with multiple subproblems. Our approach, which we refer to as the multi-agent stochastic decomposition, is a decomposition-based sequential sampling algorithm. It dynamically identifies the number of samples required to characterize the uncertainty at a particular MG and provides statistically verifiable solutions and objective function estimates.

4. A comprehensive computational analysis that highlights the scalability of the proposed algorithm to large-scale power systems. The results of our analysis illustrate the performance of the algorithm, the benefits of energy management systems, and the advantages of flexible demands.

The remainder of the chapter is organized as follows. In Section 2.2, the energy management in power systems is studied and corresponding mathematical model is presented. The multi-agent stochastic decomposition is implemented in Section 2.3. Computational experiments are conducted in Section 2.4. Finally, conclusions are offered in Section 2.5.

2.2 Problem Formulation

We consider a power system that is comprised of a main grid connected to multiple agents. The main grid can either be a transmission or distribution network. In transmission networks, the independent system operator (ISO) acts as the centralized arbiter bestowed with the responsibility of managing not only the operations (generation, transmission, etc.) of the transmission network, but also managing the transactions with distribution networks and MGs connected to it. The agents themselves are managed by autonomous decision-making entities (distribution system operators (DSO) for distribution networks and energy management systems for MGs). Similarly, the distribution system operator shares the same interactions with MGs connected to the distribution network. While the role of decision makers at individual agents is concerned with the operations on a small/local scale, the centralized arbiter is interested in optimal operations of the entire system. The formulation presented in this section encompasses any such relationship between the centralized arbiter and agents. In the remainder of the paper, we will restrict all agents to be MGs with independent energy management systems controlling their operations.

The power system uses both conventional and renewable energy resources to meet customer demands. Each entity in the system is exposed to varied sources of uncertainty (demand, renewable generation, etc.) and utilizes different energy management settings. Fig.2.1 shows the system we described above. To capture these properties of the system, we present a stochastic optimization formulation that is comprised of (a) an arbiter problem where decisions are made before the realization of any uncertainty and (b) multiple agent problems where decisions are made in

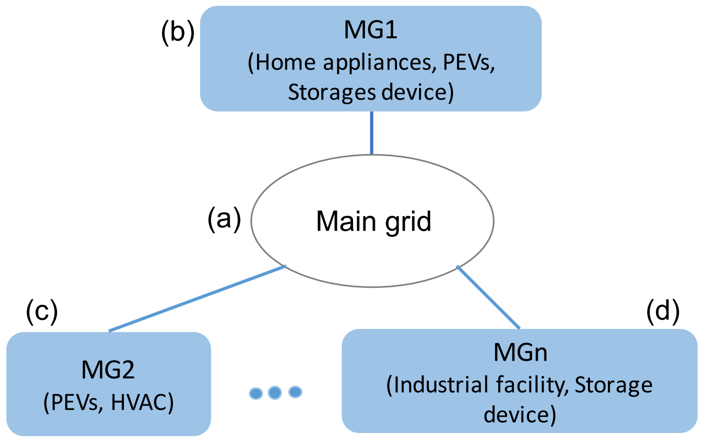

Figure 2.1: A power system: A main grid (a) connects to multiple MGs ((b) - (d)) that utilize different energy management settings

response to their respective stochastic outcomes. This formulation is an extension of the classical 2-SP and will be referred to as the multi-agent stochastic program (MA-SP). At time period t, customer demands at each agent can be met through local generation (conventional and renewable) as well as energy bought from the main grid (when $n \neq 0$). We first begin by presenting the arbiter's optimization problem.

2.2.1 Arbiter Problem

The centralized arbiter determines the conventional generation level at the main grid as well as its power transactions with all the MGs. The set of generators in the main grid is denoted by $\mathcal{G}_0$. For every generator $j \in \mathcal{G}_0$, the generation level and the corresponding cost are denoted by g_{0jt} and c^g_{0jt}, respectively. The transaction decisions b_{ijt} between the main grid and MGs are determined for all $(i,j) \in \mathcal{I}_n$ at a price of c^b_{ijt}, where $\mathcal{I}_n$ is the set of interconnection links. These generation and transaction decisions are made so as to satisfy the following power balance equation:

$$\sum_{j \in \mathcal{G}_0} g_{0jt} = \sum_{j \in \mathcal{D}_0 \bigcup \mathcal{R}_0} \partial \bar{D}_{0jt} + \sum_{(i,j) \in \mathcal{I}_n} b_{ijt} \quad \forall t \in \mathcal{T}, \tag{2.1}$$

where $\partial \bar{D}_{0jt}$ is the net demand computed using the forecasted demand ($\mathcal{D}_0$) and renewable generation ($\mathcal{R}_0$) in the main grid. In addition, generation and transaction decisions are bounded by their respective physical limits. Further, these decisions are established in a "here and now" manner and effect the state of every agent in the system. We will succinctly denote the arbiter's decision vector by $x = (x_t)_{t\in\mathcal{T}}$ and cost vector by $c = (c_t)_{t\in\mathcal{T}}$, where $x_t = ((g_{0jt})_{j\in\mathcal{G}_0}, (b_{ijt})_{(i,j)\in\mathcal{I}})$ and the corresponding cost coefficients by $c_t = ((c^g_{0jt})_{j\in\mathcal{G}_0}, (-c^b_{ijt})_{(i,j)\in\mathcal{I}})$. The feasible set characterized by (1) is denoted by $\mathcal{X}$. Once the arbiter makes its decision, each agent responds to this decision and a realization ω_n of its stochastic process $\tilde{\omega}_n$ at a recourse cost of $h_n(x, \omega_n)$. We assume that the stochastic processes affecting the agents are independent of each other.

The objective of the centralized arbiter is to minimize the energy cost and the sum of weighted expected recourse functions. Its optimization problem is given by:

$$\begin{aligned} &\min\ c^\top x + \sum_{n\in\mathcal{N}} v_n \mathbb{E}\{h_n(x, \omega_n)\} \\ &\text{s.t. } x \in \mathcal{X}, \end{aligned} \tag{2.2}$$

where the weight $v_n \geq 0\ \forall n \in \mathcal{N}$ is chosen based on the relative preference of the agents set by the centralized arbiter. For example, an agent with critical infrastructures (like hospitals) has higher priority (weight) than other agents.

2.2.2 Agent problem

Each agent in the system, that is, the main grid and all MGs, is associated with an agent problem. This problem is characterized by the energy management setting adopted and stochasticity faced by the agent. The energy resources of an agent n include the set of conventional generators $\mathcal{G}_n$ as well as renewable generators $\mathcal{R}_n$. The conventional generators at MGs ($n \neq 0$) usually have lower capacities when compared to the main grid ($n = 0$) generators. In addition to these local energy resources, the MGs can utilize a fraction of the energy available from the main grid. The generation levels g_{0jt} $\forall j \in \mathcal{G}_0$ at the main grid, which were set by the arbiter, are allowed to be updated.

These resources are used to meet customers' demands, which are denoted by $\mathcal{D}_n$. Further, all customer demands can be categorized as fixed and flexible. The fixed demand, D_{njt}, at location $j \in \mathcal{D}_n^f$ must be met in the current time period t. In other words,

$$a_{njt} \geq D_{njt}, \tag{2.3}$$

where a_{njt} is the power utilized to meet this fixed demand. The flexible demand, $\mathcal{D}_n^v$, depends on the energy management settings adopted by each agent. We will describe these settings in the following.

2.2.2.1 Energy Management Settings

Each agent may adopt (one or more) different settings. Therefore, we omit the agent index n while presenting these settings.

1. Industrial Sector: The field of production management provides flexibility in how demand at a particular facility can be met during the operation time horizon[30]. This, in turn, allows for efficiently utilizing the available energy resources. To ensure that the production demand is met, the cumulative power consumption within a production window must exceed a given threshold. Let $\mathcal{V}^i$ denote a set of industrial facilities. If for each $j \in \mathcal{V}^i$, the time window within which the demand D_j^i can be satisfied is given by $[\underline{\tau}_j^i, \bar{\tau}_j^i] \subseteq \mathcal{T}$. This

requirement is captured by:

$$\sum_{t \in [\underline{\tau}_j^i, \bar{\tau}_j^i]} a_{jt} \geq D_j^i. \tag{2.4}$$

In the above, a_{jt} is the realized power in time period t that is restricted to be within an interval $[a_j^{min}, a_j^{max}] \in \mathbb{R}$. The equipment used in industrial settings is associated with significant start-up time and set-up cost. Therefore, it is efficient to run the industrial equipment uninterrupted, which is ensured by setting $a_j^{min} > 0$.

2. Building Management: For commercial buildings, around 50% of the energy is consumed by heating, ventilation, and air conditioning (HVAC) systems to provide a comfortable indoor environment [34]. Let $\mathcal{V}^h$ denote the set of buildings that have intelligent HVAC systems. Since comfort is a qualitative term, it is best captured through a flexible range. For example, the comfortable indoor temperature ranges between 20°C to 25°C [35]. Moreover, this comfort is also associated with climate [36] and building occupancy [37]. For these reasons, the amount of energy consumed has a fixed minimum level D_{jt}^h (corresponding to the minimum comfort requirement) and a flexible portion Δ_{jt}^h for all $j \in \mathcal{V}^h$. The flexible portion can frequently fluctuate within a range without reducing the end-user's comfort significantly. This is ensured by:

$$D_{jt}^h \leq a_{jt} \leq D_{jt}^h + \Delta_{jt}^h \quad \forall j \in \mathcal{V}^h, \forall t \in \mathcal{T}. \tag{2.5}$$

Note that, while the demand in (2.4) can be met across multiple time periods, the demand here is time-dependent and should be met in its time period.

3. Storage Devices: It has been identified that storage devices will play a critical role in mitigating renewable regulation challenges [38, 39]. Apart from energy arbitrage, storage devices can provide ancillary services, capacity deferral services, and end-user services [40]. Let $\mathcal{V}^b$ denote a set of storage devices. For each $j \in \mathcal{V}^b$, a_{jt} is the charging/discharging amount during time period t. If this value is positive, it indicates a charging activity—discharging otherwise. These decisions are bounded by charging/discharging rates of the storage devices: $a_{jt} \in [a_j^{min}, a_j^{max}] \in \mathbb{R}$. Let s_{jt} denote the state of storage devices that is required to satisfy the following dynamics equation:

$$s_{jt} = s_{j,t-1} + a_{jt} \qquad \forall j \in \mathcal{V}^b,\ \forall t \in \mathcal{T}, \tag{2.6}$$

where the initial state s_{j0} is assumed to be given. This variable is also bounded by the capacity of this storage device, that is $0 \leq s_{jt} \leq s_j^{max}$. In any time period, a storage device can act both as source and sink of energy.

4. Plug-in Electric Vehicle (PEV): The operating principle of PEVs is similar to that of storage devices. However, unlike the storage devices, the charging and discharging activities depend on the utility of the vehicle. For example, it should be expected that the PEVs are connected to a residential grid during the off-work hours. Therefore, the whole operation must be completed during a time period that is desired by the customer. Using similar definitions as given for storage devices, for $j \in \mathcal{V}_p$, the set of PEVs must satisfy:

$$a_j^{min} \leq a_{jt} \leq a_j^{max},\ s_j^{min} \leq s_{jt} \leq s_j^{max} \tag{2.7a}$$

$$s_{jt} = s_{j,t-1} + a_{jt} \quad \forall t \in [\underline{\tau}_j^p, \bar{\tau}_j^p], \tag{2.7b}$$

where $[\underline{\tau}_j^p, \bar{\tau}_j^p]$ is the plug-in interval. Further, the state of the PEVs at the end of the plug-in interval must satisfy the specific customer-desired requirement[33]:

$$s_{j\bar{\tau}_j^p} = S_j \quad \forall j \in \mathcal{V}^p. \tag{2.8}$$

5. Home Appliances: The operation of some appliances, such as dishwashers and washing machines, is flexible over a time horizon. These appliances have relatively lower demand compared to the other settings described thus far. Let $\mathcal{V}^a$ denote a set of appliances. For each $j \in \mathcal{V}^a$, a_{jt} is the power utilized in time period t that must satisfy:

$$\sum_{t \in [\underline{\tau}_j^a, \bar{\tau}_j^a]} a_{jt} \geq D_j^a \tag{2.9}$$

during the desired time window $[\underline{\tau}_j^a, \bar{\tau}_j^a]$. The operation of these appliances can withstand interruptions since the start-up time and set-up cost are negligible. Moreover, power utilized in any time period should be less than the power rating of the appliance. Therefore, $a_{jt} \in [0, a_j^{max}]$. The interruptible nature of these appliances differentiates them from industrial equipment.

We restrict our attention to the above five settings, but other similar settings can also be operated within our multi-agent framework. Moreover, for agent n the flexible demand set $\mathcal{D}_n^v$ can be any combination of the above settings. The feasible region for decisions a_{njt}, where $j \in \mathcal{D}_n^v$ depends on this combination and will be denoted as $\mathcal{A}_n^v$. For example, for a household with storage devices and PEV units installed, the set $\mathcal{D}_n^v = \mathcal{V}_n^b \bigcup \mathcal{V}_n^p \bigcup \mathcal{V}_n^a$. In this case, the feasible region $\mathcal{A}_n^v$ is characterized by (6), (7), (8), and (9) along with the respective bounds.

2.2.2.2 Power Network Constraints

The power grid in both the main grid and MGs (i.e., for all $n \in \mathcal{N}$) consists of buses and lines that construct a network with a set of buses $\mathcal{B}_n$ and a set of transmission lines $\mathcal{L}_n$. At any bus $i \in \mathcal{B}_n$, the total available power should meet the total of fixed and flexible demands, thus, satisfying the following:

$$\sum_{j \in \mathcal{G}_{ni}} g_{njt} + \Bigg(\sum_{j:(j,i) \in \mathcal{L}_n} p_{njit} - \sum_{j:(i,j) \in \mathcal{L}_n} p_{nijt} \Bigg) \\ - \sum_{j \in \mathcal{D}_{ni}} (a_{njt} - u^{\ell}_{njt}) = r_i(x_t, \tilde{\omega}_{nit}) \quad \forall t \in \mathcal{T}, \tag{2.10}$$

where p_{njit} and p_{nijt} are the flow into and out of bus i, respectively. Further, u_{jit} is the purchased power that is unused. Note that this variable appears only in MG problems. The right-hand side $r_i(x_t, \tilde{\omega}_{nit})$ depends on the arbiter's decision and the renewable generation $\tilde{\omega}_{nit}$. Note that the right-hand side $r_i(x_t, \tilde{\omega}_{nit})$ for the main grid and MGs are different since the main grid acts as a seller rather than a buyer in the transactions with agents. Therefore, for any bus $i \in \mathcal{B}_n$, $r_i(x_t, \tilde{\omega}_{nit})$ is set as the following:

$$\begin{cases} -\sum_{j \in \mathcal{R}_{ni}} (\tilde{\omega}_{njt} - u^r_{njt}) + \sum_{j:(i,j) \in \mathcal{I}_n} b_{ijt} & \text{if } n = 0, \\ -\sum_{j \in \mathcal{R}_{ni}} (\tilde{\omega}_{njt} - u^r_{njt}) - \sum_{j:(j,i) \in \mathcal{I}_n} (b_{jit} - u^p_{jit}) & \text{if } n \neq 0. \end{cases} \tag{2.11}$$

On any transmission line, the real transmitted power and power losses are non-linear functions of the differences between the voltages and angles of buses in both ends of connecting lines. To make these functions suitable for linear optimization methods, we apply a linear approximation described in [41]. We ignore the power flow losses. If V_{nit} denotes the voltage of bus i, and X_{nij} denotes the reactance of line

$(i,j) \in \mathcal{L}_n$, then the power flow p_{nijt} is given by:

$$p_{nijt} = \frac{V_{nit}V_{njt}}{X_{nij}}(\theta_{nit} - \theta_{njt}) \quad \forall t \in \mathcal{T}, \tag{2.12}$$

where the decision variable θ_{nit} is the angle of bus i. Further, the power flow p_{nijt} and bus angle θ_{nit} should be within their intervals $[p_{nij}^{min}, p_{nij}^{max}]$ and $[\theta_{nij}^{min}, \theta_{nij}^{max}]$, respectively.

Each agent has the objective of minimizing the following: the total cost of generation, the penalty for under-utilizing the power already purchased, the unused renewable generation, and the unmet demands. Let c_{njt}^{g}, d_{ijt}^{p}, d_{ijt}^{r}, and d_{ijt}^{ℓ} represent the corresponding unit costs, thus, the objective is:

$$\begin{aligned} h_n(x,\omega_n) = \min \ & \sum_{t \in \mathcal{T}_n} [\sum_{j \in \mathcal{G}_n} c_{njt}^{g} g_{njt} + \sum_{\substack{(i,j) \in \mathcal{I}_n \\ n \neq 0}} d_{ijt}^{p} u_{ijt}^{p} + \\ & \sum_{j \in \mathcal{R}_n} d_{njt}^{r} u_{njt}^{r} + \sum_{j \in \mathcal{L}_n} d_{njt}^{\ell} u_{njt}^{\ell}] \\ & s.t. \ (2.3), \ (2.10), \text{and } (2.12) \\ & a_{njt} \in \mathcal{A}_n^v. \end{aligned} \tag{2.13}$$

The arbiter's decision as well as stochastic information (renewable generation) affect only the right-hand side of the above program. The agent subproblem and the arbiter's problem in (2.2), which is referred to as the first-stage problem, together constitute our MA-SP:

$$\min c^\top x + \sum_{n \in \mathcal{N}} v_n \mathbb{E}\{h_n(x,\omega_n)\} \tag{2.14a}$$

$$\text{s.t. } x \in \mathcal{X},$$

where,

$$h_n(x,\omega_n) = \min \ d_n^\top y_n \tag{2.14b}$$
$$s.t. \ W_n y_n \leq r_n(\omega_n) - T_n(\omega_n)x,$$
$$y_n \geq 0.$$

The subproblem (2.14b) is a succinct representation of the agent problem in (2.13). We resort to this representation to simplify the exposition of our algorithm in the next section. Notice that the objective function and constraints are linear functions, the first-stage decisions affect the right-hand side of (2.14b), and the recourse matrix is independent of uncertainty. Therefore, this formulation is an extension of 2-SP with fixed recourse [1].

2.3 Algorithm

The formulation introduced in Section 2.2 has an arbiter problem where decisions are made before the realization of demand and renewable generation as well as multiple agent problems that provide the recourse costs for the arbiter's decisions. If all the agents can be operated/controlled by a single decision maker, then a combined optimization program can be used to obtain their decisions (shown by the large shaded blue box in Figure 2.2a). Further, a subproblem scenario is a single vector of observation at all agents. In this setting, the problem can be formulated as a 2-SP. However, the agents have independent decision makers with heterogeneous optimization problems. They are exposed to different stochastic processes. As (2.14) shows, the proposed MA-SP has a weighted sum of expected recourse functions in the first stage. Each expected recourse function corresponds to an independent agent

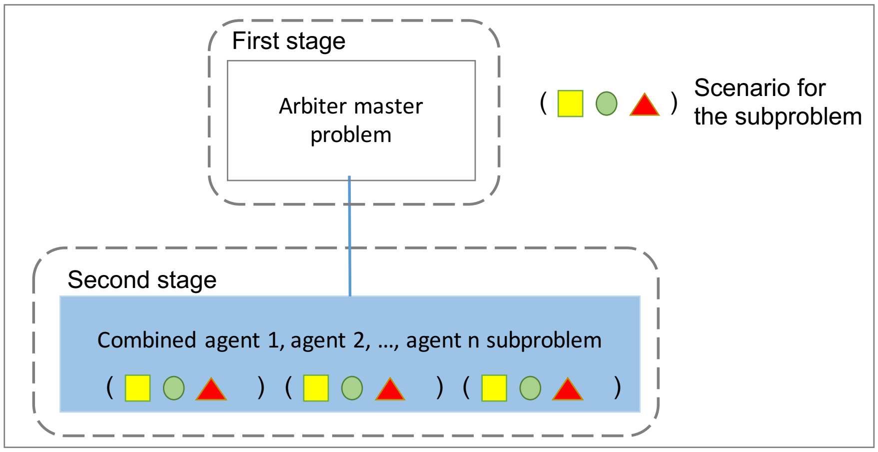

(a) Decision structure of 2-SP

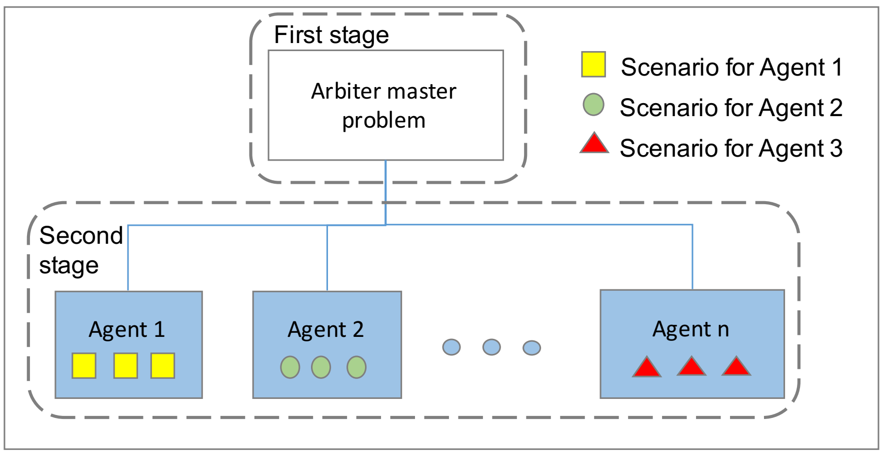

(b) Decision structure of MA-SP

Figure 2.2: Decision structures

subproblem (shown by separate and small shaded blue boxes in Figure 2.2b). In this case, every agent only observes scenarios from its stochastic process. The presence of multiple subproblems distinguishes our MA-SP from the classical formulation which only has one expected recourse function.

The classical 2-SPs are well studied in the literature. The uncertainty is represented using a set of scenarios and the expectation function is computed using the probability associated with each scenario. When the set of scenarios is not readily available, the expectation function is replaced by its sample average approximation

(SAA):

$$H(x) = \frac{1}{M}\sum_{i=1}^{M} h(x, \omega^i), \tag{2.15}$$

where M is the number of scenarios. Several algorithms, notably, Benders' decomposition [42], Dantzig-Wolfe decomposition [43], and progressive hedging [44], can be used to solve the SAA. These algorithms build lower bounding piecewise linear functions by solving a subproblem for each scenario from a set of scenarios selected a priori. For large-scale problems and/or problems with a large set of scenarios, such enumeration can prove to be computationally challenging. This is particularly the case in power systems with significant renewable integration. For such problems, sequential sampling-based bundling algorithms, such as 2-SD, have proven to be effective [45]. Recent work [46] has illustrated the advantages of sequential sampling over SAA for a wide range of applications. Motivated by these observations, we adopt a modified 2-SD solution approach to tackle our MA-SP.

Our solution approach, which we refer to as multi-agent stochastic decomposition (MA-SD), is an extension of 2-SD when multiple subproblems exist. The principal idea is to use a separate sample mean function to approximate the expected recourse function for each agent in (2.2):

$$H_n^k(x) = \frac{1}{k}\sum_{j\in\Omega_n^k} h_n(x, \omega_n^j) \qquad \forall n \in \mathcal{N}. \tag{2.16}$$

Note that the above sample mean is based on the current set of observations Ω_n^k. In any iteration k, these sample mean functions are updated by sequentially sampling scenarios (ω_n^k) from their respective stochastic processes and updating the observation set Ω_n^k. For the current arbiter decision x^k and newly sampled observation ω_n^k, the subproblem for agent-n is solved. Let π_n^{kk} denote the corresponding optimal dual solution. This solution is added to the set of previously encountered dual solutions, Π_n^k. For the remaining observations $\omega_n^j \in \Omega_n^k$, a dual solution π_n^{kj} is identified in Π_n^k, which provides the best lower bound at x^k. Using these dual solutions $\{\pi_n^{kj}\}_{j=1}^k$, we compute a lower bounding affine function for the k^{th} sample mean function $H_n^k(x)$:

$$H_n^k(x) \geq \underbrace{\frac{1}{k}\sum_{j=1}^{k}(\pi_n^{kj})^\top[r_n(\omega_n^j) - T_n(\omega_n^j)x]}_{:=\ \ell_n^k(x,\Omega_n^k)}. \tag{2.17}$$

Note that $H_n^k(x)$ approaches the expectation function as $k \to \infty$. Further, the affine function ℓ_n^j computed in iteration $j(< k)$ is a lower bound for H_n^j, and not necessarily for H_n^k.

Therefore, the previously generated affine functions are updated by multiplying ℓ_n^j by the factor $\frac{j}{k}$. Using these, the piecewise linear approximation [47] of the expected recourse function of agent n is given by:

$$L_n^k(x) = \max_{j=1,\ldots,k}\left\{\frac{j}{k} \times \ell_n^j(x, \Omega_n^k)\right\}. \tag{2.18}$$

Approximations of (2.18) are weighted and aggregated across all agents to form the first-stage problem, which is given by

$$\min\ \{c^\top x + \sum_{n=1}^{N} v_n L_n^k(x) + \frac{\sigma^k}{2}||x - \hat{x}^k||^2\ |x \in \mathcal{X}\}, \tag{2.19}$$

for a given parameter $\sigma^k > 0$. The optimal solution of the above problem x^{k+1} will be used in the subsequent iteration. Notice the use of a regularization term, centered around the incumbent solution $\hat{x}^k$, in the objective function. This term is included to stabilize our sampling-based approach. We refer the reader to [46] for a detailed exposition of incumbent updates and convergence properties of our approach. Figure 2.3 provides a flowchart representation of our algorithm.

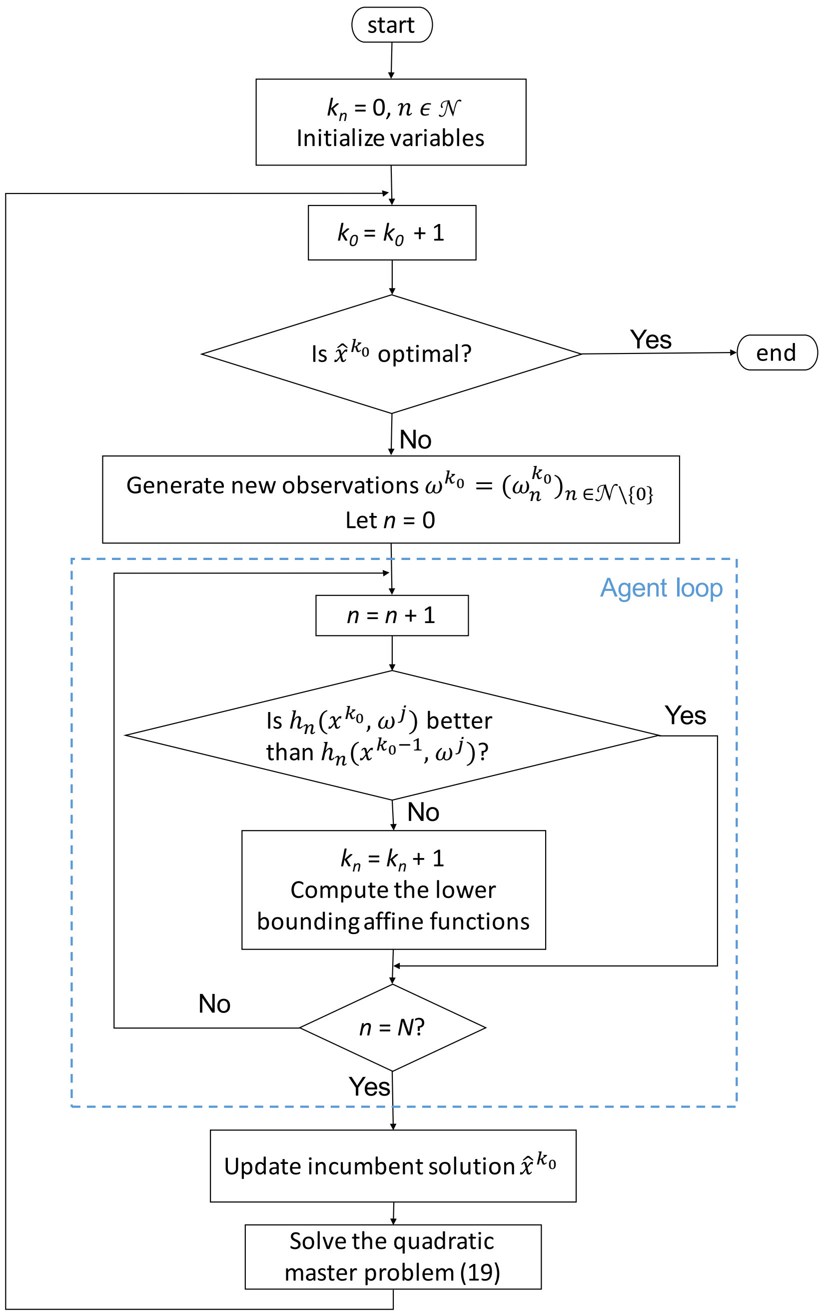

Figure 2.3: Flowchart of the MA-SD algorithm

Since each agent is exposed to an independent stochastic process, one should expect that different number of scenarios is required to characterize the uncertainty. Further, since the optimization problem is different at every agent, the number of extreme points (dual solutions) relevant to approximate the cost function is also different. In this regard, our stopping rules are based on in-sample as well as out-sample tests for stability of the observation set Ω_n^k and dual solution set Π_n^k. We refer the reader to [46] for more details. Due to the heterogeneous nature of decision processes, different agents might satisfy the stopping criteria at different iterations. Further, since the algorithm allows samples to be added sequentially during the optimization process, such a sequence can be obtained from state-of-the-art simulators that are often used by power system operators.

2.4 Computational Experiments

For our computational experiments, we used the WECC-240 data set obtained from [48]. The data consists of a detailed description of network topology, generator location, and capacity. In the data set, all 240 buses, which are located in the western part of the U.S., are originally partitioned into 21 areas (see Figure 2.4). We decomposed this data set into one main grid (shown in gray) connected to $N = 10$ MGs (shown in blue). The renewable generation data was extracted from the Western Wind and Solar Integration Study [49] based on the generators' geographical locations. This data was scaled to ensure 15% renewable penetration at each MG and used to build a model that provides a stream of simulated outcomes for renewable generation. We used the demand data in the WECC data set to create the instance, and the buses with flexible demand were selected randomly from the set of all load locations. We adopted the generation costs provided by [50]. Table 2.1 presents the details of this power system. In our computational study, we set the time horizon

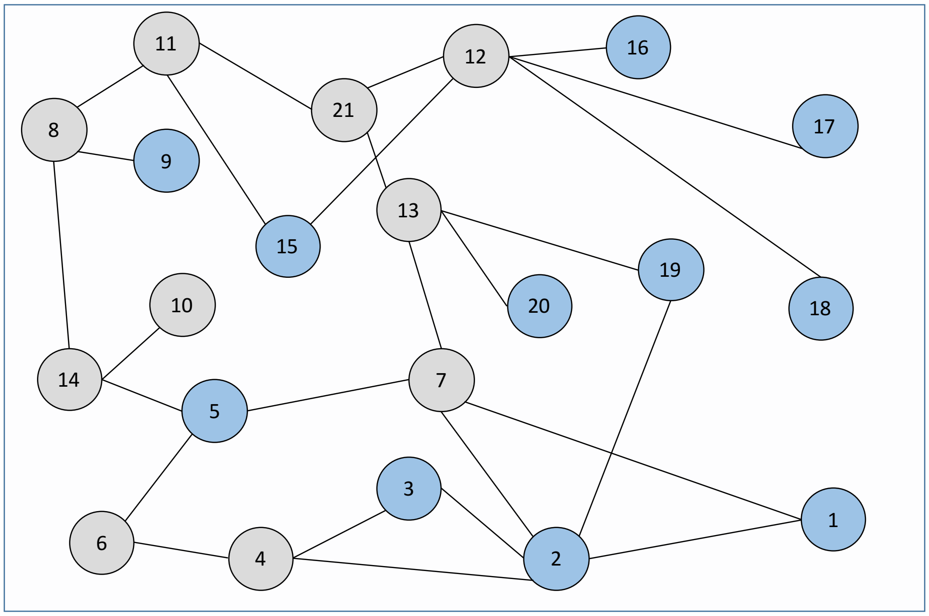

Figure 2.4: Network toplogy of WECC-240

$T = 24$ hours.

All algorithms were implemented in the C programming language on a 64-bit Intel core i7-4770 CPU @3.4GHz $\times$ 8 machine with 32 GB Memory. All linear and quadratic programs were solved using CPLEX callable subroutines. In all our experiments, we begin by using an optimization process to identify an optimal solution for the arbiter and the corresponding prediction value. Note that this prediction value is an estimate of the lower bound for the original optimization problem. This is followed by a verification phase where the arbiter's solution is fixed, and agents (MGs) subproblems are simulated using independent and identically distributed observations. The objective functions obtained are used to build a confidence interval (CI) of the upper bound estimate for each agent's expected recourse function. The CI for the arbiter objective function value is the aggregate based on the weighted sum of individual agent objective values.

Table 2.1: Details of the WECC-240 power system

Agent	Weights	# Buses	# Lines	# Generators		# Demand Locations		Energy Management Settings				
n	v_n	$\lvert\mathcal{B}_n\rvert$	$\lvert\mathcal{L}_n\rvert$	$\lvert\mathcal{G}_n\rvert$	$\lvert\mathcal{R}_n\rvert$	Fixed ($\lvert\mathcal{D}_n^f\rvert$)	Flexible ($\lvert\mathcal{D}_n^v\rvert$)	$\lvert\mathcal{V}_n^i\rvert$	$\lvert\mathcal{V}_n^h\rvert$	$\lvert\mathcal{V}_n^b\rvert$	$\lvert\mathcal{V}_n^p\rvert$	$\lvert\mathcal{V}_n^a\rvert$
0	1	81	100	24	0	40	0	0	0	0	0	0
1	1	21	24	15	3	7	6	2	1	1	1	1
2	1	2	1	2	1	0	1	0	0	0	0	1
3	1	15	18	2	1	5	7	2	1	1	2	1
4	1	14	17	3	1	3	7	2	1	0	2	2
5	1	29	36	5	1	12	11	3	1	2	3	2
6	1	33	41	16	7	5	10	3	1	1	2	3
7	1	6	5	5	1	0	3	2	0	0	0	1
8	1	29	36	17	4	11	10	2	3	1	3	1
9	1	5	4	3	1	1	2	0	0	0	1	1
10	1	5	5	3	1	1	3	1	0	0	1	1

2.4.1 Comparison of Decision Structures

We start by comparing our MA-SP with the classical 2-SP. While MA-SP includes a separate subproblem for each agent, the 2-SP considers a subproblem that aggregates together the decision processes of all agents. The uncertainty in 2-SP is captured by a single random vector, say $\tilde{\omega}_t = (\tilde{\omega}_{1t}, \tilde{\omega}_{2t}, \ldots, \tilde{\omega}_{Nt})$. The first-stage problem in both these formulations remains the same. We used the 2-SD algorithm to optimize the 2-SP. These results are summarized in Table 2.2.

Note that the total costs (i.e., prediction value) for MA-SP is within 0.5% of that predicted by the benchmark 2-SD algorithm. This indicates that the objective function value estimated by considering a separate sampling procedure for each agent is statistically similar to when a single stream of samples is used. The verification CIs, on the other hand, provide us with a tool to compare the solutions generated from the formulations. We accomplished this by testing the following hypothesis: the solutions from the two formulations are statistically indistinguishable. The p-value associated with this hypothesis test is 0.7008, which is greater than 0.05. It indicates that the hypothesis cannot be rejected at a 0.95 significance level.

The first column of Table 2.2 shows that solving an MA-SP requires a smaller number of iterations than solving a 2-SP (670 vs. 708). In 2-SP, the number of

Table 2.2: Comparison between 2-SP and MA-SP

Structure	# of optimization programs	Time per iter. (s)	Prediction value ($)	95% C.I.	p-value
2-SP	708	18.682	43,760,652	[43,499,527, 44,103,080]	-
MA-SP	670	9.849	43,951,145	[43,534,253, 44,252,131]	0.7008

scenarios (of random vector $\tilde{\omega}_t$) is equal to the number of optimization programs, while, for solving the MA-SP, the number of scenarios encountered by each agent (i.e., random variable $\tilde{\omega}_{nt}$) is different. We will discuss it in the following sub-section. The average time taken to complete an iteration of each algorithm is presented in Table 2.2 as well. Since MA-SP decomposes the subproblems into smaller linear programs, the computational requirements are lower when compared to 2-SP where a significantly larger linear program is solved. Therefore, the average time taken for an iteration in 2-SD is twice as much as MA-SD. The separation of sampling procedures and the computational advantage make the MA-SP setup suitable for parallel computing environments. We are currently working on an implementation suitable for such environments, and the results will be reported in future publications.

2.4.2 Comparison of Cut Formation Procedures

The expected recourse function for each agent is approximated using lower bounding affine functions as described in Section 2.3. These approximations are included in the master problem as linear functional constraints [51]. This implies that the size of the master problem grows by N (number of agents/MGs) in every iteration that increases the computational burden of solving quadratic programs. Alternatively, one may aggregate these affine functions as:

$$\bar{\alpha} = \sum_{n=1}^{N} v_n \alpha_n; \qquad \bar{\beta} = \sum_{n=1}^{N} v_n \beta_n, \tag{2.20}$$

where (α_n, β_n) are coefficients of individual affine functions for $n = 1, \ldots, N$, and $(\bar{\alpha}, \bar{\beta})$ are those for the aggregated affine function. This choice motivates the next set of experiments where we compare the MA-SD(m) and MA-SD(a) procedures. In MA-SD(m), N affine functions are added in every iteration, and a single aggregated function is added in MA-SD(a). The results of MA-SD(a) and MA-SD(m) are shown in Table 2.3 and Table 2.4, respectively.

These results indicate that, while the number of quadratic master programs solved is higher in the case of MA-SD(a) when compared to MA-SD(m), the corresponding running time is lower. This can be attributed to the larger size of the master problem in the MA-SD(m). As before, we can compare the prediction and verification values to establish the similarity between the two approaches. The difference in prediction values of the two approaches is around 0.3%. We also conducted a hypothesis test that there is no difference between the solutions obtained from these two algorithms. The p-value of 0.9751 (> 0.05) indicates that we cannot reject the null hypothesis of statistically indistinguishable arbiter solutions.

The results in the two tables showcase one of the principal features of our solution approach, viz. the distributed nature of our sequential sampling procedure. Since each agent is exposed to stochastic processes with different characteristics (mean, variance, etc.), the number of samples required to satisfactorily approximate the expected recourse function is also different. These numbers can be seen in the first column of Table 2.3 and Table 2.4 for each method, respectively. For sample-based stochastic programming models, it is not guaranteed that the prediction value falls within the verification CI. However, when it does, then the solutions can be accepted with greater confidence. The arbiter solution satisfies this condition as the aggregated prediction value falls within the verification CI for both methods proposed. (See the row corresponding to "master" in Table 2.3 and Table 2.4.) While this solution is statistically acceptable to the aggregated optimization problem, it might not be the case for individual agents (e.g., agent 4 in the MA-SD(a) method). Such behavior can be attributed to the fact that our approach seeks solutions that are optimal across all and not necessarily individual agents. In the remaining experiments, we will use

Table 2.3: Results of MA-SD(a)

Agents	# of optimization programs	Time per iter. (s)	Prediction value ($)	Mean	U.B. Estimate Std. dev.	95% C.I.
master	670	9.849	43,951,145	43,893,192	5,788,250	[43,534,253, 44,252,131]
0	369	0.012	0.007	0.007	0.000	[0.007, 0.007]
1	301	0.002	8,998,948	8,997,077	150,725	[8,987,730, 9,006,424]
2	475	0.002	8,755	8,749	694	[8,706, 8,792]
3	359	0.004	2,139,078	2,140,098	91,629	[2,134,416, 2,145,780]
4	343	0.004	2,076,822	1,994,509	946,845	[1,935,793, 2,053,224]
5	368	0.015	783,400	772,364	310,294	[753,122, 791,606]
6	275	0.014	4,263,634	4,205,003	2,863,423	[4,027,438, 4,382,569]
7	374	0.003	5,228,603	5,350,485	4,560,169	[5,067,701, 5,633,268]
8	265	0.006	6,692,126	6,665,261	1,822,699	[6,552,233, 6,778,290]
9	323	0.001	206,019	203,565	101,432	[197,275, 209,855]
10	351	0.002	645,443	640,605	220,237	[626,947, 654,262]

Table 2.4: Results of MA-SD(m)

Agents	# of optimization programs	Time per iter. (s)	Prediction value ($)	Mean	U.B. Estimate Std. dev.	95% C.I.
master	435	15.957	44,066,906	43,885,109	5,796,994	[43,525,628, 44,244,591]
0	311	0.012	0.004	0.004	0.000	[0.004,0.004]
1	279	0.002	8,657,521	8,654,370	142,600	[8,645,527, 8,663,213]
2	433	0.002	8,824	8,790	723	[8,745, 8,834]
3	375	0.003	2,144,479	2,146,895	98,548	[2,140,784, 2,153,006]
4	346	0.004	2,053,008	2,008,981	958,127	[1,949,566, 2,068,396]
5	393	0.019	800,002	774,888	311,272	[755,585, 794,190]
6	267	0.017	4,426,207	4,213,061	2,870,708	[4,035,044, 4,391,078]
7	314	0.002	5,173,337	5,341,604	4,560,194	[5,058,819, 5,624,389]
8	263	0.007	7,025,171	6,965,143	1,830,957	[6,851,602, 7,078,684]
9	317	0.001	197,412	192,457	92,595	[186,715, 198,199]
10	281	0.001	648,653	646,629	222,103	[632,856, 660,402]

MA-SD(a) as our method of choice to solve MA-SPs.

2.4.3 Study the Impacts of the Network Constraints

The formulation presented in Section 2.2 considers a DC approximation of the power flow constraints (2.10). Power flow on line (i, j) is bounded by the line capacity $[p_{nij}^{min}, p_{nij}^{max}]$. In order to study the impact of these constraints, we created instances without power flows ("NoNetwork"), uncapacitated power flows ("Uncapacitated"), and capacitated power flows ("Capacitated"). In the "NoNetwork" instance, system-wide power balance was ensured by including:

$$\sum_{j \in \mathcal{G}_n} g_{njt} = \sum_{j \in \mathcal{D}_n \bigcup \mathcal{R}_n} \partial \bar{D}_{njt} - \sum_{(i,j) \in \mathcal{I}_n} b_{ijt} \quad \forall t \in \mathcal{T}_n, \tag{2.21}$$

where $\partial \bar{D}_{njt}$ is the net demand computed using customer demand ($\mathcal{D}_n$) and renewable generation ($\mathcal{R}_n$) in all agents $n \in \mathcal{N}$. The results are shown in Table 2.5. Since the "NoNetwork" and "Uncapacitated" instances are relaxations of the original problem, the total cost is lower than the "Capacitated" instance. Moreover, the solution obtained for "Capacitated" is significantly different from the other instances (indicated by low p-value). It is interesting to notice that the solutions and values from "NoNetwork" and "Uncapacitated" instances are statistically indifferent. This indicates that the capacity on power flows is more critical than the power flow approximation (2.12), at least for our data set.

2.4.4 Energy Management Study

The formulation of the power system presented in Section 2.2 permitted different energy management settings to be included at agents. A main feature of these settings was the flexibility to schedule demand in a way that reduces overall system costs by efficiently managing their schedule with availabilities of renewable resources. In order to quantify the cost savings, we designed an experiment to compare a system with/without such flexible demands. Our experiment used two small instances comprised of the main grid and agents 4, 9, and 10 (all without storage devices)—one instance has inflexible customer demands and the other instance allows flexibility. All renewable generation scenarios used in this experiment are from the same data set as before.

The prediction and verification results are summarized in Table 2.6. The prediction values indicate that incorporating flexibility in energy management systems helps to reap more benefits from renewable resources and thereby results in cost savings (7.9%) for the system. This decrease in cost can be attributed to an 2.7% reduction in the conventional generation and a 10.4% reduction in the total amount of energy sold by the main grid. Further, from Figure 2.5, we see that both the main grid and agents can reduce their total costs by allowing demands to be flexible. However, the cost reduction is more prominent in the main grid than individual agents.

2.4.5 Response of Flexible Demands

In this experiment, we study the response of flexible demands to fluctuations in renewable generation over the planning horizon. The optimal first-stage solution

Table 2.5: Solution results of various network constraints

Instances	Prediction value ($)	95% C.I.	p-value
NoNetwork	37,138,279	[36,930,348, 37,366,901]	-
Uncapacitated	37,132,967	[36,926,762, 37,363,174]	0.9815
Capacitated	43,951,145	[43,534,253, 44,252,131]	0

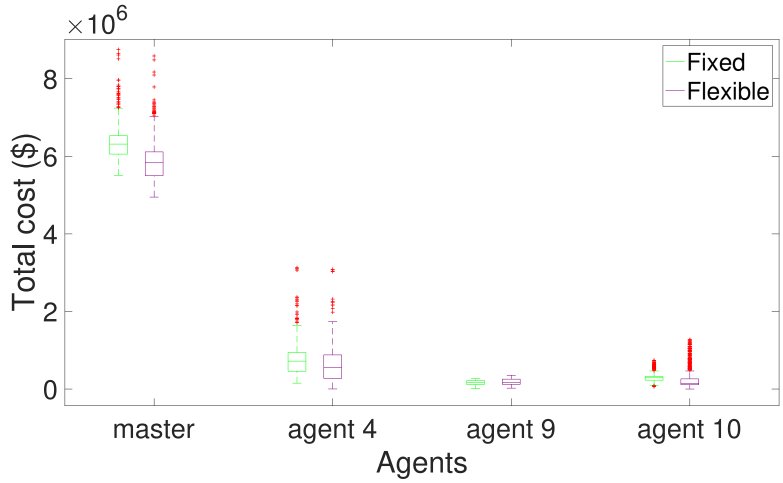

Figure 2.5: Objective values of the arbiter and agents

identified by MA-SD(a) is treated as an input to the individual agent problem. The decision process of each agent is simulated by solving an optimization problem using independent Monte-Carlo samples. Some key observations are discussed here.

Figure 2.6 shows the mean responses over 1000 samples for different settings during a day for agents 1, 3, and 6. The power purchased (which is a part of arbiter decisions), local conventional generation, and renewable generation are utilized to satisfy both flexible and fixed demand of an agent. During time window [0, 9], the requirements of industrial facilities dominate the power consumption and drive a high level of local conventional generation for all the three agents. In time period 10, when the industrial facilities stop operating, the local conventional generation reduces dramatically while the purchased power increases for agents 1 and 3 only.

Table 2.6: Solution method comparison (Fixed and Flexible)

Instances	Prediction Value($)	Conventional Generation (MW)	Selling Power (MW)	95% C.I.
Fixed	6,360,378	412,471	108,236	[6,316,083, 6,364,164]
Flexible	4,879,788	376,211	71,986	[4,818,633, 4,867,403]

Another interesting observation from Figure 2.6 is that industrial and home appliances demand realization trends complement one another. For example, when industrial demand decreases at the end of time period 9, the demand of home appliances is scheduled to be met. This behavior can be attributed to the fact that home appliances are allowed to operate over a longer time window as compared to industrial demand, which makes them more flexible. Similar complementary behavior was observed between conventional and renewable generation. We also can see from Figure 2.6 that excess renewable energy is stored (e.g., in $t \geq 10$ in agent 6) for future usage. While the realized power for the HVACs is constant for a majority of agents, this is not the case for agent 6 (see Figure 2.6). This is due to the presence of renewable resources with higher variability at this agent when compared to others. Both HVACs and storage devices help in smoothing this variability.

Further, we conducted sensitivity analysis of different type of flexible demands to investigate the effect of their variations on agents' total costs. The power system in this experiment comprises only one agent (agent 1) and the main grid. Our benchmark is to set all demands as fixed and no storage devices installed. Then we only allowed one type of energy management setting to be flexible. We conducted the same experiment for the rest of the settings. When storage devices are used, all other settings are not allowed to be flexible. The total costs for the main grid and agent 1 are shown in Figure 2.7. It was observed that the total cost savings are proportional to the power demand. This seems to be the case for industrial sectors in Figure 2.7. The figure also illustrates the role of storage devices in reducing total costs by moving energy from time periods of abundant generation to periods of low generation (also see Figure 2.6).

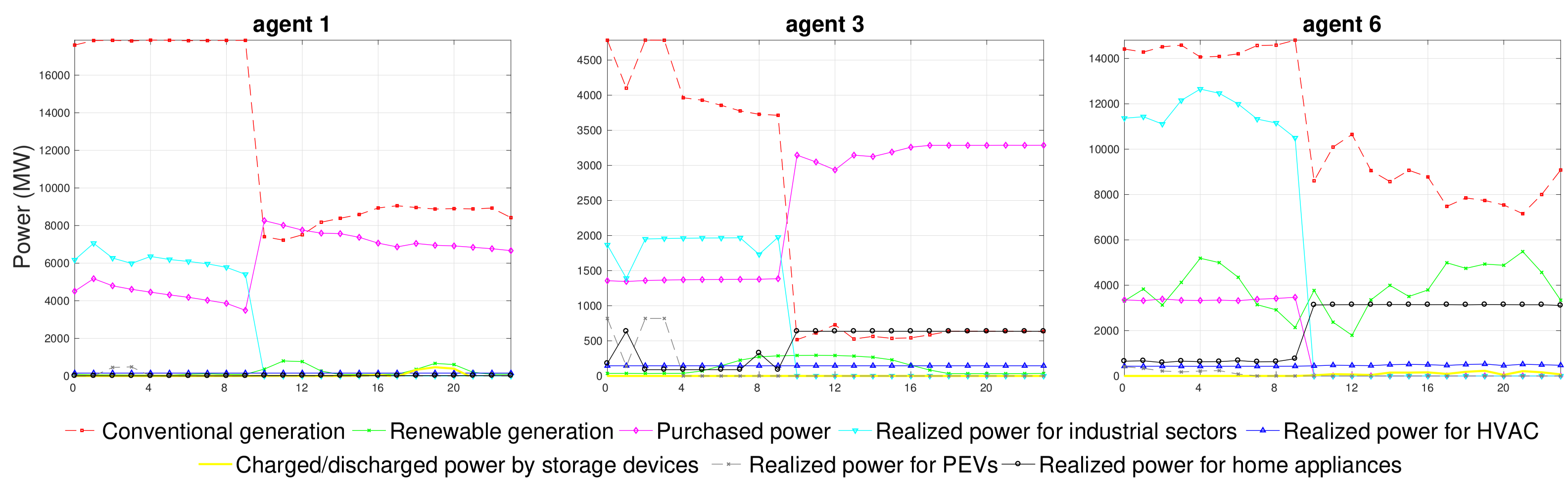

Figure 2.6: Mean agent response for different energy management settings

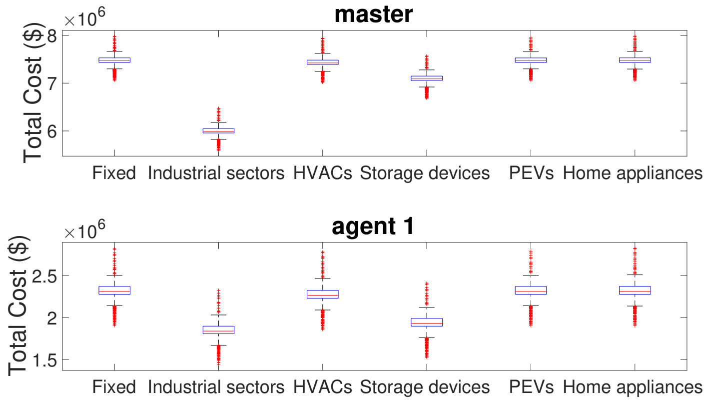

Figure 2.7: Sensitivity analysis of energy management settings

2.5 Conclusion

We presented a stochastic optimization framework that captures interactions between (a) a centralized arbiter in the main grid and (b) multiple agents with heterogeneous objectives and constraints in MGs that utilize various energy management settings. We investigated the response of each agent to intermittent renewable resources by extending the classical 2-SP model to include multiple subproblems. To the best of our knowledge, this is the first study that investigates multiple subproblems with heterogeneous decisions and stochastic processes in the second-stage. We developed stochastic decomposition-based algorithms to solve the proposed large-scale problem. The statistical results showed that our algorithm can provide reliable overall cost estimates to the proposed problem with 50% less running time as compared to the benchmark 2-SD approach. Our algorithm used two different approximation approaches: agent cuts (MA-SD(m)) and aggregated cuts (MA-SD(a)). Both these approaches yield statistical comparable results, but the aggregated approach is computationally more efficient. The results implemented with and without allowing flexible demands show that the total operational costs can be reduced significantly when customer demand is flexible by effective utilization of the renewable resources. Our experiments show that cost reductions are more prominent in the main grid than at individual agents. The sensitivity analysis reveals that the flexibility in the industrial sector has the potential to contribute the most towards the total cost reduction. The results also indicate storage devices play a critical role in cost reductions. While the inclusion of power flow equations increases the computational requirements, they are necessary to identify system congestion. This is highlighted by the increase in total cost when flow balance constraints are considered in the proposed MA-SP. Finally, we studied how the activities of these flexible demands fluctuate with variations of renewable generations during a day.

The structure of our algorithm involves solving several independent subproblems (corresponding to MGs). This structure is naturally fit for an implementation of distributed/parallel computing, which will be taken up as part of our future study. In a smart grid, MGs not only are buyers but also can sell power back to the main grid to increase utilization of renewable energy over the entire power system. Furthermore, they are allowed to make transactions with other MGs in the system as well. These features will also be addressed in our future work.

Chapter 3

Stochastic Optimization for Flow-shop Scheduling with On-site Renewable Energy Generation using a case in the United States

S. Wang, S. J. Mason, and H. Gangammanavar, "Stochastic optimization for flow-shop scheduling with on-site renewable energy generation using a case in the United States," Computers & Industrial Engineering, Vol. 149, 2020.

Nomenclature

Sets

B	set of ESSs; indexed by $i = 1, 2, \ldots \lvert B\rvert$
J	set of jobs; indexed by $j = 1, 2, \ldots \lvert J\rvert$
F	set of job families; indexed by $f, g = 1, 2, \ldots \lvert F\rvert$
M	set of machines; $m = 1, 2, \ldots \lvert M\rvert$

R	set of renewable generators; $r = 1, 2, \ldots \lvert R \rvert$
T	set of time periods; $t = 1, 2, \ldots \lvert T \rvert$

Parameters

w_j	weight (priority) of job $j \in J$
l	length of a time slot [h]
p_{mj}	processing time of job $j \in J$ on machine $m \in M$ [h]
s_{fg}	setup time between job family $f \in F$ and $g \in F$ [h]
b_i^{min}	minimum charging/discharging rate of ESS $i \in B$ [kW]
b_i^{max}	maximum charging/discharging rate of ESS $i \in B$ [kW]
E_i^{min}	minimum energy level of ESS $i \in B$ [kWh]
E_i^{max}	maximum energy level of ESS $i \in B$ [kWh]
q_{mf}^z	unit power consumed by idling at family $f \in F$ on machine $m \in M$ [kW]
q_{mfg}^l	unit power consumed by a setup between job family $f \in F$ and $g \in F$ on machine $m \in M$ [kW]
c_t^d	unit energy purchasing cost in time period $t \in T$ [$/kWh]
c_t^u	unit energy selling price in time period $t \in T$ [$/kWh]
c_{it}^E	unit energy storage cost of ESS $i \in B$ in time period $t \in T$ [$/kWh]
ρ_t	$= 1$ if the manufacturing plant is allowed to feed power into the electricity grid during time period $t \in T$ when the selling price $c_t^u \leq$ purchasing price c_t^d, 0 otherwise
$\tilde{\omega}_{rt}$	random variable, power generated by renewable generator r at time $t \in T$ [kW]

Decision Variables

x_{mjt}	$= 1$ if job $j \in J$ is started on machine $m \in M$ at the beginning of time period $t \in T$; otherwise $= 0$

y_{mjt}	$= 1$ if job $j \in J$ is processed on machine $m \in M$ during time period $t \in T$; otherwise $= 0$
z_{mft}	$= 1$ if machine $m \in M$ is idle at job family $f \in F$ during time period $[t, t+1)$; otherwise $= 0$
v_{mfgt}	$= 1$ if machine $m \in M$ starts to make a setup operation for changing job family $f \in F$ to job family $g \in F$ at the beginning of time period $t \in T$; otherwise $= 0$
o_{mfgt}	$= 1$ if machine $m \in M$ is doing a setup for changing job family $f \in F$ to job family $g \in F$ during time period $t \in T$; otherwise $= 0$
d_t	power purchased from the grid in time period $t \in T$ [kW]
u_t	power sold to the grid in time period $t \in T$ [kW]
b_{it}	ESS charging/discharging rate during time period $t \in T$ [kW]. When b_{it} is positive, the ESS $i \in B$ is in charging status; otherwise, it is in discharging status
E_{it}	Energy state of ESS $i \in B$ in time period $t \in T$ [kWh]
a_t	underutilized renewable generation in time period $t \in T$ [kW]

Acronyms and Abbreviations

GHG	greenhouse gas
TOU	time-of-use
ECA	energy-cost-aware
ESS	energy storage system
MILP	mixed-integer linear program
ESF	extensive scenario formulation
TWCT	total weighted completion time
EC	energy cost

2-SP	two-stage stochastic program
SAA	sample average approximation
CI	confidence interval

3.1 Introduction

Today, protecting the environment is one of the most critical issues faced by citizens of the world. While, with the development of economic globalization, global demand for almost any type of product is continuously growing. As a result, the industrial sector has a high energy demand to satisfy production demand. For example, the industrial sector accounted for 32% of total U.S. energy consumption in 2018 [52] according to a report from the U.S. Energy Information Administration. The main energy sources used by the sector are natural gas, petroleum, electricity, renewable sources, and coal. Although the share of renewable sources has been increasing over the past 60 years, it is still less than 10% of all energy sources. As we know, non-renewable energy sources can cause environmental issues, especially the emission of greenhouse gas (GHG). Another U.S. Energy Information Administration report claims that the industrial sector consumes about 25% of all electricity in use [53]. To meet excessive peak electricity demands and decrease GHG emissions, load shifting and utilizing renewable resources are under consideration by Governments, society, and industry. Load shifting, which is also known as demand response, allows to curtail or shift energy demands in response to economic incentives. In a smart grid, any kind of end-use customer can gain benefits from adopting a demand response program. While, industrial sector has the potential to take more advantage of cost reduction by utilizing demand response [54].

Time-of-use (TOU) electricity pricing schemes vary prices during the day.

Higher (lower) costs are charged during peak (off-peak) demand hours. TOU pricing schemes are used by utilities to motivate manufacturing plants to reduce consumption at peak times by shifting energy use from peak hours to off-peak hours. This shifting activity, which is referred to as demand response, can increase time-related scheduling objectives. Energy-cost-aware (ECA) manufacturing is a way to utilize demand response. Its objective is to minimize energy costs at the operational level by determining optimal job scheduling and/or lot-sizing while considering time-varying electricity prices [55]. Using on-site electricity generators, some industrial facilities produce electricity for use. In an ECA manufacturing system, industrial facilities also can sell some of the electricity that they generate back to the power grid for compensation.

An effective way to reduce GHG emissions is to utilize environment-friendly renewable energy resources, which have received significant research attention in recent years. Renewable resources are the fastest growing among all energy resources, with their consumption expected to increase by an average 2.3% per year between 2015 and 2040, according to the U.S. Energy Information Administration [56]. Moreover, some governments and organizations such as RE100 have committed to encouraging businesses to consider using 100% renewable power. According to its website, UPS invested $18 million in on-site solar panels, which expanded UPS's solar power generating capacity by 10 megawatts in 2017. Further, it is estimated that on-site wind energy resource development is feasible for about 44% of the continental U.S.'s buildings, according to a report by the National Renewable Energy Laboratory [57].

Unfortunately, the availability of wind and solar energy, which are two significant renewable energy resources, is uncertain, as it fluctuates with weather variations. Generation can vary at different times over a day and at the same time period over different days. Properly addressing the uncertainties inherent in renewable energy resources can mitigate potential scheduling solution inaccuracies. Further, developing effective strategies for handling the intermittent nature of renewable energy resources can improve the effectiveness of renewable energy utilization in production environments. To mitigate renewable energy availability challenges, energy storage systems (ESSs) are utilized to store intermittent renewable energy and use it when needed.

To the best of our knowledge, Liu [58] presents the first study that integrates renewable energy supply into production scheduling while considering the uncertainty of renewable energy availability using interval number theory. Unfortunately, little research has been done since that simultaneously considers both ECA production scheduling and the utilization of uncertain renewable resources for energy generation. Given this motivation, we study a flow shop scheduling problem with sequence-dependent setups under a TOU pricing scheme. Power purchased from the main grid, generated by grid-connected on-site renewable generators such as wind turbines and solar panels, and discharged from ESSs are available energy sources for the manufacturing process under study. Energy consumption is machine status-related, as job processing, production setups, and machine idling consume different amounts of energy.

Figure 3.1 describes the methodological approaches used in this research. We first formulate a two-stage, bi-objective stochastic ECA problem. Then the problem is solved through a ϵ-constraint framework with L-shaped method. Finally, experiments were conducted to illustrate the performance of our proposed algorithm and its effectiveness in realizing energy-related objectives in manufacturing. The main contributions of this research are threefold: (1) we study an ECA problem that integrates an energy procurement problem with a flow shop scheduling problem to minimize total weighted completion time and energy costs simultaneously by determining optimal job schedules and energy supply decisions; (2) we develop a two-stage,

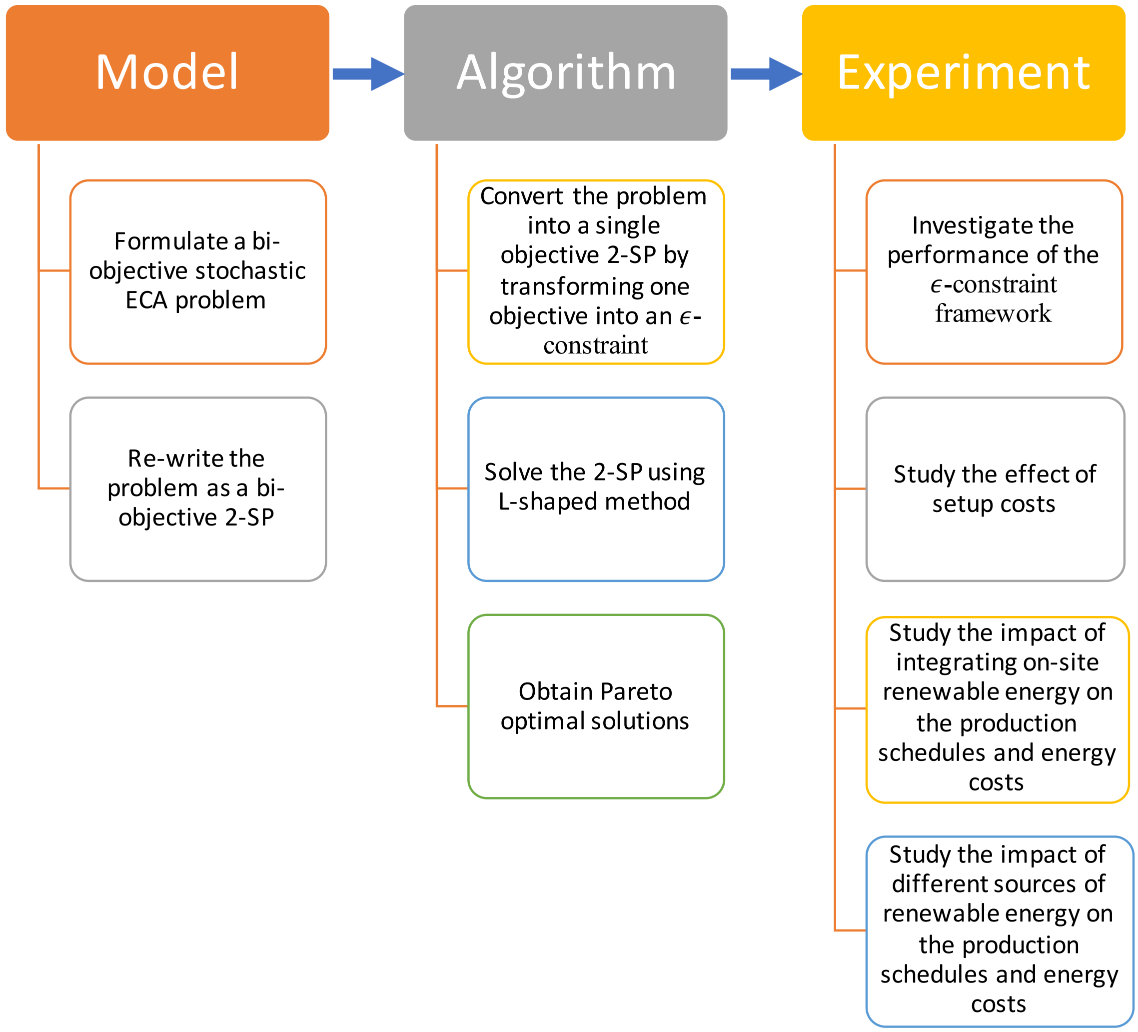

Figure 3.1: Flow chart of methodological approaches performed in this research

multi-objective stochastic problem for the ECA problem. In the first stage, we propose a time-indexed, mixed-integer linear program (MILP) which captures several practical features of the flow shop scheduling problem. The second stage determines the energy transactions between the manufacturing plant and the power grid in the context of uncertain renewable energy and ESSs under a TOU pricing scheme; (3) we conduct a case study to investigate the performance of our algorithm, the effects of setups on energy cost, and demonstrate the potential benefits of utilizing on-site renewable resources and ESSs.

The rest of the paper is organized as follows. After the current literature is reviewed in Section 3.2, our mathematical model is presented in Section 3.3. Then, two-stage, multi-objective decomposition algorithms are implemented in Section 3.4, followed by a discussion of our computational experiments in Section 3.5 Finally, we offer conclusions and future research directions in Section 3.6.

3.2 Literature Review

As many areas of the world are facing environmental issues surrounding the consumption of fossil fuels and concomitant GHG emissions, efforts to make production scheduling sustainable have become a key focus for many companies. Lots of literature on energy-aware production scheduling has evolved in recent years. Giret *et al.* [59], Biel and Glock [60], and Gahm *et al.* [61] present a comprehensive review of this research stream. Giret *et al.* [59] review the existing literature on sustainable scheduling and focus on environmental and economic development. Biel and Glock [60] provide a survey on decision support models for energy-efficient production planning. Gahm *et al.* [61] develop a framework for energy-efficient scheduling and classify the literature into three aspects–energetic coverage, energy supply, and energy demand. Gahm *et al.* [61] state that machine processing states and job-related features both impact energy consumption during production operations, non-processing states such as machine idling, system on/off, and setups can also affect energy consumption requirements.

Yildirim and Mouzon [62] propose a multi-objective framework for a single machine scheduling problem to minimize both energy consumption and job completion time by turning off the machine instead of leaving it idle when not in use. Liu *et al.* [63] study a flow shop scheduling problem with state-dependent setup times to minimize energy consumption and tardiness penalties. After introducing fuzzy set theory to describe the uncertainty of processing time and due dates, an improved hybrid genetic algorithm is developed for solving the problem.

Luo *et al.* [64] investigate a hybrid flow shop scheduling problem under a four-period TOU pricing scheme to minimize makespan and power consumption. Their experimental results show that increasing the length of each TOU period can reduce electricity costs without affecting makespan. Similarly, under a TOU tariff, Ding *et al.* [65] propose a time-interval-based mixed-integer, linear model and a column generation heuristic for a parallel machine scheduling problem to minimize electricity costs while keeping the makespan within a given production deadline. Understanding the tradeoff between electricity costs and makespan can provide insights for management to help determine the maximum acceptable production time under TOU pricing schemes.

Moon and Park [66] investigate production scheduling problems integrated with on-site renewable generation, fuel cells, and ESSs. They propose a model with two subproblems for a flexible job shop to minimize the sum of makespan-related production costs, the cost of purchasing power from the grid, the cost of distributed generations, and the cost of an ESS under a TOU pricing scheme. The first subproblem is a production scheduling problem with a given energy schedule, while the second subproblem is an energy scheduling problem for a given flexible job shop. By solving these two subproblems alternately and repeatedly, a near-optimal solution is found. In their model, Moon and Park [66] assume that the minimum and maximum amounts of renewable energy available for each time period within the planning horizon are known in advance. Then the amount of energy generated for a given time period is determined by the model. Zhai *et al.* [67], who study a flow shop scheduling problem in the context of a real-time pricing scheme, also consider on-site renewable generation. Time series models are used to forecast hourly wind speeds and electricity prices, which increase data accuracy as compared to using the fixed intervals adopted by Moon and Park [66]. After obtaining forecast data, hourly wind speeds and electricity prices are fed into a manufacturing scheduling model to minimize energy costs. Unfortunately, this procedure requires that all data is predetermined without any consideration of uncertainty. Similarly, Zhang *et al.* [68] investigate the effect of on-site photovoltaic and ESSs on a flow shop under a TOU pricing scheme. However, the uncertainty of solar generation is not considered in the study.

Liu [58] presents a mathematical model for a single-machine scheduling problem integrated with renewable generation and an ESS. Liu [58] represents the uncertainty of renewable energy resources by using interval number theory. The energy generated by renewable energy resources during each time period is bounded by an interval and the interval boundaries are randomly generated from a uniform distribution. The author assumes that the plant will purchase any power needed from the main grid if the renewable energy stored in batteries runs out in any time period. Two models are considered: 1) simultaneously minimizing total weighted flow time and GHG emissions using a lexicographic-weighted Tchebycheff method and 2) minimizing total weighted flow time by considering a GHG emission constraint.

Biel *et al.* [69] propose a two-stage stochastic optimization procedure for a flow shop scheduling problem with on-site wind power under a TOU pricing scheme to minimize total weighted flow time and energy costs. In the first stage, a bi-objective MILP is used to evaluate a number of generated wind power scenarios which form an extensive scenario formulation (ESF). A weighted sum algorithm is used to tackle multiple objective functions. Then, based on real-time wind power data, energy supply decisions are adjusted in the second stage. Fazli Khalaf and Wang [70] propose a two-stage stochastic MILP for a flow shop problem with on-site renewable resources and ESS under day-ahead and real-time electricity pricing schemes. The first stage determines job schedules and minimizes energy purchase cost procured from the day-ahead plan by considering forecasted renewable energy generation, while the second stage compensates for the mismatch between forecasted and actual renewable energy and minimizes energy costs under a real-time pricing scheme.

As Table 3.1 shown, only a few research studies have considered ECA production scheduling with stochastic renewable energy sources simultaneously. Further, sequence-dependent setups, which occur when production switches between different job families Wang *et al.* [71], have been ignored in the literature. These setups not only affect time-related objectives but also affect energy costs and demand requirements [72]. Motivated by these gaps in the literature, the main goal of our study is to examine these important topics.

3.3 Problem Formulation

Consider a flow shop comprised of $|M|$ production machines. A set of jobs J of varying weights (priorities) w_j is released at the beginning of the time horizon of interest. Each job $j \in J$ must be processed with processing time p_{mj} on each machine $m \in M$ sequentially. A sequence-dependent setup time is required for changeovers when the job family changes from $f \in F$ to $g \in F \setminus \{f\}$ on any machine. Different machine statuses (i.e., job processing, setup, and idling) consume different amounts of energy. The energy required for operating machines can be purchased from the main power grid, generated by on-site renewable generators, and/or discharged from ESSs. On-site renewable generation can be used to run production, charge ESSs, and/or be sold to the main grid for compensation (Figure 3.2). In our study, electricity prices are governed by a TOU pricing scheme containing three different electricity

Table 3.1: Summary of reviewed ECA production scheduling problems

Study	Machine environment	Machine Status	RES	Stochastic	ESS
Yildirim and Mouzon (2012)	Single machine	Processing, idling, and ON/OFF	-	-	-
Liu et al. (2017)	Flow shop	Processing, idling, state-dependent setup, and ON/OFF	-	-	-
Luo et al. (2013)	Hybrid flow shop	Processing and idling	-	-	-
Ding et al. (2016)	Parallel machine	Processing	-	-	-
Moon and Park (2014)	Flexible job shop	Processing and idling (no cost)	Yes	No	Yes
Zhai et al. (2017)	Flow shop	Processing, idling, and ON/OFF	Wind	No	-
Zhang et al., (2017)	Hybrid flow shop	Processing	Solar	No	Yes
Liu (2016)	Single machine	Processing	Yes	Yes	Yes
Biel et al. (2018)	Flow shop	Processing	Wind	Yes	-
Fazli Khalaf and Wang (2018)	Flow shop	Processing	Wind & Solar	Yes	Yes

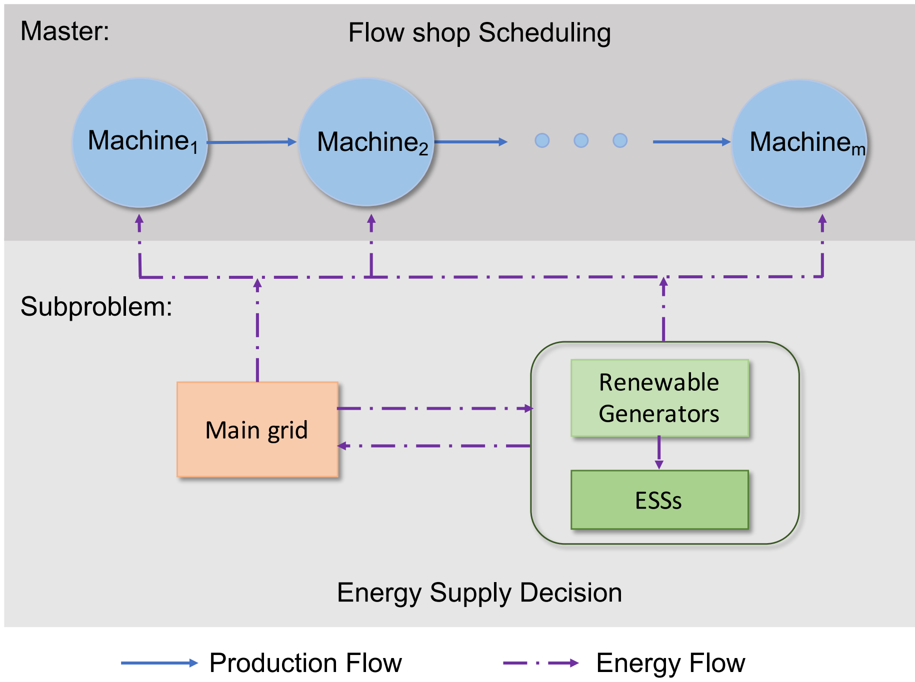

Figure 3.2: A flow shop system with production and energy flow

rates each day: peak load, mid-load, and off-peak load, depending on the time of day. We consider two major decisions simultaneously: (1) assigning jobs to machines and determining machine statuses in each time period $t \in T$ to minimize total weighted completion time (TWCT) and (2) determining energy transactions between the main grid, the manufacturing plant, and operating ESSs to minimize energy cost (EC).

3.3.1 Model

Apart form what has already been stated, we further make the following assumptions for our problem:

1. All machines and jobs are available at the beginning of our time horizon T;

2. All jobs are required to be processed completely by the end of the time horizon T;

3. The processing order of jobs can differ among flowshop stages;

4. Each machine can process only one job at a time;

5. Each machine must complete job j before undergoing a setup or processing another job $j' \in J \setminus \{j\}$;

Using the above notation, the objective function and constraints of the proposed MILP model for flow shop scheduling and energy supply decisions are given as follows:

$$\min \text{TWCT} = \sum_{j \in J} w_j \sum_{t \in T} (tl + p_{|M|j} - l) x_{|M|jt} \tag{3.1}$$

$$\min \text{EC} = \sum_{t \in T} (c_t^d d_t l + \sum_{i \in B} c_{it}^E E_{it} - c_t^u u_t \rho_t l) \tag{3.2}$$

Subject to

$$y_{m-1,jt} + y_{mjt} \leq 1 \qquad \forall m \in M \setminus \{1\}, j \in J, t \in T, \tag{3.3}$$

$$\sum_{\tau=1}^{t} x_{m-1,j\tau} \geq \sum_{\tau=1}^{t} x_{mj\tau} \qquad \forall m \in M \setminus \{1\}, j \in J, t \in T, \tag{3.4}$$

$$\sum_{\tau \geq 1}^{\tau \leq |T| - \frac{p_{mj}}{l} + 1} x_{mjt} = 1 \qquad \forall m \in M, j \in J, \tag{3.5}$$

$$y_{mjt} + \sum_{k \in J \setminus \{j\}} x_{mkt} \leq 1 \qquad \forall m \in M, j \in J, t \in T \tag{3.6}$$

$$l \sum_{\tau \geq t}^{\tau \leq t + \frac{p_{mj}}{l} - 1} y_{mj\tau} \geq x_{mjt} \cdot p_{mj} \qquad \forall m \in M, j \in J, t \in \{1, 2, \ldots, |T| - \frac{p_{mj}}{l} + 1\}, \tag{3.7}$$

$$l \sum_{\tau \geq t}^{\tau \leq t + \frac{s_{fg}}{l} - 1} o_{mfg\tau} \geq v_{mfgt} \cdot s_{fg} \qquad \forall m \in M, f \in F, g \in F \setminus \{g\}, t \in T, \tag{3.8}$$

$$\sum_{j\in J} y_{mjt} + \sum_{f\in F} z_{mft} + \sum_{k\in F}\sum_{h\in F\setminus\{k\}} \sum_{\tau>t-\frac{s_{kh}}{l}}^{\tau\leq t} v_{mkh\tau} = 1 \qquad \forall m \in M, t \in T, \tag{3.9}$$

$$z_{mft-1} + \sum_{F_j=f} y_{mj,t-1} + \sum_{g\in F\setminus\{f\}} v_{mgf,t-\frac{s_{gf}}{l}} = z_{mft} + \sum_{F_j=f} y_{mjt} +$$

$$\sum_{g\in F\setminus\{f\}} v_{mfgt} \qquad \forall m \in M, f \in F, t \in T \setminus \{1\}. \tag{3.10}$$

$$d_t - u_t\rho_t - \sum_{i\in B} b_{it} - a_t = \sum_{m\in M}\sum_{j\in J} y_{mjt} q^y_{mj} + \sum_{m\in M}\sum_{f\in F} z_{mft} q^z_{mf}$$

$$+ \sum_{m\in M}\sum_{f,g\in F: f\neq g} o_{mfgt} q^l_{mfg} - \sum_{r\in R} \tilde{\omega}_{rt} \qquad \forall t \in T, \tag{3.11}$$

$$b_i^{min} \leq b_{it} \leq b_i^{max} \qquad \forall i \in B, t \in T, \tag{3.12}$$

$$E_{it} = E_{i,t-1} + b_{it} l \qquad \forall i \in B, t \in T, \tag{3.13}$$

$$E_{it}^{min} \leq E_{it} \leq E_{it}^{max} \qquad \forall i \in B, t \in T, \tag{3.14}$$

$$u_t l \leq \sum_{r\in R} r_{rt} \qquad \forall t \in T, \tag{3.15}$$

$$x_{mjt}, y_{mjt}, z_{mft}, o_{mfgt}, v_{mfgt} \in \{0,1\} \qquad \forall m \in M, j \in J, f, g \in F, t \in T, \tag{3.16}$$

$$d_t, u_t, E_{it}, a_t \geq 0 \qquad \forall i \in B, t \in T, \tag{3.17}$$

$$b_{it} \text{ unrestricted} \qquad \forall i \in B, t \in T. \tag{3.18}$$

Equations (3.1) and (3.2) define the two objective functions that our model seeks to simultaneously minimize: (1) total weighted completion time and (2) energy costs, which we calculate as the cost of purchasing power from the grid plus the cost of storing energy in ESSs, minus the revenue generated from selling power back to the grid. Constraint set (3.3) ensures that job j can only be processed by one machine during any time period $t \in T$. Next, constraint set (3.4) guarantees that any job j must be processed on machine $(m-1)$ before it can be processed on machine m due to the flow shop environment under study. Constraint set (3.5) requires that any job

j can only be processed by each machine m once. Next, constraint set (3.6) ensures that any machine m can process job j only after job j is assigned to the machine. Any machine m cannot be interrupted once it starts processing a job, which is guaranteed by constraint set (3.7). Similarly, constraint set (3.8) ensures that a setup operation on machine m cannot be interrupted once it starts.

The constraints for representing the three machine states of interest are inspired by [73]. Constraint set (3.9) ensures that any machine can only be in exactly one state, job processing, setup, or idling, in each time period $t \in T$. Further, any change of machine state induces a setup operation (3.10). The power needed for running the flow shop's machines includes power purchased from the grid, power discharged from ESSs, and power generated by on-site renewable generators. Constraint set (3.11) is a power balance equation which specifies that the total available power should meet the total power demand at every time period. In (3.11), b_{it} is the charging/discharging rate of ESS $i \in B$ during time period $t \in T$. The value of b_{it} will be positive if the ESS $i \in B$ is charging; otherwise, it is in a discharging mode. These decisions are bounded by the charging/discharging rates of the ESS (3.12). Constraint set (3.13) is the system dynamics equations which specify the state of ESS $i \in B$ (see [54] for details). In (3.13), the initial state E_{i0} is assumed to be given. Constraint set (3.14) ensures that the state of ESS $i \in B$ is always between its lower and upper bounds. The quantity of renewable generation determines the upper bound of the power sold to the main grid (3.15). Finally, constraint sets (3.16) - (3.18) provide variable types and limits on the decision variables in our model.

3.3.2 Formulation of the Two-stage Stochastic Programming Model

The proposed scheduling and energy supply problem can be written as a two-stage stochastic program (2-SP) to model the stochastic nature of on-site renewable energy resources. Since scheduling decisions are made prior to the realization of renewable energy availability, they are non-anticipative in nature [1]. We succinctly use a single decision vector $x \in \mathcal{X}$ to collectively denote scheduling variables x_{mjt}, y_{mjt}, z_{mft}, o_{mfgt} and v_{mfgt}, where $\mathcal{X}$ denotes the feasible set. Once scheduling decisions are made, energy supply requirements are informed by this decision vector and the realization of renewable generation ω of its stochastic process $\tilde{\omega}$. This allows us to write the entire model as:

$$\min \sum_{j \in J} w_j \sum_{t \in T} (tl + p_{|M|j} - l) x_{|M|jt} + \mathbb{E}\{h(x, \omega)\} \tag{3.19a}$$

$$\text{s.t. } (3.3) – (3.10) \text{ and } (3.16),$$

where the recourse function $h(x, \omega)$ is given by:

$$h(x, \omega) = \min \sum_{t \in T} (c_t^d d_t - c_t^u u_t + \sum_{i \in B} c_{it}^E E_{it}) \tag{3.19b}$$

$$\text{s.t. } (3.11) – (3.15), (3.17), \text{and } (3.18).$$

According to the general formulation of a stochastic problem [1], problem (3.19a) is commonly referred to as the master problem, while problem (3.19b) is known as the subproblem. Note that the decision variables in the master problem (3.19a) are binary variables, while the decision variables in subproblem (3.19b) are continuous. While first-stage decisions affect the right-hand side of equation (3.11) (renewable generation), the recourse matrix characterized by the left-hand side in equation (3.11) and the transfer matrix characterized by the right-hand side of equation (3.11) are independent of uncertainty. Therefore, the above formulation is a 2-SP with fixed recourse [1].

3.4 Two-Stage, Multi-Objective Stochastic Solution Scheme

Our problem is a bi-objective problem whose solution is described by a Pareto-optimal set, rather than a unique solution. In general, the resolution of multi-objective stochastic problems involves two kinds of transformations: transforming the multi-objective problem into a single-objective problem and converting the stochastic problem into its equivalent deterministic problem [74, 75]. Caballero *et al.* [76] classify the existing techniques for the solution of multi-objective stochastic problems according to the order in which transformations are carried out. The *multi-objective* approach first transforms the stochastic multi-objective problem into its equivalent multi-objective, deterministic problem. Alternatively, the *stochastic* approach transforms the stochastic multi-objective problem into a single-objective stochastic problem in the first step.

Multi-objective stochastic optimization approaches have been studied in various fields. Tricoire *et al.* [77] formulate a bi-objective stochastic covering tour problem using a sample average approximation (SAA) technique, which is then solved by a branch-and-cut method within an ϵ-constraint algorithm. Osorio *et al.* [78] provide an approach which combines the SAA method and the augmented ϵ-constraint algorithm. Biel *et al.* [69] propose a two-stage stochastic optimization framework for flow shop scheduling problems with on-site wind power. In the first stage, a bi-objective MILP is formulated via an ESF considering all generated wind power scenarios simultaneously. The bi-objective objective function is transformed into a single objective using a weighted sum approach. In the second stage, energy supply decisions are adjusted according to the realization of actual wind power. Compared to the ϵ-constraint algorithm, weighted sum approach has two main drawbacks [77]: (1) it is difficult for decision-makers to define weights for conflicting objectives a priori; and (2) it can only find supported solutions and missing other attractive candidates. So motivated by [79], our solution approach for solving the bi-objective stochastic problem adopts an ϵ-constraint framework to transform the multi-objective problem into a problem with only one objective. The L-shaped method is used to tackle the 2-SP. The details of ϵ-constraint framework and the L-shaped method described in the following subsections.

3.4.1 ϵ-constraint Framework

The ϵ-constraint algorithm [80] consists of transforming a multi-objective problem into a single objective problem. To do this, decision-makers must select one objective function to remain as the objective function and transform all others into constraints bounded by a set of parameters ϵ. These additional constraints are named as ϵ-constraints.

To enumerate all Pareto optimal solutions, the algorithm iteratively solves single-objective optimization problems for each value of the ϵ parameters. The formulation introduced in Section 3.3 has two objective functions: TWCT and EC. The discrete-time periods result in integer values of TWCT. If we convert TWCT into an ϵ-constraint, it is easy to change the value of parameter ϵ by one unit from one iteration to the next [79]. Therefore, for computational convenience, we choose EC as the main objective function and TWCT is transformed into an ϵ-constraint. By introducing these changes, the master problem (3.19a) can be reformulated as:

$$
\begin{aligned}
&\min \mathbb{E}\{h(x,\omega)\} \qquad (3.20)\\
&\text{s.t.} \sum_{j\in J} w_j \sum_{t\in T}(tl + p_{|M|j} - l)x_{|M|jt} \le \epsilon\\
&\qquad (3.3) - (3.10), (3.16).
\end{aligned}
$$

Note that the two-stage stochastic programming framework in problem (3.20) is maintained by converting TWCT to an ϵ-constraint.

Figure 3.3 shows a flow chart for the two decomposition algorithms integrated with the ϵ-constraint framework [79]. Given the negative correlation between our two objective functions (i.e., TWCT increases as EC decreases), the maximum (minimum) value of TWCT, which is denoted as b (a), is obtained when EC reaches its smallest (largest) value. Let V denote a set of paired objective functions EC and TWCT. We begin our algorithm by setting the value of parameter $\epsilon = b$. The ϵ value is decreased by one unit (δ) in each iteration. We call this an ϵ-iteration within which one pair of optimal solutions is obtained using our decomposition algorithms. Note that ϵ is an upper bound of TWCT, not the value of TWCT. The actual TWCT value can be calculated using the ϵ-constraint during each ϵ-iteration. The ϵ-iteration stops when $\epsilon = a$. Finally, the Pareto front is identified from the set V.

3.4.2 L-shaped Method

Classical 2-SPs are well studied in the literature and several algorithms have been proposed to analyze these problems. To achieve computational tractability, many of these methods represent uncertainty through a finite number of realizations

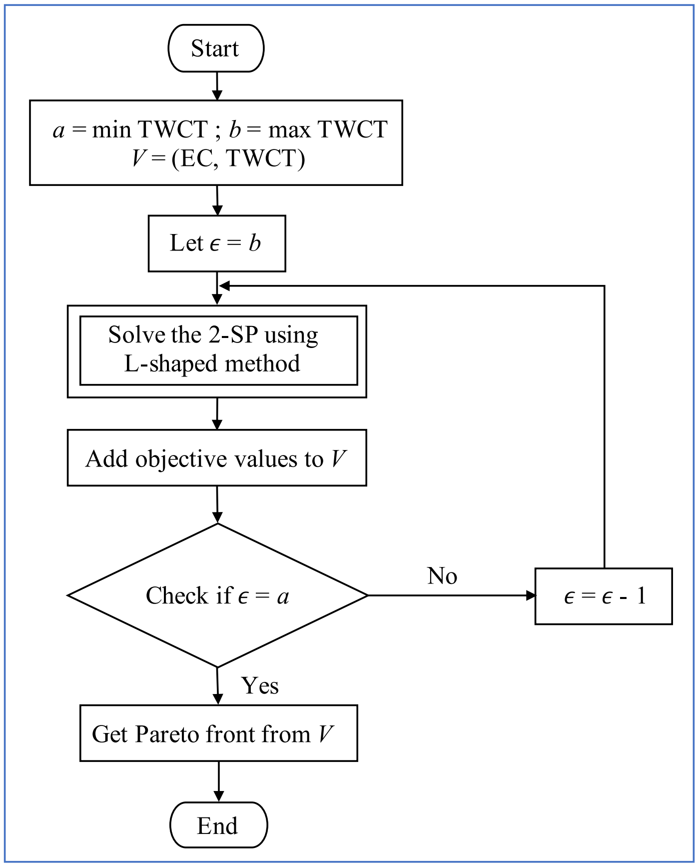

Figure 3.3: Flowchart of two-stage multi-objective stochastic solution scheme[79]

(scenarios). The expected value of the second stage function is computed by taking the average of M individual objective values obtained from each scenario. The expectation function can be replaced by its SAA and re-stated as follows [81]:

$$H(x) = \frac{1}{M} \sum_{i=1}^{M} h(x, \omega^i). \tag{3.21}$$

Decomposition-based methods, such as Dantzig-Wolfe decomposition [43], progressive hedging [44], and L-shaped method [82], have proven effective in solving the SAA. These methods iteratively build piece-wise affine approximations to the expected recourse function by solving a subproblem for each scenario from a set of scenarios. Dantzig-Wolfe decomposition is not directly applicable for MILP problems as it solves the dual of the master problem. Progressive hedging, which is a scenario-based decomposition method, requires selecting an appropriate proximal parameter which is instance-dependent and hard to determine. We base our solution approach on the L-shaped method.

To simplify our exposition of L-shaped method, we use a succinct representation of the 2-SP model [1]:

$$\begin{aligned} &\min\ c^\top x + \mathbb{E}\{h(x,\omega)\} \\ &\text{s.t. } x \subset \mathbb{Z}^{n_1} \times \mathbb{R}^{n_2}, \end{aligned} \tag{3.22a}$$

where

$$\begin{aligned} h(x,\omega) = \min\ & d^\top y \\ s.t.\ & Wy \leq r(\omega_n) - T(\omega)x, \\ & y \geq 0. \end{aligned} \tag{3.22b}$$

Auxiliary variable η is used to represent the approximation of the expected recourse function $\mathbb{E}\{h(x,\omega)\}$. At the beginning of the algorithm, the value of η is set as $-\infty$ or an appropriate approximation value. The algorithm begins with the original constraints only, $\mathcal{X}^0 := \{x,\eta|Ax = b\} \subset \mathbb{Z}_+ \times \mathbb{R}_+$. In iteration k, the algorithm first solves the MILP

$$\min\{c^\top x + \eta|(x,\eta) \in \mathcal{X}^k\}, \tag{3.23}$$

to obtain the solution x^k. Then, with this solution and a realization $\omega_i \in \Omega$, the optimal dual solution π^k is identified by solving the subproblem $h(x^k,\omega_i)$. This procedure is enumerated for every realization $\omega_i \in \Omega$. Using these dual solutions, we obtain a lower bounding optimality cut as follows:

$$l^k(x,\eta) := \sum_{i\in S} p_i \pi_i^\top [r(\omega^i - T(\omega^i)x^k)] - \eta \leq 0, \tag{3.24}$$

where p_i is the probability of scenario ω_i and S is the number of scenarios. Then, the feasible region is updated as:

$$\mathcal{X}^{k+1}(x) = \mathcal{X}^k(x) \cap (l^k(x,\eta) \leq 0). \tag{3.25}$$

Note that our subproblem (3.19b) satisfies the relative complete recourse property which means our subproblem has feasible solutions for all $\omega_i \in \Omega$ and $x \in \mathcal{X}^0$. Therefore, we omit feasibility cuts here. For more details, we refer the reader to [1].

3.5 Computational Experiments

We consider a three-machine flow shop in which three jobs need to be processed within the planning horizon (T = 24 hours). The length of each time slot is one hour and 10 random problem instances are created. The data for weights of the jobs (w_j), job processing times (p_{mj}), and the processing power requirements of machines (q^y_{mj}) are from [69]. Setup times (s_{fg}) and the power consumed during setup (q^l_{mfg}) are randomly generated from uniform distributions [1 h, 3 h] and [1 kW, 15 kW], respectively.

One energy storage system is installed and available near the plant. Renewable generation data was extracted from the Western Wind and Solar Integration Study [49]. An experiment utilizes solar generation if no specific details are given. To reduce the impact of seasonal variations, we only adopt the renewable generation data from spring. The number of scenarios considered in building our instances is

1000. Electricity prices follow a day-ahead TOU pricing scheme (Figure 3.4) which is derived from a rate schedule for industrial customers of California's Pacific Gas and Electric Company [83]. The feed-in electricity price is set to 0.08923 USD/kWh as found in the Electric-Renewable Market Adjusting Tariff of the Pacific Gas and Electric Company [84].

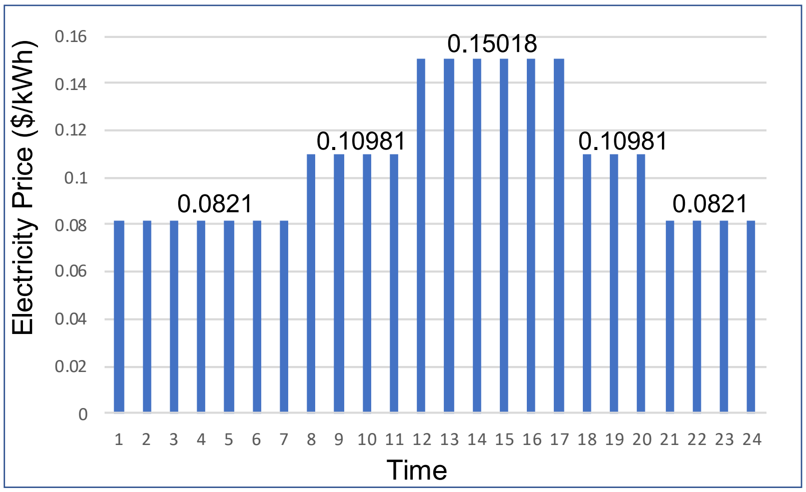

Figure 3.4: TOU Pricing Scheme

Our L-shaped method-based ϵ-constraint algorithm was implemented in C on a MacBook Pro running an Intel Core i7 CPU@3.3GHz (Dual-Core) with 16 GB Memory @2133 MHz. All MILPs were solved using CPLEX 12.7 callable subroutines.

During each ϵ-iteration, we begin by using an optimization process to identify the optimal solution for the master problem and the corresponding prediction value. Then, a verification phase is applied, where the solution of the master problem is fixed, and the subproblem is simulated using independent and identically distributed observations. Using the objective values, a confidence interval (CI) of the upper bound estimate is built for the expected recourse function.

We begin by illustrating how the ϵ-constraint framework works using instance 3 ("Ins3s"). The input ϵ value, corresponding TWCT, and predicted EC are summarized in Table 3.2. As mentioned in Section 3.4.1, the actual TWCT is not necessarily equal to the input ϵ, which is shown in the results in the 2nd, 5th, and 8th columns in Table 3.2. For example, when ϵ is equal to 138, the actual TWCT is 135. Another feature that should be noted is that TWCT is 135 whenever the input ϵ is set to 138 or 135. The predicted EC obtained when ϵ is set to 138 is smaller than the value obtained when ϵ is changed to 135. Therefore, (TWCT = 138, EC = 233.737) is Pareto optimal as (TWCT = 138, EC = 233.737) dominates (TWCT = 135, EC = 234.104), although this Pareto point is obtained when the input ϵ is 138 not 135. We say a point (TWCT, EC) dominates another point (TWCT', EC') when TWCT' $\geq$ TWCT and EC $\leq$ EC'. Therefore, seven Pareto optimal solutions are found for instance 3, marked by "*" in Table 3.2. Figure 3.5 presents the Pareto frontier of the ten instances. As we expected, there is a trade-off between TWCT and the predicted objective value EC: as the TWCT decreases, the predicted EC increases.

Next, we continue to use instance 3 to study the effect of setup costs in our scheduling problem with both time and energy cost considerations. We create another problem using Ins3s without considering setup costs, Ins3. Ins3 also contains seven Pareto optimal solutions which obtain the same TWCT as Ins3s. Figure 3.6 presents

Table 3.2: Input ϵ, corresponding TWCT, and predicted EC of Ins3s

ϵ	TWCT (hr)	Predicted EC ($)	ϵ	TWCT (hr)	Predicted EC ($)	ϵ	TWCT (hr)	Predicted EC ($)
*138	135	233.737	130	129	240.391	122	120	253.878
137	135	234.104	*129	129	240.391	121	120	253.878
136	135	234.104	128	126	245.790	*120	120	253.878
135	135	234.104	127	126	245.790	119	117	257.558
134	132	234.988	*126	126	245.790	118	117	257.558
133	132	234.988	125	123	250.909	*117	117	257.558
*132	132	234.988	124	123	250.909			
131	129	240.391	*123	123	250.909			

*Pareto optimal solution

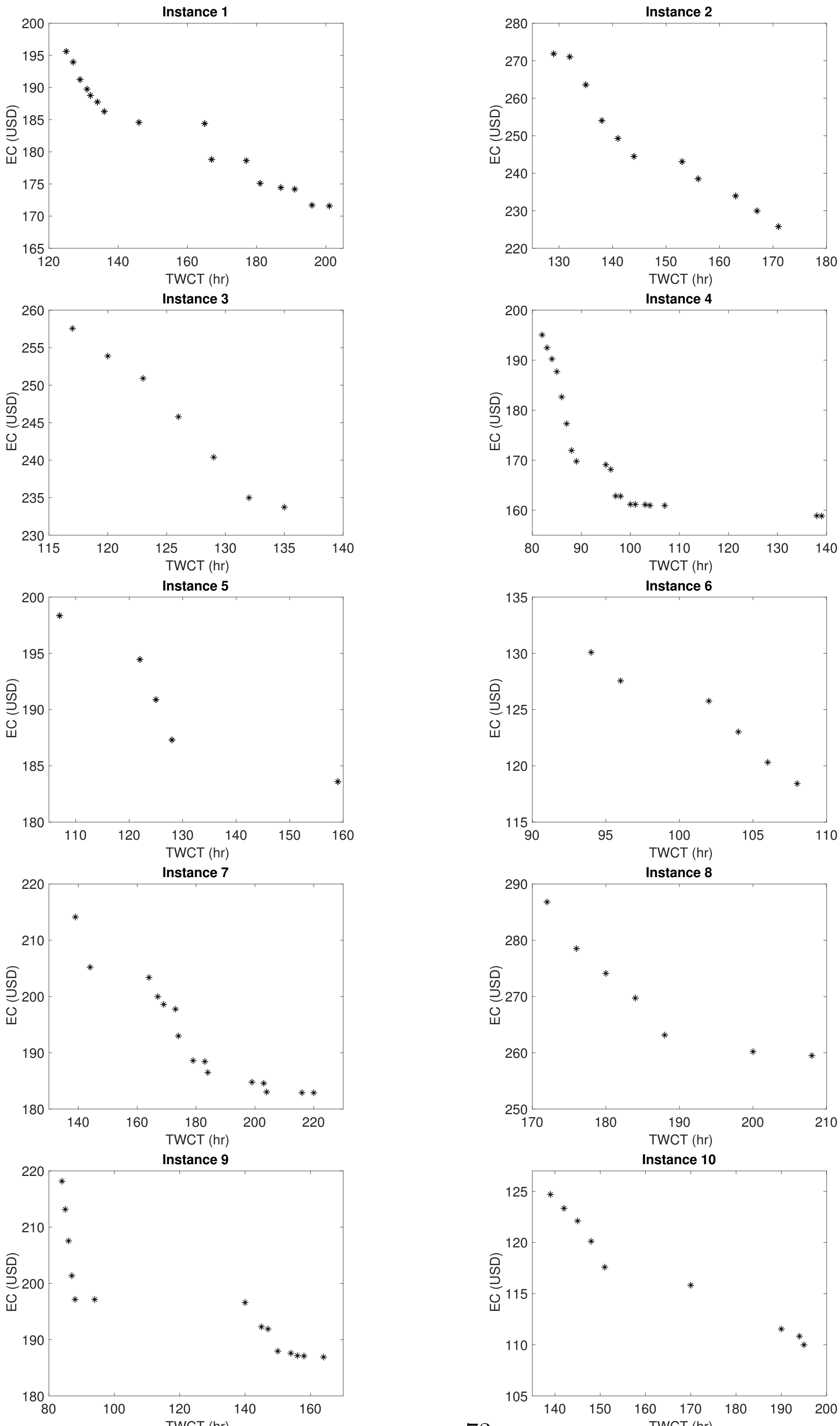

Figure 3.5: Pareto fronts of all 10 instances

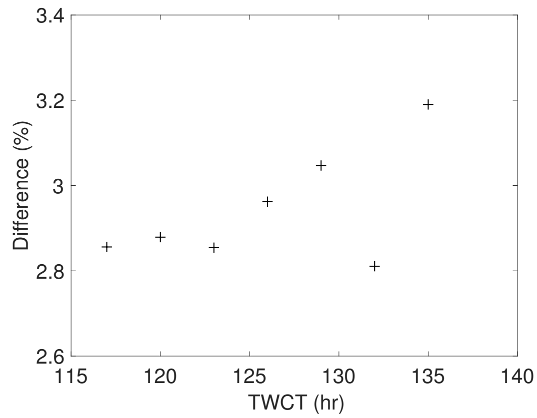

Figure 3.6: Cost differences between instance Ins3s and Ins3

the differences in energy costs between these two problem instances. We see that the differences consistently fall in the range [2.85%, 3.2%] for each TWCT. The average difference value is 2.94%, while the average power requirement for setup operations is approximately 6.5% of the power required by job processing. This analysis confirms for decision-makers that the energy costs of setup operations cannot be ignored, especially for some industries in which setup operations consume a large amount of energy.

Next, we study the impact of integrating on-site renewable energy and different sources of renewable energy on the production schedules and energy costs for problem Ins3s. Two more instances are created—one with wind energy as the renewable energy source and the other instance has no renewable energy at all. Wind and solar penetrations are kept the same in the first two instances. In the no-renewable instance, the random variable $\tilde{\omega}_{rt}$ is set to 0 for all generators at every time period. To this end, the studied bi-objective stochastic model is turned into a bi-objective deterministic program. Figure 3.7 shows the Pareto frontier of the studied example problems with wind energy and without renewable energy. Both of these two instances found seven Pareto optimal solutions as the same TWCT as Ins3s did. All three instances have

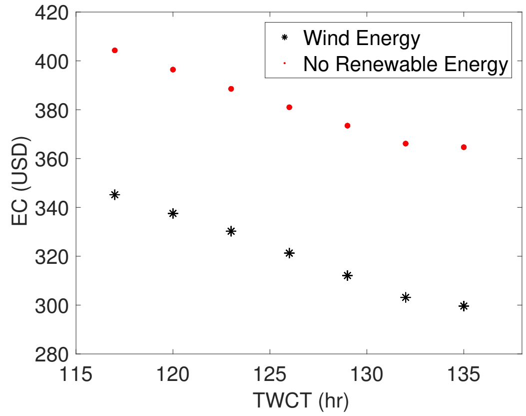

Figure 3.7: Pareto front for instance 3 with wind energy and without renewable energy

the same trend of reducing EC when increasing TWCT.

During the verification phase, 100 samples are used for different ϵ parameters to evaluate the solution. Figure 3.8 presents the energy costs observed at every TWCT of all three problem instances during the verification phase. It clearly shows that incorporating renewable energy helps to reduce energy costs for production. On average, using solar energy and wind energy saves 35.8% and 15.9% over no renewable generation utilized, respectively. Another observation from Figure 3.8 is that cost reduction is more prominent when utilizing solar energy than with wind energy as the average savings is 23.6%. This decrease can be attributed to the different distributions of solar and wind generation within the time horizon of interest (Figure 3.9). Wind power distributes evenly during the entire time horizon (Figure 3.9b), while solar provides more generation during the day time when electricity prices are high (Figure 3.4). Therefore, solar energy can satisfy some or all power demand during these high electricity price periods. Moreover, surplus solar energy can be stored in energy storage devices for future use or fed back into the main grid for compensation.

To further study the impact of on-site renewable energy on production schedules and energy costs, we use the optimal first-stage solution as an input to the

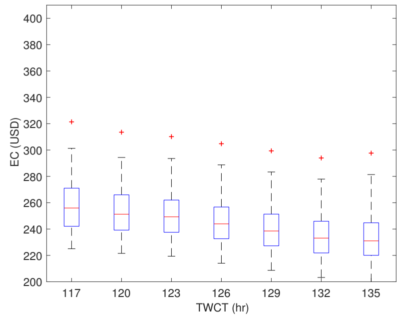

(a) Objective values of instance 3 with solar energy

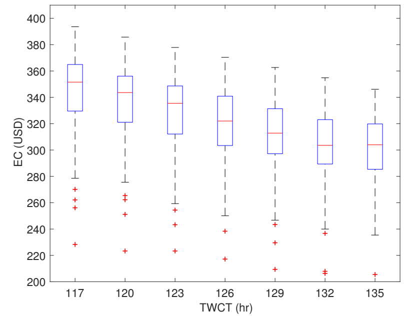

(b) Objective values of instance 3 with wind energy

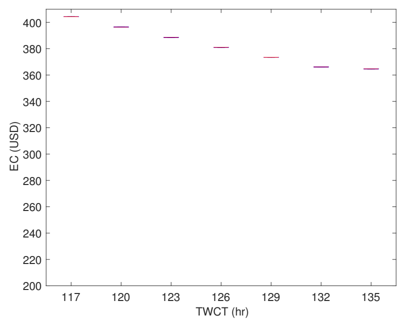

(c) Objective values of instance 3 without renewable energy

Figure 3.8: Objective values of instance 3

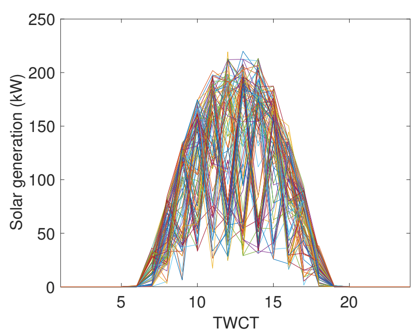

(a) Distribution of solar generation

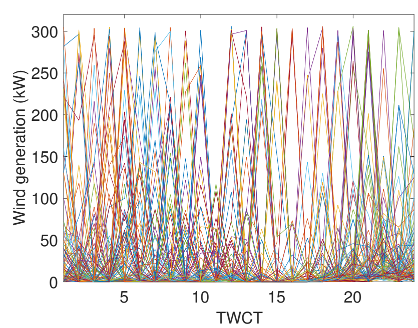

(b) Distribution of wind generation

Figure 3.9: Distributions of solar and wind generation

subproblem. The decision process of the subproblem is simulated by solving an optimization problem using independent Monte Carlo samples. Figure 3.10 shows the results with and without solar energy when TWCT = 132. Production processes, which consume more energy, are scheduled within low-electricity-price periods as much as possible to save energy costs in both of these two cases. With the help of renewable energy, production and setups can be performed in time periods with higher electricity prices. For example, the start of job 2's processing on machine 2 is scheduled four time slots earlier when solar energy is available than in the schedule when no renewable energy is available. Another example is that the setup operation of changing family 1 to family 2 on machine 3 is moved from time window [18,19] to [14,15] to fully utilize renewable energy. Figure 3.10 also shows that during time periods [8,16], renewable energy not only satisfies production requirements but also is sold back to the grid for compensation. Another interesting observation from Figure 3.10 is that the storage device is charged during time periods 7 and 11, the last periods before the electricity prices increase, regardless of whether renewable energy is used or not. The stored energy then is released to the system for production in future high electricity price time periods. These charging and discharging activities help to reduce total energy costs. The energy device only stores energy for one time period after each charging activity as the trade-off between storage cost and power

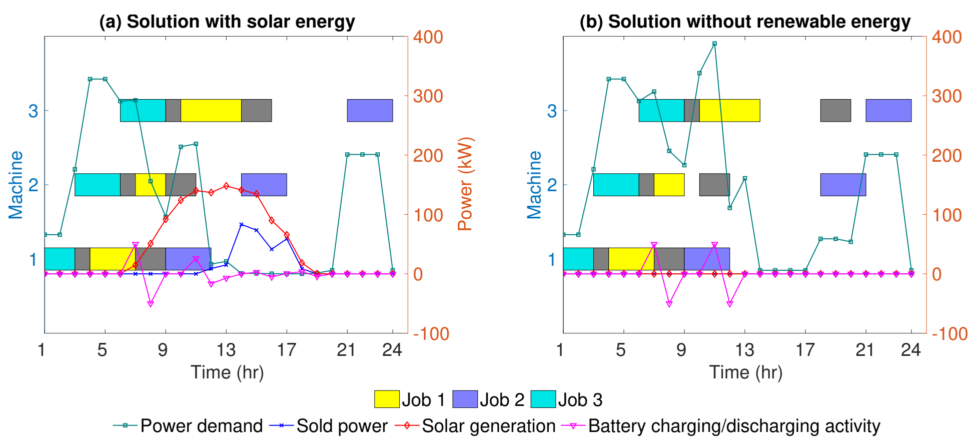

Figure 3.10: Comparison of production schedules of instance 3 with and without solar energy

purchasing cost determines the length of storage periods.

3.6 Conclusions and Future Research

In this paper, we study a flow shop scheduling problem with sequence-dependent setups, on-site renewable generation, and an available energy storage system. The model is formulated as a two-stage, multi-objective stochastic MILP. In the first stage, a time-indexed MILP is proposed to capture sequence-dependent setups. The optimal production schedule is determined to minimize the total weighted completion time. The second stage determines the energy supply decisions according to the production schedule and the realization of renewable energy generation to minimize energy costs under a TOU electricity price scheme. To solve this problem, we first adopt a ϵ-constraint approach to transform the multi-objective problem into a two-stage, single-objective stochastic MILP which is then tackled by Benders' decomposition.

Experiments based on machine power requirements, real renewable generation, a current TOU tariff, and a renewable feed-in tariff produce sets of Pareto optimal solutions for decision-makers who want to minimize total weighted completion time and energy cost in scheduling production process. Among sets of Pareto optimal solutions, decision-makers can choose the Pareto solution according to their preferences to determine job processing sequence and operate on-site ESSs. Sensitivity analysis shows that the energy cost of setup operations is relatively high compared to the power requirements of setup operations such that they cannot be ignored. Our experiments also reveal that both solar generation and wind generation are capable of reducing energy costs. However, energy cost reductions are more prominent by using solar energy than by using wind energy. This is because solar and wind generation follow different distributions during the time horizon under study. Finally, we studied how production schedules and energy supply change with the utilization of solar energy during the day.

The obtained results are associated with the available data of specific region and season. Further, we do not differentiate the electricity prices between working days and weekends. The number of working hours in one day is assumed as 24 hours in our numerical example that maybe not the usual schedule of some manufacturing factories. However, our developed methodology can be applied and customized to any given data including the electricity prices and renewable generation data in other regions/seasons, and any number of working hours in a workday. From the case study, several managerial implications can be derived: (1) Our model can be used as a managerial tool to optimize production scheduling and energy cost simultaneously with regards to one day-ahead TOU electricity pricing scheme and stochastic renewable generation; (2) manufacturing factories need to consider scheduling setups while optimizing time-dependent energy cost; (3) renewable generation resources, especially the solar panel, play a crucial role in reducing energy cost and promoting environmental goals in manufacturing.

There are several potential extensions for our study. First, we worked with small flow shop instances for computational efficiency. To address large-scale problems effectively, future research should focus on developing heuristic/meta-heuristic algorithms for this challenging problem. Another area for further research is to consider other machine environments such as job shops, which are prevalent in practice. Further, investigating production schedules and energy supply decisions under hour-ahead real-time tariffs would introduce additional uncertainty to the problem for another interesting line of research.

Chapter 4

A Hybrid Multi-objective Evolutionary Algorithm for Job-shop Scheduling with On-site Renewable Energy Generation and Real-time Electricity Pricing

Nomenclature

Sets

J	Set of jobs; indexed by $j = 1, 2, \ldots \lvert J\rvert$
O	Set of job operations; indexed by $o = 1, 2, \ldots \lvert O_j\rvert$
F	Set of job families; indexed by $f, g = 1, 2, \ldots \lvert F\rvert$
M	Set of machines; $m = 1, 2, \ldots \lvert M\rvert$
B	Set of ESSs; indexed by $i = 1, 2, \ldots \lvert B\rvert$

R	Set of renewable generators; $r = 1, 2, \ldots \lvert R \rvert$
S	Set of scenarios; $s = 1, 2, \ldots \lvert S \rvert$
T	Set of time periods; $t = 1, 2, \ldots \lvert T \rvert$

Parameters

ρ_s	probability of scenario $s \in S$
w_j	weight (priority) of job $j \in J$
l	length of a time slot
p_{mj}	processing time of job $j \in J$ on machine $m \in M$
s_{fg}	setup time between job family $f \in F$ and $g \in F$
$\sigma_{o,j}$	indicator, indicates job $j \in J$'s oth operation is processed by machine $m \in M$
b_i^{min}	minimum charging/discharging rate of ESS $i \in B$
b_i^{max}	maximum charging/discharging rate of ESS $i \in B$
E_i^{min}	minimum energy level of ESS $i \in B$
E_i^{max}	maximum energy level of ESS $i \in B$
q_{mj}^y	unit power consumed by processing job $j \in J$ on machine $m \in M$
q_{mf}^z	unit power consumed by idling at family $f \in F$ on machine $m \in M$
q_{mfg}^l	unit power consumed by a setup between job family $f \in F$ and $g \in F$ on machine $m \in M$
c_t^u	unit energy selling price in time period $t \in T$
c_{it}^E	unit energy storage cost of ESS $i \in B$ in time period $t \in T$
$\tilde{c}_t^{s,d}$	random variable, unit energy purchasing cost in time period $t \in T$ in scenario $s \in S$
$\tilde{\omega}_{rt}^s$	random variable, power generated by renewable generator $r \in R$ at time $t \in T$ in scenario $s \in S$

Decision Variables

x_{mjt}	$= 1$ if job j is started on machine m at the beginning of time period t
y_{mjt}	$= 1$ if job j is processed on machine m during time period t
z_{mft}	$= 1$ if machine m is idle at job family f during time period $[t, t+1)$
v_{mfgt}	$= 1$ if machine m starts to make a setup operation for changing job family f to job family g at the beginning of time period t
o_{mfgt}	$= 1$ if machine m is doing a setup for changing job family f to job family g during time period t
d_t^s	power purchased from the grid in time period t in scenario s
u_t^s	power sold to the grid in time period t in scenario s
b_{it}^s	ESS charging/discharging rate during time period t in scenario s
E_{it}^s	Energy state of ESS i in time period t in scenario s
a_t^s	underutilized renewable generation in time period t in scenario s

4.1 Introduction

We now extend the flow shop scheduling work of [85] to a job shop environment with the same two objectives: minimizing total weighted completion time and energy costs. We refer the reader to [85] for details about the integrated scheduling and energy procurement problem. In this study, an additional uncertainty, hour-ahead real-time electricity prices, is introduced to the model. Under conventional electricity pricing schemes such as time-of-use pricing tariffs, electricity prices are fixed for months or years. Under hour-ahead real-time pricing tariffs, electricity prices are released to customers only hours in advance of consumption, thereby introducing operational uncertainty to the energy cost-related problem under study. Many studies confirm that the job shop scheduling problem is a member of the class of intractable optimization problems known as NP-hard ([86, 87, 88]). To analyze our motivating problem effectively, we present a hybrid multi-objective evolutionary algorithm based on the Non-dominated Sorting Genetic Algorithm II (NSGA-II) [89].

4.2 Literature Review

A number of previous research studies investigate job shop scheduling problems with various objectives and processing characteristics in the literature. Zhang *et al.* [90] provide a review of models and solution approaches for job shop problems. Similarly, Çaliş and Bulkan [91] review artificial intelligence approaches such as neural networks and genetic algorithms on job shop problems.

With energy shortage and environmental challenges becoming increasingly severe problems, energy-aware scheduling and energy-cost-aware scheduling are attracting much more attention in the literature than before. Energy-efficient scheduling focuses on minimizing total energy consumption while energy-cost-aware scheduling seeks to minimize energy costs under various electricity pricing schemes. Liu *et al.* [92] employed NSGA-II to minimize total electricity consumption and total weighted tardiness for a classical job shop problem. Wu and Sun [93] study a flexible job shop problem considering machine turn on/off and choosing machine speed level to minimize makespan, energy consumption, and the total number of turning-on/off machines. Gong *et al.* [94] not only consider makespan and energy costs but also labor cost, workload, and total workload for a flexible job shop problem under real-time pricing and time-of-use pricing. Similarly, Mokhtari and Hasani [95] study energy-efficient of a flexible job shop to minimize total completion time, total energy cost of both production and maintenance operations, and to maximize the total availability of the system. However, most of these studies do not consider the utilization of renewable energy resources.

Moon and Park [66] study a flexible job shop scheduling problem integrated with on-site renewable generation, fuel cells, and energy storage systems to minimize the sum of makespan-related production costs, the cost of purchasing power from the grid, the cost of distributed generation, and the cost of an energy storage system (ESS) under a time-of-use pricing scheme. The model determines the amount of renewable energy generated for a given time period within the given minimum and maximum limits. Zhai *et al.* [67] consider on-site renewable generation in the context of flow shop scheduling under a real-time pricing scheme. Hourly wind speeds and electricity prices are first calculated by time series models and then fed to a manufacturing scheduling model to minimize energy costs. Unfortunately, this procedure requires that all data is predetermined without any consideration of uncertainty. Similarly, Zhang *et al.* [68] investigate a grid-connected hybrid flow shop problem with consideration of maintenance and buffers. On-site photovoltaics and ESSs are utilized to minimize electricity costs under a time-of-use pricing scheme. However, the uncertainty of solar generation is not considered by the authors.

Integrating renewable energy resources with scheduling has started to be investigated just recently. To the best of our knowledge, Liu [58] presents the first study that integrates a single-machine scheduling problem with renewable generation and an ESS. Interval number theory is used to represent the uncertainty of renewable energy availability. In the theory, the energy generated by renewable energy resources during each time period is bounded by an interval and the interval boundaries are randomly generated from a uniform distribution.

Biel *et al.* [69] study a flow shop scheduling problem with on-site wind power under a time-of-use pricing scheme. A two-stage stochastic procedure is proposed to minimize total weighted flow time and energy costs. Khalaf and Wang [70] propose a two-stage stochastic mixed-integer linear program for a flow shop problem with on-site renewable energy resources and ESS under day-ahead and real-time electricity pricing schemes. In the first stage, job schedules are determined to minimize energy purchase cost procured from the day-ahead plan by considering forecasted renewable energy generation. Then, the second stage compensates for the mismatch between forecasted and actual renewable energy to minimize energy costs under a real-time pricing scheme.

Wang *et al.* [85] investigate a flow shop problem with on-site renewable energy resources and an ESS to minimize total weighted completion time and energy costs under time-of-use electricity pricing schemes. Sequence-dependent setups and machine status (i.e., job processing, setup, and idling)-related energy costs are considered. Golpîra *et al.* [96] propose a risk-based Robust Mixed Integer Linear Programming model for a job shop problem with wind power generation to cope with the uncertainties of wind speed and heat/wind demands. Both lot sizing and job scheduling are considered in their problem.

To date, only a few studies have considered energy-cost-aware job shop scheduling with stochastic renewable energy simultaneously. Further, machine state-related energy consumption is usually ignored in the literature. Motivated by the insufficiency of the previous studies, the main goal of this study is to fill these gaps.

4.3 Model

4.3.1 Problem Description

A job shop is comprised of $|M|$ machines. Each job j with weight (priority) w_j in the set of jobs J is released at the beginning of the time horizon of interest. Each job associated with a predetermined sequence of operations needs to be completed on given machines in a specific order. A sequence-dependent setup is required for changeovers when the job family changes from $f \in F$ to $g \in F \setminus \{f\}$ on each machine. Further, different amounts of energy are required by the three different machine states under study (i.e., job processing, setup, and idling). The energy required to run the machines can be purchased from the main power grid, generated by on-site renewable generators, and/or discharged from ESSs. Energy generated by renewable generators can be used to run production, charge ESSs, and/or be fed into the main grid for compensation according to current hour-ahead real-time electricity prices. A valid production schedule decision assigns jobs to machines and determines machine states in each time period $t \in T$ to minimize total weighted completion time (TWCT). The energy supply decision determines energy transactions between the main grid, the manufacturing plant, and operating ESSs to minimize total energy cost (EC).

4.3.2 Formulation

Our proposed MILP model for job shop scheduling and energy supply decisions, which is inspired by [85], seeks to simultaneously minimize two objectives. The first one is to minimize total weighted completion time (TWCT):

$$\min \text{TWCT} = \sum_{j \in J} w_j \sum_{t \in T} (tl + p_{|M|j} - l) x_{|M|jt}. \tag{4.1}$$

Uncertainties are incorporated into the MILP model by means of a large number of scenarios containing renewable generation and real-time electricity prices in each time period. The second objective minimizes the expected value of energy cost (EC), which consists of the cost of purchasing power from the grid plus the cost of storing energy in ESSs, minus the revenue generated from selling power back to the grid:

$$\min \text{EC} = \sum_{s \in S} \rho_s \sum_{t \in T} (\tilde{c}_t^{s,d} d_t^s l + \sum_{i \in B} c_{it}^E E_{it}^s - c_t^u u_t^s l). \tag{4.2}$$

The model constraint sets are partitioned into two parts: production process and energy supply. Constraint sets (4.3)-(4.12) describe the production flow in the job shop:

$$\sum_{t \in T} x_{mjt} = 1 \qquad \forall m \in M, j \in J, \tag{4.3}$$

$$\sum_{j \in J} \sum_{\tau \geq t - \frac{p_{mj}}{l} + 1}^{t} x_{mj\tau} \leq 1 \qquad \forall m \in M, j \in J, t \in T, \tag{4.4}$$

$$\sum_{t \in T} (t + \frac{p_{\sigma_{o-1}^j, j}}{l}) x_{\sigma_{o-1}^j, jt} \leq \sum_{t \in T} t \cdot x_{\sigma_o^j, jt} \qquad \forall j \in J, o \in O \setminus \{1\}, \tag{4.5}$$

$$y_{mjt} + y_{m'jt} \leq 1 \qquad \forall m, m' \in M, j \in J, t \in T, \tag{4.6}$$

$$y_{mjt} + \sum_{j' \in J \setminus \{j\}} x_{mj't} \leq 1 \qquad \forall m \in M, j \in J, t \in T, \tag{4.7}$$

$$\sum_{\tau \geq t}^{t + \frac{p_{mj}}{l} - 1} y_{mj\tau} \geq x_{mjt} \cdot \frac{p_{mj}}{l} \qquad \forall m \in M, j \in J, t \in T, \tag{4.8}$$

$$\sum_{\tau \geq t}^{t + \frac{s_{fg}}{l} - 1} o_{mfg\tau} \geq v_{mfgt} \cdot \frac{s_{fg}}{l} \qquad \forall m \in M, f \in F, g \in F \setminus \{g\}, t \in T, \tag{4.9}$$

$$\sum_{j \in J} y_{mjt} + \sum_{f \in F} z_{mft} + \sum_{k \in F} \sum_{h \in F \setminus \{k\}} \sum_{\tau > t - \frac{s_{kh}}{l}}^{\tau \leq t} v_{mkh\tau} = 1 \qquad \forall m \in M, t \in T, \tag{4.10}$$

$$\begin{aligned} & z_{mft-1} + \sum_{j: F_j = f} y_{mj,t-1} + \sum_{g \in F \setminus \{f\}} v_{mgf,t-\frac{s_{gf}}{l}} = z_{mft} + \sum_{j: F_j = f} y_{mjt} + \\ & \sum_{g \in F \setminus \{f\}} v_{mfgt} \qquad \forall m \in M, f \in F, t \in T \setminus \{0\}, \end{aligned} \tag{4.11}$$

$$x_{mjt}, y_{mjt}, z_{mft}, o_{mfgt}, v_{mfgt} \in \{0, 1\} \qquad \forall m \in M, j \in J, f, g \in F, t \in T, \tag{4.12}$$

Constraint set (4.3) ensures that any job j can only start processing on each machine m once during the entire time horizon. Constraint set (4.4) guarantees that each machine m can only process one job at a time. Constraint set (4.5) specifies the precedence relationship of two consecutive job operations. Job operation o can be started if and only if previous job operation $(o-1)$ was previously started. Constraint set (4.6) ensures that job j can only be processed by one machine during any time period $t \in T$. Any machine m can process job j only after job j is assigned to the machine, which is guaranteed by constraint set (4.7). Constraint set (4.8) ensures that once machine m starts to process a job, it cannot be interrupted. Similarly, any machine m cannot be interrupted once it starts a setup, which is enforced by constraint set (4.9). In each time period $t \in T$, constraint set (4.10) ensures that any machine can only be in exactly one state: job processing, setup, or idling. Further, a setup operation is induced if machine m has any state change (4.11). Constraint set (4.12) prescribes the binary character of variables used in the model.

Next, constraint sets (4.13)-(4.19) specify the energy supply and consumption of the job shop system:

$$d_t^s - u_t^s - \sum_{i \in B} b_{it}^s - a_t^s = \sum_{m \in M} \sum_{j \in J} y_{mjt} q_{mj}^y + \sum_{m \in M} \sum_{f \in F} z_{mft} q_{mf}^z$$
$$+ \sum_{m \in M} \sum_{f,g \in F: f \neq g} o_{mfgt} q_{mfg}^l - \sum_{r \in R} \tilde{\omega}_{rt}^s \qquad \forall t \in T, s \in S, \tag{4.13}$$

$$E_{it}^s = E_{i,t-1}^s + b_{it}^s l \qquad \forall i \in B, t \in T, s \in S, \tag{4.14}$$

$$b_i^{min} \leq b_{it}^s \leq b_i^{max} \qquad \forall i \in B, t \in T, s \in S, \tag{4.15}$$

$$E_{it}^{min} \leq E_{it}^s \leq E_{it}^{max} \qquad \forall i \in B, t \in T, s \in S, \tag{4.16}$$

$$u_t^s \cdot l \leq \sum_{r \in R} \tilde{\omega}_{rt}^s \qquad \forall t \in T, s \in S, \tag{4.17}$$

$$d_t^s, u_t^s, E_{it}^s, a_t^s \geq 0 \qquad \forall i \in B, t \in T, s \in S, \tag{4.18}$$

$$b_{it}^s \text{ unrestricted} \qquad \forall i \in B, t \in T, s \in S. \tag{4.19}$$

At any time period t, the total available power should meet total demand, according to a power balance equation (4.13). The total available power includes power purchased from the grid, power discharged from ESSs, and power generated by on-site renewable generators. The state of ESS i is required to satisfy the governing dynamics equation (4.14): the charging/discharging rate b_{it} will be positive if the ESS i is charging; otherwise, it is discharging. Further, these decisions are bounded by the charging/discharging rates of the ESS (4.15). Constraint set (4.16) guarantees that the state of the ESS is bounded by its capacity. Constraint set (4.17) ensures that the power sold to the main grid cannot exceed the power generated by renewable generators. While, constraint sets (4.18) - (4.19) provide variable types and limits on the decision variables in the energy supply model, respectively.

An ϵ-constraint algorithm [80] is applied to the bi-objective optimization model. We keep EC as the objective function and convert TWCT into an ϵ-constraint [85]. Therefore, the transformed single formulation can be reformulated as follows:

$$\min \text{ EC} = \sum_{s \in S} \rho_s \sum_{t \in T} (\tilde{c}_t^{s,d} d_t^s l + \sum_{i \in B} c_{it}^E E_{it}^s - c_t^u u_t^s l) \tag{4.20}$$

$$\text{s.t.} \sum_{j \in J} w_j \sum_{t \in T} (tl + p_{|M|j} - l) x_{|M|jt} \leq \epsilon,$$

$$(4.3) - (4.19).$$

4.4 A Hybrid Multi-objective Evolutionary Algorithm

To efficiently solve the problem presented in the previous section, we develop a hybrid multi-objective evolutionary algorithm that integrates a mathematical approach with NSGA-II [89]. Introduced by Deb *et al.* [89], NSGA-II is one of the best algorithms for multi-objective problems with respect to fitness and solution diversity ([97, 98]). In our algorithm, a genetic algorithm (GA) is applied to the scheduling part of our problem to generate feasible schedules with TWCT. Under a given feasible production schedule, we use a commercial solver to compute the optimal EC, as the energy supply problem is a linear program. Finally, fast non-dominated sorting and crowding-distance approaches are applied to obtain the Pareto frontier of non-dominated solutions.

Figure 4.1 shows a flow chart of NSGA-II. The algorithm begins with randomly generating an initial population P_0 of size N. At generation k, we have the parent population P_k of size N. Then, the offspring population Q_k of size N is generated using genetic operations such as crossover and mutation. Next, P_k and Q_k are combined to form mating pool R_k. Fast non-dominated sorting scheme is performed to classify individuals in R_k into a non-decreasing order of fronts $(F_1, F_2, ...)$ based on the individuals' fitness. After that, individuals from the sorted list are added to the next generation P_{k+1} until the size of P_{k+1} exceeds N. If the current $|P_{k+1}| + F_i \leq N$, then all individuals in the F_i are added to the next generation P_{k+1}. Otherwise, we first sort the individuals in F_i in non-increasing order according to their crowding distance. Then, the remaining members of P_{k+1} are chosen from F_i based on their crowding distance. Since only non-dominated individuals (lowest rank front) are selected to add to the next generation population, elitism is ensured.

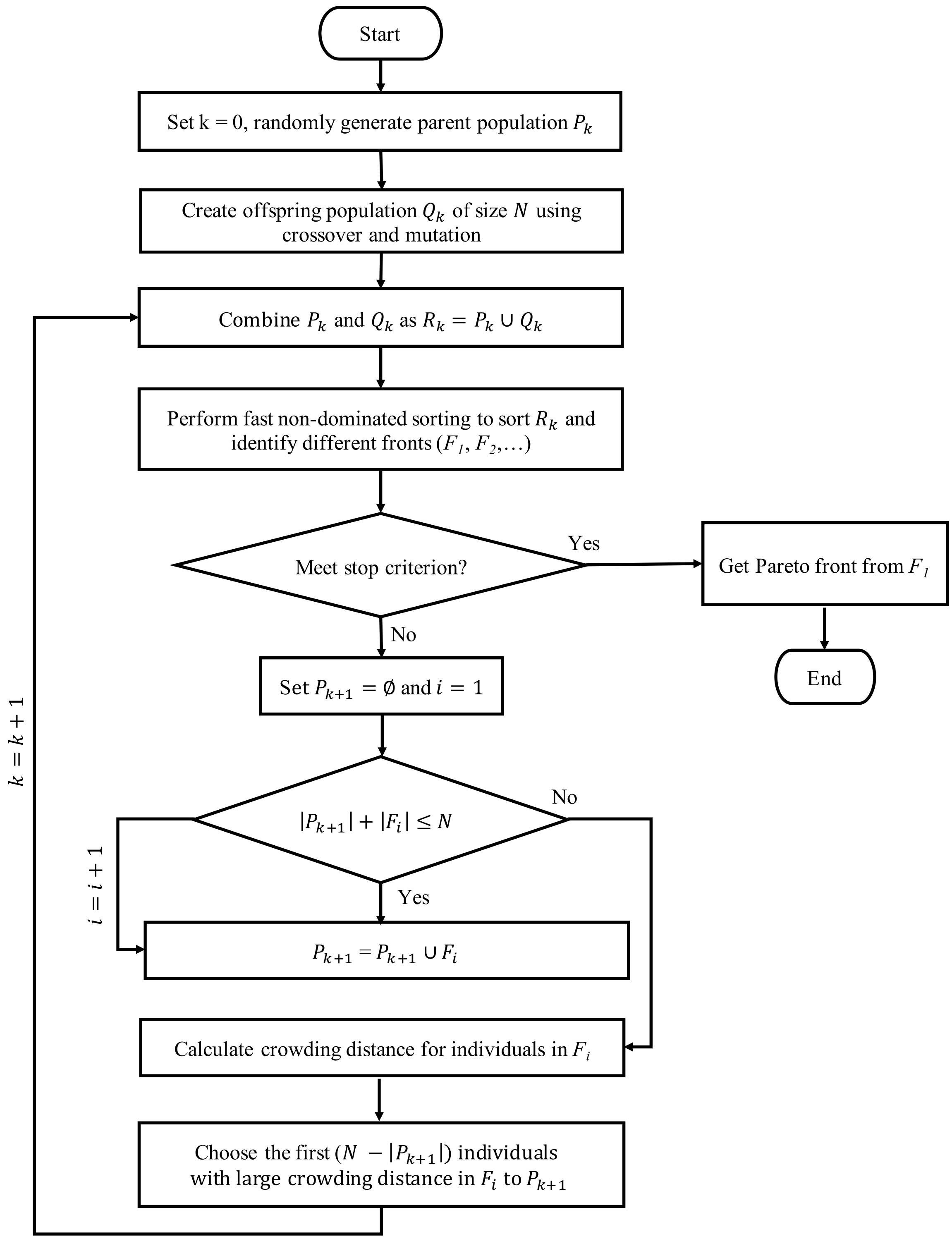

Figure 4.1: Flow chart of the NSGA-II [89]

4.4.1 Chromosome Representation

The GA in our proposed algorithm is used to generate job operation sequences that are represented by chromosomes. Then, the start time of job processing and machine setups associated with these sequences are determined using a heuristic method embedded in our evaluation process. In our algorithm, we start by sampling $n \times m$ $U(0, 1)$ random numbers where n is the number of jobs and m is the number of machines. For example, when three jobs need to be processed on four machines, let the 12 randomly generated numbers be (0.6984, 0.1639, 0.1174, 0.2976, 0.5354, 0.0165, 0.2958, 0.5882, 0.7355, 0.1715, 0.8359, 0.2955). Then, we sort these random numbers in ascending order: (0.0165, 0.1174, 0.1639, 0.1715, 0.2955, 0.2958, 0.2976, 0.5354, 0.5882, 0.6984, 0.7355, 0.8359). We record the sorted numbers' indices as (6, 3, 2, 10, 12, 7, 4, 5, 8, 1, 9, 11). Finally, we divide each index number by the total number of machines (four) and then round up to the next integer. Thus, the encoding for this example is (2, 1, 1, 3, 3, 2, 1, 2, 2, 1, 3, 3). Here, 1, 2, and 3 represent job j_1, j_2 and j_3, respectively. The different appearances of the same job j represent different operations of the job. For example, job j_1 shows up at the 2nd, 3rd, 7th, and 10th position in the sequence, which means job j_1 has four operations. The 1st appearance of job j_1 (i.e., at 2nd position) means the 1st operation (O_{11}) of job j_1. Therefore, the corresponding job-operation sequence of the encoding sequence is (O21, O11, O12, O31, O32, O22, O13, O23, O24, O14, O33, O34).

4.4.2 Genetic Operators

Genetic algorithms use ideas borrowed from the concepts of genetics and biological evolution. The main idea is to improve the quality of offsprings over multiple generations. Genetic operators are used to generate more promising candidate solutions that replace less promising solutions. In our algorithm, crossover and mutation operators are employed.

Crossover - Crossover is performed on two parent chromosomes that are randomly selected from the population. In our algorithm, we adopt a random two-point crossover operator. Two crossover points are randomly chosen from the parent chromosomes. Then, genes in between the two points are swapped between the parent chromosomes (Figure 4.2). Thus, two child chromosomes are obtained.

Parent 1	0.6984	0.1639	0.1174	0.2976	0.5354	0.0165	0.2958	0.5882	0.7355	0.1715	0.8359	0.2955
Parent 2	0.2004	0.8668	0.0731	0.5703	0.4241	0.3424	0.1863	0.7934	0.8901	0.7585	0.3345	0.5788
Child 1	0.6984	0.1639	0.1174	0.2976	0.4241	0.3424	0.1863	0.7934	0.8901	0.1715	0.8359	0.2955
Child 2	0.2004	0.8668	0.0731	0.5703	0.5354	0.0165	0.2958	0.5882	0.7355	0.7585	0.3345	0.5788

Figure 4.2: Example crossover operation

Mutation - Mutation preserves genetic variation with the intent to escape from local minima. It involves selecting a chromosome and two points at random, and then generating new $U(0,1)$ genes at these points (Figure 4.3).

Parent	0.6984	0.1639	0.1174	0.2976	0.5354	0.0165	0.2958	0.5882	0.7355	0.1715	0.8359	0.2955
Child	0.6984	0.2344	0.1174	0.2976	0.5354	0.0165	0.2958	0.5882	0.7355	0.4692	0.8359	0.2955

Figure 4.3: Example mutation operation

4.4.3 Heuristic Objective Functions

As described in Section 4.3, the model decomposes into two parts: (1) job shop scheduling decisions with constraint sets (4.3)-(4.12) and (2) energy supply decisions with constraint sets (4.13)-(4.19). For the job shop problem, given the job operation sequences decoded from our chromosome, we created a heuristic method to generate the start times of both job processing and machine setups between different job families. As a result, TWCT can be calculated for any chromosome. The EC objective function is computed optimally using our mathematical model after production schedule is fixed in the model as an input. Our heuristic method uses five approaches to generate job start times on machines.

1 Earliest start time: Algorithm 1 describes the earliest start time method. Each job operation is required to be started as early as possible within the time horizon while respecting job operation sequences and machine availability re-

Algorithm 1 Algorithm of earliest start time

Input: decoded job operation sequence
for i = the first job operation to the last job operations **do**
    if $t_j \leq t_m$ **then**
        $t_{start} \leftarrow t_j$
    else
        $t_{start} \leftarrow t_m$
    end if
    $t_m = t_j \leftarrow t_{start}+$ job j's processing time on machine m
    on machine m, find job operation i's job family f and its next job operation i''s job family g
    if i is not the last job operation assigned on machine m **then**
        $t_{comp} \leftarrow t_m$
        the start time of setup $t_{StartSetup} \leftarrow t_m$
        the completion time of setup $t_{CompSetup} \leftarrow t_m+$ setup time between job family f and g
        Record $t_{start}, t_{comp}, t_{StartSetup}$, and $t_{CompSetup}$
    else
        $t_{comp} \leftarrow t_m$
        Record t_{start} and t_{comp}
    end if
    $t_m \leftarrow t_m+$ setup time between job family f and g
end for

quirements. In addition, all job family-related setup operations are performed at the earliest possible time.

2 Latest start time: In this method, we assign job operations to begin processing as late as possible. Given a job operation sequence, our algorithm starts from the last job operation and progresses to the first one, placing each hob as late in the schedule as possible (Algorithm 2). As was the case in Algorithm 1, all job operations, machine availability, and setup requirements are enforced.

Methods 3 - 5 are similar to the earliest start time (method 1). The difference lies in generating the starting time of job operations (lines 3-6, Algorithm 1). Besides the decoded job operation sequence, methods 3 - 5 also require as input the latest

---

Algorithm 2 Algorithm of latest start time

Input: decoded job operation sequence
for $i =$ the #of job operations to the first job operation **do**
    if $t_j \leq t_m$ **then**
        $t_{comp} \leftarrow t_j$
    else
        $t_{comp} \leftarrow t_m$
    end if
    $t_m = t_j \leftarrow t_{comp}-$ job j's processing time on machine m
    on machine m, find job operation i's job family g and its previous job operation i''s job family f
    if i is not the first job operation assigned on machine m **then**
        $t_{start} \leftarrow t_m$
        the completion time of setup $t_{CompSetup} \leftarrow t_m$
        the start time of setup $t_{StartSetup} \leftarrow t_m-$ setup time between job family f and g
        Record $t_{start}, t_{comp}, t_{StartSetup}$, and $t_{CompSetup}$
    else
        $t_{start} \leftarrow t_m$
        Record t_{start} and t_{comp}
    end if
    $t_m \leftarrow t_m-$ setup time between job family f and g
end for

---

start time of each job operation (which can be obtained from method 2).

3 Lowest price start time: This method seeks to find the time period with the lowest electricity price, which is denoted as $t_{LowestPrice}$, within time window [t_j, the latest start time of job operation i] if job j becomes available before machine m (Algorithm 3). Otherwise, find $t_{LowestPrice}$ within time window [t_m, the latest start time of job operation i] and set start time t_{start} equal to $t_{LowestPrice}$.

4 Highest renewable generation start time: Similar to method 3, this method seeks the time period with the highest renewable generation $t_{highestRenewable}$ within time period [t_j, the latest start time of job operation i] or [t_m, the latest start

Algorithm 3 Algorithm of start time with the lowest price

Input: decoded job operation sequence
for i = the first job operation to the last job operations **do**
  if $t_j \leq t_m$ **then**
    $t_{start} \leftarrow$ the time period with the average lowest electricity price within time window [t_j, the latest start time of job operation i]
  else
    $t_{start} \leftarrow$ the time period with the average lowest electricity price within time window [t_m, the latest start time of job operation i]
  end if
  $t_m = t_j \leftarrow t_{start}+$ job j's processing time on machine m
  on machine m, find job operation i's job family f and its next job operation i''s job family g
  if i is not the last job operation assigned on machine m **then**
    $t_{comp} \leftarrow t_m$
    the start time of setup $t_{StartSetup} \leftarrow t_m$
    the completion time of setup $t_{CompSetup} \leftarrow t_m+$ setup time between job family f and g
    Record $t_{start}, t_{comp}, t_{StartSetup}$, and $t_{CompSetup}$
  else
    $t_{comp} \leftarrow t_m$
    Record t_{start} and t_{comp}
  end if
  $t_m \leftarrow t_m+$ setup time between job family f and g
end for

time of job operation i], based on whether $t_j \geq t_m$ or $t_j < t_m$, respectively.

5 Random start time: Within time window [t_j, the latest start time of job operation i] or [t_m, the latest start time of job operation i], start time t_{start} is randomly generated in this method.

In all of the five methods, any required setup between two job operations on a machine is scheduled right after the first job operation is completed. Thus, the start time of the setup is as early as possible. To improve solution diversity, we also randomly generate setup start times for the schedules obtained by the five methods. With 50% probability, we generate a start time for a setup within the time frame of its earliest start time and latest start time. The earliest start time is equal to the completion time of job operation i and the latest start time is equal to the start time of i' minus the setup time between i and i'.

4.4.4 Fast non-dominated sorting and crowding distance

Fast non-dominated sorting and crowding distance are two main features of NSGA-II which are used to evaluate each solution in R_k as shown in Figure 4.1. Let n_p and S_p denote the number of solutions that dominate solution p and a set of solutions that the solution p dominates, respectively. First, we put all solutions with $n_p = 0$ in the first non-dominated front F_1. Then, for each solution in F_1, we visit each individual q in its set S_q and reduce n_q by one. If any individual q's n_q becomes 0, we put it into a new non-dominated front. This process continues until all individuals are considered and all fronts are identified. We refer the reader to [89] for a detailed exposition of the fast non-dominated sorting scheme.

The crowding distance measure first sorts individual solutions in front F_k in non-decreasing order of the n^{th} objective function value. The crowding distance CD_{in}

of each solution i with respect to objective n is calculated as:

$$CD_{in} = \frac{f_n(i+1) - f_n(i-1)}{f_n^{max} - f_n^{min}}, \tag{4.21}$$

where f_n^{max} and f_n^{min} are the maximum and minimum values of the n^{th} objective function of the solution. The boundary solutions (solutions with the smallest and largest objective function value) are assigned to an infinite distance value. The total crowding distance of each solution i is calculated as:

$$CD_i = \sum_{n=1}^{N} CD_{in}, \tag{4.22}$$

where N is the number of objectives.

4.5 Computational Experiments

To test the performance of our proposed mathematical model and algorithm, 30 instances are generated (Table 4.1). We consider three different sets of jobs (3, 6, and 9) processed on three machines in the 30 instances and two sets of time periods: 24 and 96. As each day has 24 hours, the length of each time period is 1 hour (15 minutes) when there are 24 (96) time periods. Table 4.2 provides the values of other scheduling-related parameters in the test instances.

Renewable generation data is from [85] wherein solar generation data is adopted. The hour-ahead real-time pricing scheme is derived from the Commonwealth Edison (ComEd) company [99]. To illustrate the problem under study and our algorithms, we generate four scenarios, each with an equal probability of occurrence. The feed-in electricity price is set to 0.08923 USD/kWh as found in the Electric-Renewable Market Adjusting Tariff of the Pacific Gas and Electric Company [84]. One ESS is

Table 4.1: Experiment design

Instances	# of jobs	# of time periods	Processing time	Power requirement by processing jobs
1-5	3	24	DU(2,6)	DU(50,200)
6-10	3	96	DU(10,30)	DU(20,100)
11-15	6	24	DU(1,4)	DU(50,200)
16-20	6	96	DU(4,16)	DU(20,100)
21-25	9	24	DU(2,6)	DU(50,200)
26-30	9	96	DU(2,6)	DU(20,100)

Table 4.2: Common parameters for 30 instances

Parameter	Value description
Weight	DU(1,10)
Family	DU(1,3)
Setup times	DU(1,3)
Setup power requirement	DU(5,15)
Ideling power requirement	1

installed and available near the plant.

Both our mathematical model and heuristic algorithm were implemented using JuMP and Gurobi 7.0.1 on a MacBook Pro running an Intel Core i7 CPU@3.3GHz (Dual-Core) with 16 GB Memory @2133 MHz. For employing NSGA-II, both population size and number of generations are set to 50. Further, crossover probability and mutation probability are defined as 0.8 and 0.2, respectively.

As electricity prices are released one hour ahead, each instance can be analyzed for at most one hour. When the ϵ parameter is set to a big number such as 10000, we can obtain the smallest EC for every instance. Optimal solutions were found for instances 1-25 using the original MILP formulation. Instances 26-30 stopped at the one-hour time limit before finding an optimal solution. Thus, we only compare the mathematical model and our proposed algorithm using the smallest EC. Let Δ denote the gap between the EC obtained from the mathematical model and the NSGA-II such that $\Delta = (EC_{NSGA-II} - EC_{MILP})/EC_{NSGA-II}$. Table 4.3 summarizes results from the two solution methods. Our NSGA-II algorithm can produce competitive solutions with an average $\Delta = 3.29\%$ compared to the mathematical model. When the number of jobs increases from 3 to 6 and then to 9, the average solution gap Δ increases from 1.5% to 2.14%, and then to 6.22%. Similarly, Δ increases from 1.73% to 4.85% as the number of time periods increases from 24 to 96.

Overall, the quality of our NSGA-II-based solutions decreases as problem instances become more complicated. However, NSGA-II can produce solutions fairly quickly, especially for large problems. The 5^{th} column in Table 4.3 provides the solution time of the mathematical model. These times are only for one ϵ parameter. Tens or 100s of ϵ parameters need to be considered for each instance for full Pareto results. When there are nine jobs and 96 time periods considered in a job shop, the MILP cannot determine an optimal solution, even for only one ϵ parameter within one hour. In contrast, our NSGA-II algorithm can produce all Pareto frontiers of non-dominated solutions within 1700s (6^{th} column in Table 4.3).

The algorithm presented in section 4.4 considers five methods simultaneously to generate schedules (NSGA-II_5). Now, we modify the algorithm by randomly selecting one method to generate a schedule for each chromosome, which is denoted as NSGA-II_1. Tabel 4.4 summarizes the results of solutions produced by NSGA-II_1. Here, Δ is the gap between the EC obtained from the mathematical model and NSGA-II_1. On average, the Δ is 4.36% for all 30 instances. The gap between EC obtained from NSGA-II_5 and NSGA-II_1 is 1.14%. However, the running time reduces 716.24s (83.6%) on average, when choosing NSGA-II_1.

Now, we further examine the performance of NSGA-II_5 and NSGA-II_1. To

Table 4.3: Mathematical Model vs. NSGA-II

Instance	EC ($)			Running time (s)	
	MILP	NSGA-II	Δ	MILP	NSGA-II
1	773.789	789.773	2.02%	6.27	810.19
2	649.518	654.647	0.78%	9.31	192.61
3	548.143	557.496	1.68%	7.68	209.93
4	623.966	644.218	3.14%	6.31	605.90
5	634.242	634.277	0.01%	6.11	657.16
6	225.175	230.588	2.35%	37.65	1371.40
7	356.036	361.631	1.55%	33.85	1322.77
8	279.760	280.597	0.30%	29.25	1390.68
9	210.707	217.21	2.99%	31.98	1194.64
10	252.472	252.988	0.20%	9.61	1139.29
11	872.868	885.939	1.48%	21.91	205.31
12	890.330	890.619	0.03%	25.39	844.72
13	850.172	858.564	0.98%	47.43	699.99
14	777.846	779.683	0.24%	48.10	891.76
15	859.454	870.203	1.24%	53.75	784.82
16	339.162	349.449	2.94%	1376.53	1525.95
17	229.493	239.206	4.06%	1071.31	1535.39
18	270.511	279.15	3.09%	3607.25	1647.76
19	354.436	368.287	3.76%	1259.32	1497.42
20	223.755	232.055	3.58%	2064.15	1697.14
21	895.048	918.938	2.60%	191.07	220.87
22	907.968	938.514	3.25%	293.19	221.76
23	789.433	815.575	3.21%	199.80	229.95
24	965.238	984.047	1.91%	785.38	215.24
25	964.817	997.933	3.32%	19.17	245.32
26	422.372	456.407	7.46%	3606.24	667.78
27	129.445	134.936	4.07%	3623.14	1691.38
28	97.965	107.953	9.25%	3606.57	690.49
29	50.227	60.7778	17.36%	3606.29	692.64
30	114.298	126.686	9.78%	3605.86	597.24

Table 4.4: Solution results of NSGA-II_1

Instance	EC ($)	Δ	Running time (s)	Instance	EC ($)	Δ	Running time (s)
1	841.754	8.07%	57.27	16	349.158	2.86%	235.55
2	664.277	2.22%	61.60	17	242.441	5.34%	205.22
3	592.382	7.47%	64.66	18	286.689	5.64%	211.79
4	647.642	3.66%	64.66	19	371.365	4.56%	212.46
5	647.794	2.09%	68.45	20	237.626	5.84%	207.98
6	230.588	2.35%	188.46	21	939.473	4.73%	75.70
7	364.564	2.34%	187.33	22	942.778	3.69%	91.43
8	280.976	0.43%	191.38	23	821.843	3.94%	68.02
9	220.815	4.58%	184.63	24	987.215	2.23%	73.14
10	252.988	0.20%	191.72	25	1010.210	4.49%	73.42
11	882.583	1.10%	72.93	26	448.027	5.73%	209.68
12	890.619	0.03%	143.07	27	137.361	5.76%	219.54
13	865.544	1.78%	68.64	28	109.427	10.47%	217.22
14	788.409	1.34%	65.59	29	60.945	17.59%	214.85
15	865.568	0.71%	70.27	30	126.51	9.65%	213.55

have a better understanding of solution quality, we combine all Pareto solutions of a problem instance into a new set of non-dominated solutions called a super front. Let $N(T)$ be the number of Pareto front solutions and $N(H)$ be the number of non-dominated solutions produced by an algorithm in the aggregated set. The performance ratio of a particular algorithm H, $PR(H) = \frac{N(H)}{N(T)}$. As Table 4.5 shows, NSGA-II_5 performs better than NSGA-II_1 for 23 of the 30 instances. The average performance ratios of NSGA-II_5 and NSGA-II_1 are 74.24% and 34.67%, respectively.

Table 4.5: Performance ratios of NSGA-II_5 and NSGA-II_1

Instance	NSGA-II_5	NSGA-II_1	Instance	NSGA-II_5	NSGA-II_1
1	87.5%	25.0%	16	87.5%	87.5%
2	85.7%	28.6%	17	100.0%	0.0%
3	100.0%	14.3%	18	88.9%	11.1%
4	66.7%	44.4%	19	66.7%	33.3%
5	100.0%	0.0%	20	75.0%	25.0%
6	50.0%	100.0%	21	100.0%	0.0%
7	71.4%	28.6%	22	40.0%	60.0%
8	90.0%	30.0%	23	55.6%	44.4%
9	100.0%	7.7%	24	53.3%	46.7%
10	50.0%	83.3%	25	100.0%	0.0%
11	83.3%	16.7%	26	27.8%	72.2%
12	100.0%	28.6%	27	100.0%	0.0%
13	62.5%	25.0%	28	26.1%	69.6%
14	100.0%	0.0%	29	83.3%	11.1%
15	66.7%	83.3%	30	22.7%	63.6%

We now use instances 1 and 11 to illustrate how we calculate the performance ratio. Figure 4.4 shows the plot of non-dominated solutions of NSGA-II_5, along with solutions achieved with NSGA-II_1, for the example problem instances. Initially, NSGA-II_5 and NSGA-II_1 generate eight and five Pareto solutions for instance 1, respectively. Among all eight Pareto solutions for instance 1, NSGA-II_1 has one same solution (188, 850.527) as NSGA-II_5 does and one non-dominated solution at (200, 842.363). Besides the shared solution (188, 850.527), NSGA-II_5 provides six additional non-dominated solutions. Therefore, the performance ratios of NSGA-II_5 and NSGA-II_1 are 87.5%(7/8) and 25%(2/8), respectively. For instance 11, 10 of 12 and 2 of 12 non-dominated solutions are obtained by NSGA-II_5 and NSGA-II_1, respectively, which result in performance ratios of 83.3% and 16.7%. The purpose of generating a super front is to let decision-makers evaluate trade-offs between different solution options effectively [97].

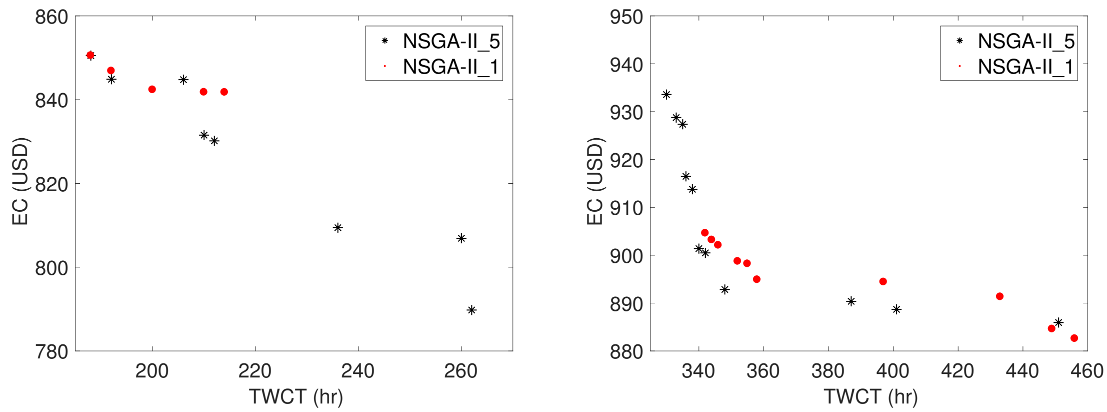

(a) Pareto fronts of instance 1 (b) Pareto fronts of instance 11

Figure 4.4: Pareto fronts of instance 1 and 11

4.6 Conclusions and Future Research

In this paper, we study a job shop scheduling problem with on-site renewable generation and an energy storage system under hour-ahead real-time pricing schemes to simultaneously minimize the total weighted completion time and energy costs. Our model is formulated as a time-indexed, mixed-integer linear program. To solve the problem, we adopt an ϵ-constraint approach to transform TWCT into an $\epsilon-$constraint and minimize energy costs. To improve computational efficiency, we develop a hybrid multi-objective evolutionary algorithm based on NSGA-II [89]. Five methods are embedded in the algorithm to generate production schedules. Then, under a given feasible production schedule, energy costs are calculated by a commercial solver.

Experimental results confirm that both mathematical modeling and our developed algorithm are competitive. The gap between the EC obtained from the MILP and our NSGA-II is 3.29%, on average. For large problem instances (nine jobs and 96 time periods), the MILP cannot obtain optimal solution for even one ϵ parameter within a one-hour time limit. In contrast, our heuristic algorithm can produce all Pareto fonts within 1700 seconds for any instance. Using sets of Pareto optimal solutions, decision-makers can choose the desired solution according to their preferences to determine production schedules and energy requirements. Computational tests also show that NSGA-II_1 can produce solutions more quickly than NSGA-II_5, but with slightly lower quality. This result indicates that both NSGA-II_5 and NSGA-II_1 can be used as managerial tools to provide solutions on minimizing production scheduling and energy cost simultaneously with regards to hour-ahead real-time electricity pricing scheme and stochastic renewable generation. However, there is a trade-off between solution quality and computational time that decision-makers must consider.

Future studies can investigate how production schedules and energy supply decisions change with different pricing schemes. Other objective functions also can be studied such as minimizing greenhouse gas emissions. Another interesting research topic could be to examine the performance of other heuristic methods such as Tabu search on the problem of interest.

Chapter 5

Conclusions and Future Research

With energy shortage and environmental challenges becoming increasingly severe problems, interest in renewable energy resources has grown in recent years. This dissertation considers utilizing renewable energy resources in two major locations: the power grid side and the end-use customer side of power systems. As renewable energy resources like solar and wind energy typically fluctuate with weather variations, the inherent stochastic nature of renewable energy resources makes the decision making of utilizing renewable generation complex. To this end, we study how to effectively utilize renewable energy in power systems.

5.1 Research Conclusions

In the first phase of this dissertation, we focus on managing energy of networked microgrids in a power grid with the integration of renewable energy resources. A centralized arbiter in the main grid regulates power generation and supply for the whole power system. Each microgrid contains various energy management settings, and as an agent, seeks to minimize cost within the microgrid area after receiving the arbiter's decision and an observation of the renewable generation and customer demand. We present a two-stage stochastic optimization framework for this multi-agent system by extending the classical 2-SP model to include multiple subproblems. To the best of our knowledge, this is the first study that investigates multiple subproblems with heterogeneous decisions and stochastic processes in the second-stage. To optimize this energy management problem, we develop stochastic decomposition-based algorithms. Compared to the benchmark 2-SD approach, our algorithm can provide reliable overall cost estimates to the proposed problem with 50% less solution time. Both of our proposed approximation approaches, which are agent cuts (MA-SD(m)) and aggregated cuts (MA-SD(a)), yield statistically comparable results, but MA-SD(a) is computationally more efficient.

In the second phase, we focus on studying renewable generators installed and available in a flow shop. A two-stage, multi-objective stochastic MILP is developed for the flow shop scheduling problem with energy decisions. In the first stage, a time-indexed MILP is proposed to minimize total weighted completion time. The second stage determines the energy supply decisions according to the production schedule and a realization of renewable energy generation to minimize energy costs under a TOU electricity price scheme. First, we employ a ϵ-constraint approach to transform the multi-objective problem into a two-stage, single-objective stochastic MILP which is then solved by an L-shaped method. In our experiments, a set of Pareto optimal solutions are provided for decision-makers to minimize total weighted completion time and energy costs in scheduling the production process. Decision-makers can choose a solution according to their preference among all Pareto optimal solutions. Our experiments show that although using solar generation or wind generation can reduce energy costs, using solar energy can reduce more cost than using wind energy for the problem under study.

In the third and final phase of this dissertation, we extend the flow shop scheduling with on-site renewable generation problem to a job shop environment. We present a time-indexed, mixed-integer linear program to simultaneously minimize the total weighted completion time and energy costs under hour-ahead real-time pricing schemes. An ϵ-constraint approach is used to transform the total weighted completion time into an $\epsilon-$ constraint and minimize energy costs. Since the problem is NP-hard, we develop a hybrid multi-objective evolutionary algorithm based on NSGA-II to improve computational efficiency. First, production schedules are generated using five methods which are embedded in the algorithm. Then, energy costs are calculated by a commercial solver under a given feasible production schedule. Computational tests show that both mathematical modeling and our developed algorithm are competitive. However, our heuristic algorithm can produce all Pareto fonts more quickly than the MILP. When used as a managerial tool, our algorithm reveals trade-offs between solution quality and computational time that decision makers must consider.

5.2 Future Research Directions

There are a number of research opportunities in the future that could enhance this research study. In Chapter 2, the structure of our algorithm involves solving several independent subproblems (corresponding to MGs) that is naturally fit for a distributed/parallel computing implementation. Bi-direction transactions can be investigated in a smart grid in which microgrids not only purchase power from the main grid but also can sell power back to the grid to increase the utilization of renewable energy over the entire power system. Further, transactions between microgrids also could be addressed.

For the scheduling problems with on-site renewable energy in Chapters 3 and

4, different objective functions such as due-date related lateness can be investigated. In addition, comparisons of production schedules and energy supply changes under different pricing schemes can be studied. Different time horizon lengths also need to be investigated as not all manufacturing facilities work 24 hours per day. Finally, another interesting research topic could be to examine the performance of other heuristic methods such as Tabu search on the problem of interest.

Bibliography

[1] J. R. Birge and F. Louveaux, *Introduction to stochastic programming*. Springer Science & Business Media, 2011.

[2] M. Shahidehpour and J. F. Clair, "A functional microgrid for enhancing reliability, sustainability, and energy efficiency," *The Electricity Journal*, vol. 25, no. 8, pp. 21–28, 2012.

[3] F. M. P. Júnior, A. C. Z. de Souza, M. Castilla, D. Q. Oliveira, P. F. Ribeiro *et al.*, "Control strategies for improving energy efficiency and reliability in autonomous microgrids with communication constraints," *Energies*, vol. 10, no. 9, pp. 1–16, 2017.

[4] D. T. Ton and M. A. Smith, "The US department of energy's microgrid initiative," *The Electricity Journal*, vol. 25, no. 8, pp. 84–94, 2012.

[5] N. Hamsic, A. Schmelter, A. Mohd, E. Ortjohann, E. Schultze, A. Tuckey, and J. Zimmermann, "Increasing renewable energy penetration in isolated grids using a flywheel energy storage system," in *2007 International Conference on Power Engineering, Energy and Electrical Drives*. IEEE, 2007, pp. 195–200.

[6] I. Stadler, "Power grid balancing of energy systems with high renewable energy penetration by demand response," *Utilities Policy*, vol. 16, no. 2, pp. 90–98, 2008.

[7] A. Evans, V. V. Strezov, and T. J. Evans, "Assessment of utility energy storage options for increased renewable energy penetration," *Renewable and Sustainable Energy Reviews*, vol. 16, no. 6, pp. 4141–4147, 2012.

[8] C. Bueno and J. A. Carta, "Wind powered pumped hydro storage systems, a means of increasing the penetration of renewable energy in the Canary Islands," *Renewable and Sustainable Energy Reviews*, vol. 10, no. 4, pp. 312–340, 2006.

[9] R. Segurado, G. Krajačić, N. Duić, and L. Alves, "Increasing the penetration of renewable energy resources in S. Vicente, Cape Verde," *Applied Energy*, vol. 88, no. 2, pp. 466–472, 2011.

[10] M. L. Pinedo, *Scheduling: Theory, Algorithms, and Systems.* Springer, 2015.

[11] B. Ekşioğlu, S. D. Ekşioğlu, and P. Jain, "A tabu search algorithm for the flowshop scheduling problem with changing neighborhoods," *Computers & Industrial Engineering*, vol. 54, no. 1, pp. 1–11, 2008.

[12] S. Mason, S. Jin, and C. Wessels, "Rescheduling strategies for minimizing total weighted tardiness in complex job shops," *International Journal of Production Research*, vol. 42, no. 3, pp. 613–628, 2004.

[13] M. L. Bell and D. L. Davis, "Reassessment of the lethal london fog of 1952: novel indicators of acute and chronic consequences of acute exposure to air pollution." *Environmental health perspectives*, vol. 109, no. Suppl 3, p. 389, 2001.

[14] Y. Chen, S. Lu, Y. Chang, T. Lee, and M. Hu, "Economic analysis and optimal energy management models for microgrid systems: A case study in Taiwan," *Applied Energy*, vol. 103, pp. 145–154, 2013.

[15] P. Basak, S. Chowdhury, S. Halder nee Dey, and S.P. Chowdhury, "A literature review on integration of distributed energy resources in the perspective of control, protection and stability of microgrid," *Renewable and Sustainable Energy Reviews*, vol. 16, no. 8, pp. 5545–5556, 2012.

[16] R. H. Lasseter, "MicroGrids," in *2002 IEEE Power Engineering Society Winter Meeting. Conference Proceedings (Cat. No.02CH37309)*, vol. 1, 2002, pp. 305–308.

[17] A. Zakariazadeh, J. Shahram, and P. Siano, "Smart microgrid energy and reserve scheduling with demand response using stochastic optimization," *International Journal of Electrical Power & Energy Systems*, vol. 63, pp. 523–533, 2014.

[18] T. Ackermann, G. Andersson, and L. Söder, "Distributed generation: a definition," *Electric Power Systems Research*, vol. 57, no. 3, pp. 195–204, 2001.

[19] H. Gangammanavar and S. Sen, "Two-scale stochastic optimization for controlling distributed storage devices," *IEEE Transactions on Smart Grid*, vol. 9, no. 4, pp. 2691–2702, 2016.

[20] M. Marzband, N. Parhizi, M. Savaghebi, and J. M. Guerrero, "Distributed smart decision-making for a multimicrogrid system based on a hierarchical interactive architecture," *IEEE Transactions on Energy Conversion*, vol. 31, no. 2, pp. 637–648, 2016.

[21] A. R. Malekpour and A. Pahwa, "Stochastic energy management in distribution systems with correlated wind generators," *IEEE Transactions on Power Systems*, 2017.

[22] K. Boroojeni, M. H. Amini, A. Nejadpak, T. Dragičević, S. S. Iyengar, and F. Blaabjerg, "A novel cloud-based platform for implementation of oblivious power routing for clusters of microgrids," *Ieee Access*, vol. 5, pp. 607–619, 2017.

[23] Z. Wang, B. Chen, J. Wang, M. M. Begovic, and C. Chen, "Coordinated energy management of networked microgrids in distribution systems," *IEEE Transactions on Smart Grid*, vol. 6, no. 1, pp. 45–53, 2015.

[24] H.S.V.S. Kumar Nunna and S. Doolla, "Multiagent-based distributed-energy-resource management for intelligent microgrids," *IEEE Transactions on Industrial Electronics*, vol. 60, no. 4, pp. 1678–1687, 2013.

[25] T. Logenthiran, D. Srinivasan, and A. M. Khambadkone, "Multi-agent system for energy resource scheduling of integrated microgrids in a distributed system," *Electric Power Systems Research*, vol. 81, no. 1, pp. 138–148, 2011.

[26] T. Dai and W. Qiao, "Trading wind power in a competitive electricity market using stochastic programing and game theory," *IEEE Transactions on Sustainable Energy*, vol. 4, no. 3, pp. 805–815, 2013.

[27] S. W. Wallace and S.-E. Fleten, "Stochastic programming models in energy," *Handbooks in operations research and management science*, vol. 10, pp. 637–677, 2003.

[28] A. Sheikhi, A. Maani, and A. Ranjbar, "Evaluation of intelligent distribution network response to plug-in hybrid electric vehicles," in *PowerTech (POWERTECH), 2013 IEEE Grenoble*. IEEE, 2013, pp. 1–6.

[29] D. T. Nguyen and L. B. Le, "Optimal energy management for cooperative microgrids with renewable energy resources," in *2013 IEEE International Conference on Smart Grid Communications (SmartGridComm)*. IEEE, 2013, pp. 678–683.

[30] Y. M. Ding, S. H. Hong, and X. H. Li, "A demand response energy management scheme for industrial facilities in smart grid," *IEEE Transactions on Industrial Informatics*, vol. 10, no. 4, pp. 2257–2269, 2014.

[31] G. Goddard, J. Klose, and S. Backhaus, "Model development and identification for fast demand response in commercial HVAC systems," *IEEE Transactions on Smart Grid*, vol. 5, no. 4, pp. 2084–2092, 2014.

[32] N. Li, L. Chen, and S. H. Low, "Optimal demand response based on utility maximization in power networks," in *2011 IEEE power and energy society general meeting*. IEEE, 2011, pp. 1–8.

[33] Z. Chen, L. Wu, and Y. Fu, "Real-time price-based demand response management for residential appliances via stochastic optimization and robust optimization," *IEEE Transactions on Smart Grid*, vol. 3, no. 4, pp. 1822–1831, 2012.

[34] P. Zhao, S. Suryanarayanan, and M. G. Simoes, "An energy management system for building structures using a multi-agent decision-making control methodology," *IEEE Transactions on Industry Applications*, vol. 49, no. 1, pp. 322–330, 2013.

[35] R. de Dear and G. S. Brager, "The adaptive model of thermal comfort and energy conservation in the built environment," *International Journal of Biometeorology*, vol. 45, no. 2, pp. 100–108, 2001.

[36] D. J. Sailor and A. A. Pavlova, "Air conditioning market saturation and long-term response of residential cooling energy demand to climate change," *Energy*, vol. 28, no. 9, pp. 941–951, 2003.

[37] Y. Agarwal, B. Balaji, R. Gupta, J. Lyles, M. Wei, and T. Weng, "Occupancy-driven energy management for smart building automation," in *Proceedings of the 2nd ACM Workshop on Embedded Sensing Systems for Energy-Efficiency in Building*. ACM, 2010, pp. 1–6.

[38] A. Etxeberria, I. Vechiu, H. Camblong, and J. M. Vinassa, "Hybrid energy storage systems for renewable energy sources integration in microgrids: A review," in *IPEC, 2010 Conference Proceedings*. IEEE, 2010, pp. 532–537.

[39] P. Denholm, E. Ela, B. Kirby, and M. Milligan, "The role of energy storage with renewable electricity generation. NREL/TP-6A247187. National Renewable Energy Laboratory," 2010, Accessed: 2020-1-5. [Online]. Available: https://www.nrel.gov/docs/fy10osti/47187.pdf

[40] R. Sioshansi, P. Denholm, and T. Jenkin, "Market and policy barriers to deployment of energy storage," *Economics of Energy & Environmental Policy*, vol. 1, no. 2, pp. 47–63, 2012.

[41] A. L. Motto, F. D. Galiana, A. J. Conejo, and J. M. Arroyo, "Network-constrained multiperiod auction for a pool-based electricity market," *IEEE Transactions on Power Systems*, vol. 17, no. 3, pp. 646–653, 2002.

[42] J. F. Benders, "Partitioning procedures for solving mixed-variables programming problems," *Numerische Mathematik*, vol. 4, no. 1, pp. 238–252, 1962.

[43] G. B. Dantzig and P. Wolfe, "Decomposition principle for linear programs," *Operations Research*, vol. 8, no. 1, pp. 101–111, 1960.

[44] R. T. Rockafellar and R. J. B. Wets, "Scenarios and policy aggregation in optimization under uncertainty," *Mathematics of Operations Research*, vol. 16, no. 1, pp. 119–147, 1991.

[45] H. Gangammanavar, S. Sen, and V. M. Zavala, "Stochastic optimization of sub-hourly economic dispatch with wind energy," *IEEE Transactions on Power System*, vol. 31, no. 2, pp. 949–959, 2015.

[46] S. Sen and Y. Liu, "Mitigating uncertainty via compromise decisions in two-stage stochastic linear programming: Variance reduction," *Operations Research*, vol. 64, no. 6, pp. 1422–1437, 2016.

[47] J. Higle and S. Sen, "Finite master programs in regularized stochastic decomposition," *Mathematical Programming*, vol. 67, no. 1-3, pp. 143–168, 1994.

[48] J. E. Price and J. Goodin, "Reduced network modeling of WECC as a market design prototype," in *2011 IEEE Power and Energy Society General Meeting*. IEEE, 2011, pp. 1–6.

[49] National Renewable Energy Laboratory (NREL), "Western wind and solar integration study," Accessed: 2020-1-5. [Online]. Available: https://www.nrel.gov/grid/wwsis.html

[50] U.S. Energy Information Administration (EIA), "Levelized cost and levelized avoided cost of new generation resources in the annual energy outlook 2015," Accessed: 2020-1-5. [Online]. Available: https://www.eia.gov/outlooks/archive/aeo

[51] J. L. Higle and S. Sen, "Duality and statistical tests of optimality for two stage stochastic programs," *Mathematical Programming*, vol. 75, no. 2, pp. 257–275, 1996.

[52] U.S. Energy Information Administration (EIA), "Use of energy explained," Accessed: 2020-1-5. [Online]. Available: https://www.eia.gov/energyexplained/use-of-energy/industry.php

[53] U.S. Energy Information Administration (EIA), "EIA monthly energy review," Accessed: 2020-1-5. [Online]. Available: https://www.eia.gov/totalenergy/data/monthly/pdf/mer.pdf

[54] S. Wang, H. Gangammanavar, S. D. Ekşioğlu, and S. J. Mason, "Stochastic optimization for energy management in power systems with multiple microgrids," *IEEE Transactions on Smart Grid*, vol. 10, no. 1, pp. 1068–1079, 2019.

[55] A. Sharma, F. Zhao, and J. W. Sutherland, "Econological scheduling of a manufacturing enterprise operating under a time-of-use electricity tariff," *Journal of Cleaner Production*, vol. 108, pp. 256–270, 2015.

[56] U.S. Energy Information Administration (EIA), "International Energy Outlook 2017," Accessed: 2020-9-8. [Online]. Available: https://www.eia.gov/outlooks/ieo/pdf/0484(2017).pdf

[57] E. Lantz, B. Sigrin, M. Gleason, R. Preus, and I. Baring-Gould, "Assessing the future of distributed wind: Opportunities for behind-the-meter projects," Accessed: 2018-1-12. [Online]. Available: https://www.nrel.gov/docs/fy17osti/67337.pdf

[58] C.-H. Liu, "Mathematical programming formulations for single-machine scheduling problems while considering renewable energy uncertainty," *International Journal of Production Research*, vol. 54, no. 4, pp. 1122–1133, 2016.

[59] A. Giret, D. Trentesaux, and V. Prabhu, "Sustainability in manufacturing operations scheduling: A state of the art review," *Journal of Manufacturing Systems*, vol. 37, pp. 126–140, 2015.

[60] K. Biel and C. H. Glock, "Systematic literature review of decision support models for energy-efficient production planning," *Computers & Industrial Engineering*, vol. 101, pp. 243–259, 2016.

[61] C. Gahm, F. Denz, M. Dirr, and A. Tuma, "Energy-efficient scheduling in manufacturing companies: A review and research framework," *European Journal of Operational Research*, vol. 248, no. 3, pp. 744–757, 2016.

[62] M. B. Yildirim and G. Mouzon, "Single-machine sustainable production planning to minimize total energy consumption and total completion time using a multiple objective genetic algorithm," *IEEE transactions on engineering management*, vol. 59, no. 4, pp. 585–597, 2012.

[63] G. Liu, Y. Zhou, and H. Yang, "Minimizing energy consumption and tardiness penalty for fuzzy flow shop scheduling with state-dependent setup time," *Journal of Cleaner Production*, vol. 147, pp. 470–484, 2017.

[64] H. Luo, B. Du, G. Q. Huang, H. Chen, and X. Li, "Hybrid flow shop scheduling considering machine electricity consumption cost," *International Journal of Production Economics*, vol. 146, no. 2, pp. 423–439, 2013.

[65] J.-Y. Ding, S. Song, R. Zhang, R. Chiong, and C. Wu, "Parallel machine scheduling under time-of-use electricity prices: New models and optimization approaches," *IEEE Transactions on Automation Science and Engineering*, vol. 13, no. 2, pp. 1138–1154, 2016.

[66] J.-Y. Moon and J. Park, "Smart production scheduling with time-dependent and machine-dependent electricity cost by considering distributed energy resources and energy storage," *International Journal of Production Research*, vol. 52, no. 13, pp. 3922–3939, 2014.

[67] Y. Zhai, K. Biel, F. Zhao, and J. W. Sutherland, "Dynamic scheduling of a flow shop with on-site wind generation for energy cost reduction under real time electricity pricing," *CIRP Annals*, vol. 66, no. 1, pp. 41–44, 2017.

[68] H. Zhang, J. Cai, K. Fang, F. Zhao, and J. W. Sutherland, "Operational optimization of a grid-connected factory with onsite photovoltaic and battery storage systems," *Applied Energy*, vol. 205, pp. 1538–1547, 2017.

[69] K. Biel, F. Zhao, J. W. Sutherland, and C. H. Glock, "Flow shop scheduling with grid-integrated onsite wind power using stochastic MILP," *International Journal of Production Research*, pp. 1–23, 2017.

[70] A. Fazli Khalaf and Y. Wang, "Energy-cost-aware flow shop scheduling considering intermittent renewables, energy storage, and real-time electricity pricing," *International Journal of Energy Research*, vol. 42, no. 12, pp. 3928–3942, 2018.

[71] S. Wang, M. Kurz, S. J. Mason, and E. Rashidi, "Two-stage hybrid flow shop batching and lot streaming with variable sublots and sequence-dependent setups," *International Journal of Production Research*, vol. 57, no. 22, pp. 6893–6907, 2019.

[72] A. Allahverdi and H. Soroush, "The significance of reducing setup times/setup costs," *European Journal of Operational Research*, vol. 187, no. 3, pp. 978–984, 2008.

[73] F. Sourd, "Earliness–tardiness scheduling with setup considerations," *Computers & operations research*, vol. 32, no. 7, pp. 1849–1865, 2005.

[74] I. M. Stancu-Minasian, *Stochastic programming with multiple objective functions*. D Reidel Pub Co, 1984, vol. 13.

[75] F. B. Abdelaziz, P. Lang, and R. Nadeau, "Dominance and efficiency in multicriteria decision under uncertainty," *Theory and Decision*, vol. 47, no. 3, pp. 191–211, 1999.

[76] R. Caballero, E. Cerdá, M. del Mar Muñoz, and L. Rey, "Stochastic approach versus multiobjective approach for obtaining efficient solutions in stochastic multiobjective programming problems," *European Journal of Operational Research*, vol. 158, no. 3, pp. 633–648, 2004.

[77] F. Tricoire, A. Graf, and W. J. Gutjahr, "The bi-objective stochastic covering tour problem," *Computers & operations research*, vol. 39, no. 7, pp. 1582–1592, 2012.

[78] A. F. Osorio, S. C. Brailsford, and H. K. Smith, "Whole blood or apheresis donations? A multi-objective stochastic optimization approach," *European Journal of Operational Research*, vol. 266, no. 1, pp. 193–204, 2018.

[79] Y. Cardona-Valdés, A. Álvarez, and D. Ozdemir, "A bi-objective supply chain design problem with uncertainty," *Transportation Research Part C: Emerging Technologies*, vol. 19, no. 5, pp. 821–832, 2011.

[80] Y. Haimes, "On a bicriterion formulation of the problems of integrated system identification and system optimization," *IEEE transactions on systems, man, and cybernetics*, vol. 1, no. 3, pp. 296–297, 1971.

[81] A. J. Kleywegt, A. Shapiro, and T. Homem-de Mello, "The sample average approximation method for stochastic discrete optimization," *SIAM Journal on Optimization*, vol. 12, no. 2, pp. 479–502, 2002.

[82] R. M. Van Slyke and R. Wets, "L-shaped linear programs with applications to optimal control and stochastic programming," *SIAM Journal on Applied Mathematics*, vol. 17, no. 4, pp. 638–663, 1969.

[83] Pacific Gas and Electric Company, "Industrial/general service (E-20)," Accessed: 2018-12-23. [Online]. Available: https://www.pge.com/tariffs/electric.shtml#INDUSTRIAL

[84] Pacific Gas and Electric Company, "ReMat feed-in tariff (senate bill 32)," Accessed: 2018-12-23. [Online]. Available: https://www.pge.com/en_US/for-our-business-partners/floating-pages/remat-feed-in-tariff/remat-feed-in-tariff.page

[85] S. Wang, S. J. Mason, and H. Gangammanavar, "Stochastic optimization for flow-shop scheduling with on-site renewable energy generation using a case in the united states," *Computers & Industrial Engineering*, vol. 149, p. 106812, 2020.

[86] M. R. Garey, D. S. Johnson, and R. Sethi, "The complexity of flowshop and jobshop scheduling," *Mathematics of operations research*, vol. 1, no. 2, pp. 117–129, 1976.

[87] A. S. Jain and S. Meeran, "Deterministic job-shop scheduling: Past, present and future," *European journal of operational research*, vol. 113, no. 2, pp. 390–434, 1999.

[88] C. S. Chong, M. Y. H. Low, A. I. Sivakumar, and K. L. Gay, "A bee colony optimization algorithm to job shop scheduling," in *Proceedings of the 2006 winter simulation conference*. IEEE, 2006, pp. 1954–1961.

[89] K. Deb, A. Pratap, S. Agarwal, and T. Meyarivan, "A fast and elitist multiobjective genetic algorithm: Nsga-ii," *IEEE transactions on evolutionary computation*, vol. 6, no. 2, pp. 182–197, 2002.

[90] J. Zhang, G. Ding, Y. Zou, S. Qin, and J. Fu, "Review of job shop scheduling research and its new perspectives under industry 4.0," *Journal of Intelligent Manufacturing*, vol. 30, no. 4, pp. 1809–1830, 2019.

[91] B. Çaliş and S. Bulkan, "A research survey: review of ai solution strategies of job shop scheduling problem," *Journal of Intelligent Manufacturing*, vol. 26, no. 5, pp. 961–973, 2015.

[92] Y. Liu, H. Dong, N. Lohse, S. Petrovic, and N. Gindy, "An investigation into minimising total energy consumption and total weighted tardiness in job shops," *Journal of Cleaner Production*, vol. 65, pp. 87–96, 2014.

[93] X. Wu and Y. Sun, "A green scheduling algorithm for flexible job shop with energy-saving measures," *Journal of cleaner production*, vol. 172, pp. 3249–3264, 2018.

[94] X. Gong, T. De Pessemier, L. Martens, and W. Joseph, "Energy-and labor-aware flexible job shop scheduling under dynamic electricity pricing: A many-objective optimization investigation," *Journal of Cleaner Production*, vol. 209, pp. 1078–1094, 2019.

[95] H. Mokhtari and A. Hasani, "An energy-efficient multi-objective optimization for flexible job-shop scheduling problem," *Computers & Chemical Engineering*, vol. 104, pp. 339–352, 2017.

[96] H. Golpîra, S. A. R. Khan, and Y. Zhang, "Robust smart energy efficient production planning for a general job-shop manufacturing system under combined demand and supply uncertainty in the presence of grid-connected microgrid," *Journal of cleaner production*, vol. 202, pp. 649–665, 2018.

[97] E. Cakici, S. J. Mason, and M. E. Kurz, "Multi-objective analysis of an integrated supply chain scheduling problem," *International Journal of Production Research*, vol. 50, no. 10, pp. 2624–2638, 2012.

[98] J. Long, Z. Zheng, X. Gao, and P. M. Pardalos, "A hybrid multi-objective evolutionary algorithm based on nsga-ii for practical scheduling with release times in steel plants," *Journal of the Operational Research Society*, vol. 67, no. 9, p. 0, 2016.

[99] Commonwealth Edison (ComEd) Company, "Comed's hourly pricing program," Accessed: 2020-10-20. [Online]. Available: https://www.hourlypricing.comed.com/live-prices/